Stony Brook University

The official electronic file of this thesis or dissertation is maintained by the University Libraries on behalf of The Graduate School at Stony Brook University.

Circulation and Transport Across the Iceland Faroes Shetland Ridge

A Dissertation presented

by

Katelin Childers

to

The Graduate School

in Partial Fulfillment of the

Requirements

for the Degree of

Doctor of Philosophy

in

Marine and Atmospheric Science

Stony Brook University

December 2014

Stony Brook University

The Graduate School

Katelin Childers

We, the dissertation committee for the above candidate for the
Doctor of Philosophy degree, hereby recommend
acceptance of this dissertation

Dr. Charles N. Flagg
Research Professor, School of Marine and Atmospheric Science

Dr. Robert Wilson
Associate Professor, School of Marine and Atmospheric Science

Dr. Christopher Wolfe
Assistant Professor, School of Marine and Atmospheric Science

Dr. Thomas Rossby
Emeritus Professor of Oceanography, University of Rhode Island

Dr. Robert Hallberg
Oceanographer and Ocean Group Head, NOAA Geophysical Fluid Dynamics Lab

This dissertation is accepted by the Graduate School

Charles Taber
Dean of the Graduate School

Abstract of the Dissertation

Circulation and Transport Across the Iceland Faroes Shetland Ridge

by

Katelin Childers

Doctor of Philosophy

in

Marine and Atmospheric Science

Stony Brook University

2014

The pathways and variability of warm Atlantic Water crossing over the
Iceland Faroes Scotland Ridge to the Nordic Seas are an important compo-
nent of the large scale Atlantic circulation. This dissertation presents the
spatial and temporal characteristics of the currents crossing the ridge from
both an observational and modeling perspective. Previous analyses of the
volume flux across the ridge have relied on moored velocity data and stan-
dard hydrographic sections. A unique velocity dataset collected weekly by
the M/F Norröna along repeated routes significantly improves the spatial res-
olution of observations between Iceland and Denmark. Output from a global
climate model complements this work by establishing the mean circulation
between the observational sections.

Following an introduction in Chapter 1, an analysis of the first 4.5 years
of weekly observational data collected by the Norröna program is presented
in Chapter 2. Surface inflows enter over the eastern half of each section and
transport 1.5±0.19 and 4.6±0.46 Sv through the Faroe Shetland Channel
(FSC) and across the Iceland Faroes Ridge (IFR), respectively. Fluctuations
in the FSC inflows depend primarily on the southward flux over the Faroe
shelf and slope, while the inflow width drives IFR interannual variability.
The description of regional circulation is expanded southward in Chapter 3,

using historic data from an additional ship of opportunity. Inflow paths from the North Atlantic Current to the Nordic Seas are presented.

Output from a high resolution ($1/12^o$), hourly, data assimilating run of the ECCO2 configuration of the MITgcm enhances the description of the mean flow between the observational routes and offers insight into the mesoscale features which perturb the time averaged circulation in Chapter 4. A streamline analysis in Chapter 5, predicts the flow paths from the IFR around the north of the Faroes and into the FSC. The recirculation of Atlantic Water onto the Faroes shelf and slope is shown to be split between a larger component ($\sim$1 Sv) , which is entrained into the Shetland Slope Current over the eastern FSC, and a smaller flow ($\sim$0.5 Sv), which circulates anticyclonically around the Faroes.

Contents

List of Figures

List of Abbreviations

ADCP Acoustic Doppler Current Profiler

AIW   Arctic Intermediate Water

AMO   Atlantic Multidecadal Oscillation

AVHRR Advanced Very High Resolution Radiometer

ECCO2 Estimating the Circulation and Climate of the Ocean, phase II

AMOC   Atlantic Meridional Overturning Circulation

ENAW East North Atlantic Water

FBC   Faroe Bank Channel

FSC   Faroe Shetland Channel

FSCDW Faroe Shetland Channel Deep Water

GIFR   Greenland Iceland Faroes Ridge

IFF   Iceland Faroes Front

IFR   Iceland Faroes Ridge

MEIW Mediterranean Intermediate Water

MITgcm Massachusetts Institute of Technology global climate model

MNAW Modified North Atlantic Water

NAC   North Atlantic Current

NAO   North Atlantic Oscillation

NADW North Atlantic Deep Water

NSAIW Norwegian Sea Arctic Intermediate Water

NAW   North Atlantic Water

NSDW Norwegian Sea Deep Water

NSW Norwegian Sea Deep Water

NwAC Norwegian Atlantic Current

PV Potential Vorticity

RAFOS SOund Fixing And Ranging (backwards)

RR Reykjanes Ridge

Sv Sverdrup, $10^6 m^3/s$

SSC Shetland Slope Current

SST Sea Surface Temperature

WNAW West North Atlantic Water

XBT eXpendable BathyThermograph

Acknowledgements

Chapter 1

Introduction

The Iceland-Faroes-Scotland Ridge serves as the gateway between warm Atlantic Waters and the Arctic Mediterranean. Surface waters carried north by the Gulf Stream approach the ridge as part of the North Atlantic Current bound for the Nordic and Arctic Seas through two primary routes: via the deep Faroe Shetland Channel (FSC) and over the eastern half of the shallow Iceland Faroes Ridge (IFR). Once north of the ridge, Atlantic waters are cooled and later return southward as deep and intermediate water masses. This branch of the Atlantic Meridional Overturning Circulation (AMOC) transports Atlantic Water north and exports deep nutrient rich waters south, in addition to influencing the climate of western Europe.

Observations of the hydrography and regional circulation near the ridge extend over 100 years (Helland-Hansen and Nansen, 1909; Tait, 1957; Mosby, 1970; Dooley and Meincke, 1981; Hansen et al., 2008). The basic current structure of the northern Atlantic is characterized by: several large northward currents that branch off of the North Atlantic Current, smaller southward flowing surface currents, and deep southward overflows (Figure 1.1). Throughout this dissertation, "inflow" will be used to describe currents entering the Nordic Seas from the north Atlantic and "outflow" refers to water entering the Atlantic from the north. The northward surface inflows are topographical split into three branches: the Iceland Branch, between Iceland and Greenland; the Faroe Branch, between Iceland and the Faroe Islands; and the Shetland Branch, between the Faroe Islands and the Shetland Islands north of Scotland. The Iceland Branch is the smallest, transporting only 1 Sv of Atlantic Water to the Nordic Seas (Hansen et al., 2008), while the remaining volume flux is split between the FSC ($\sim$1.5 Sv) and the IFR

($\sim$4.6 Sv) of surface inflow (Chapter 2).

Figure 1.1: Simple cartoon of the large scale circulation of the North Atlantic (from nasa.gov). Not included is the additional inflow over the eastern IFR.

The Greenland Current, and several deep overflows are the primary Nordic Seas outflows (Hansen et al., 2008). West of Iceland the outflow is strong, bottom intensified, and topographically steered (Dickson et al., 2008). This current lacks a seasonal component and is forced by density gradients (Dickson et al., 2008). To the east, overflows crossing the IFR are much more irregular both in magnitude and location (Hansen et al., 2008) providing a flux of approximately 1 Sv toward the Atlantic (Østerhus et al., 2008). The Faroe Shetland Channel has a surface outflow of recirculating Modified North Atlantic Water (MNAW) along its western slope, as well as a larger deep overflow of Faroe Shetland Channel Deep Water (FSDW), a mixture of Norwegian Sea Deep Water (NSW) and Norwegian Sea Arctic Intermediate

Water (NSAIW) (Carollo et al., 2005). It is steered through the channel by the steep topography and directed toward the west by the Wyville Thomson Ridge.

The focus of this dissertation is to characterize the mean and temporally varying volume flux of surface water across the Iceland Faroes Scotland Ridge. This introduction first presents a very brief description of the two primary inflow passageways between the Atlantic and Nordic Seas, followed by an explanation of the observational data used as the basis for this analysis. It concludes with a statement of the specific objectives addressed in each chapter.

1.1   The Faroe Shetland Channel

The Faroe Shetland Channel is the deepest entryway to the Nordic seas, reaching a maximum depth of approximately 1500 m (Carollo et al., 2005). Surface inflows primarily occur over the eastern portion of the passage and are dominated by the rapid Shetland Slope Current, which carries highly saline water from south of the Rockall Trough into the Nordic Seas (Hansen et al., 2008). The inflow waters are comprised primarily of North Atlantic Water (NAW) with some contributions of Modified North Atlantic Water (MNAW), bounded below by Arctic Intermediate Water (AIW) and NSAIW) (Carollo et al., 2005), shown in Figure 1.2. After crossing through the channel, inflow waters join the inner branch of the Norwegian Atlantic Current (NwAC) (Rossby and Flagg, 2012). The northward volume transport through the channel is characterized by Sherwin et al. (2008) as seasonal with variations of approximately 0.8 Sv from its maximum in August to its minimum in the late spring or early summer. The spring minimum is likely tied to an increase in southward flowing MNAW which enters near the Faroes and decreases the integrated northward volume transport (Sherwin et al., 2008), a further discussion of which is found in Chapters 4 and 5.

After crossing the IFR, flows are split into two major currents, the Western or offshore branch of the NwAC and the Eastern or inshore branch of the NwAC (Orvik et al., 2001). The western branch is the northern extension of the Iceland Faroes Front (IFF) and is wider and less stable than its eastern counterpart, extending approximately 400 m deep and reaching speeds up to 87 cm/s (Orvik et al., 2001). The eastern branch follows the shelf topography through the FSC north to the Nordic Seas, reaching maximum speeds up to
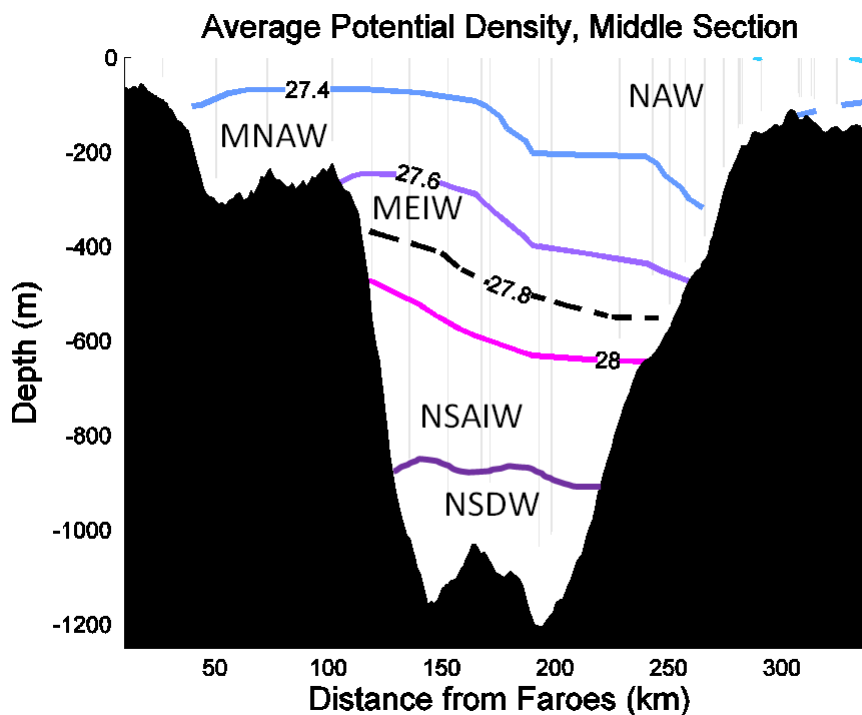
Figure 1.2: Average density and water masses along the Norröna's Middle transect across the Faroe Shetland Channel. Density values are based on ICES hydrographic data and described in greater detail in Chapter 2.

117 cm/s (Orvik et al., 2001). The western and eastern branches transport an annual average of 3.4 Sv and 4.2 Sv, respectively (Orvik et al., 2001). Waters passing northward through the FSC likely terminate in the Nordic and Barents Seas (Hansen et al., 2008).

Outflows through the FSC are split into a surface component over the western channel and a deep overflow. Southward flowing bottom waters through the FSC are made up of a mixture of Norwegian Sea Deep Water (NSDW) and NSAIW, forming Faroe Shetland Channel Deep Water (FSCDW) (Carollo et al., 2005). Overflow from the FSC is topographically controlled and blocked from flowing southward by the Wyville Thomson Ridge (Carollo et al., 2005). It is forced to the west, where it passes through the Faroe Bank Channel (FBC) (Carollo et al., 2005), which is the deepest passage across the GIFR and consequently the largest single outflow from the Nordic Seas to the North Atlantic (Østerhus et al., 2008). The overflow

4

through the FSC varies up to 10% seasonally, but shows no clear interannual trends or relationships with the density structure of the Norwegian Seas (Østerhus et al., 2008).

1.2   The Iceland Faroes Ridge

Flows over the IFR are more variable, both spatially and temporally, than their eastern counterparts in the FSC. The IFR is deepest on the eastern end, where most waters cross the ridge, and has sill depths ranging from 400 - 550 m. Atlantic water crossing the IFR forms a wedge that intersects the Faroe Plateau at 400 - 500 m depth and approaches the surface along the Iceland Faroes Front (IFF) (Hansen and Østerhus, 2000). Once across the IFR warmer Atlantic water inflows encounter the colder, fresher Faroe Current flowing eastward along the IFF (Hansen et al., 2008). This generally confines the northward flux of Atlantic waters to the eastern portion of the IFR and directs the flow eastward along the front and to the north of the Faroes about which there is an anticyclonic recirculation (Rossby and Flagg, 2012). The total detided northward flux across the IFR is roughly 4 Sv with 4.4 Sv found by Rossby and Flagg (2012)and 3.5 Sv reported by Hansen et al. (2008). Monthly averages range from 2.2 to 5.8 Sv northward resulting in seasonal fluctuations that are small compared with the range of monthly transports (Hansen et al., 2008). Flow across the IFR is subject to high eddy activity (Rossby et al., 2009) with meanders ranging from 30 - 50 km being carried eastward by the Iceland Faroes Front (IFF) (Carollo et al., 2005). A RAFOS float study showed that Atlantic water inflow moves southeast along the IFF before splitting into a recirculating component that flows southward through the FSC and a northward component that joins the inner Norwegian Atlantic Current (NwAC) (Rossby et al., 2009).
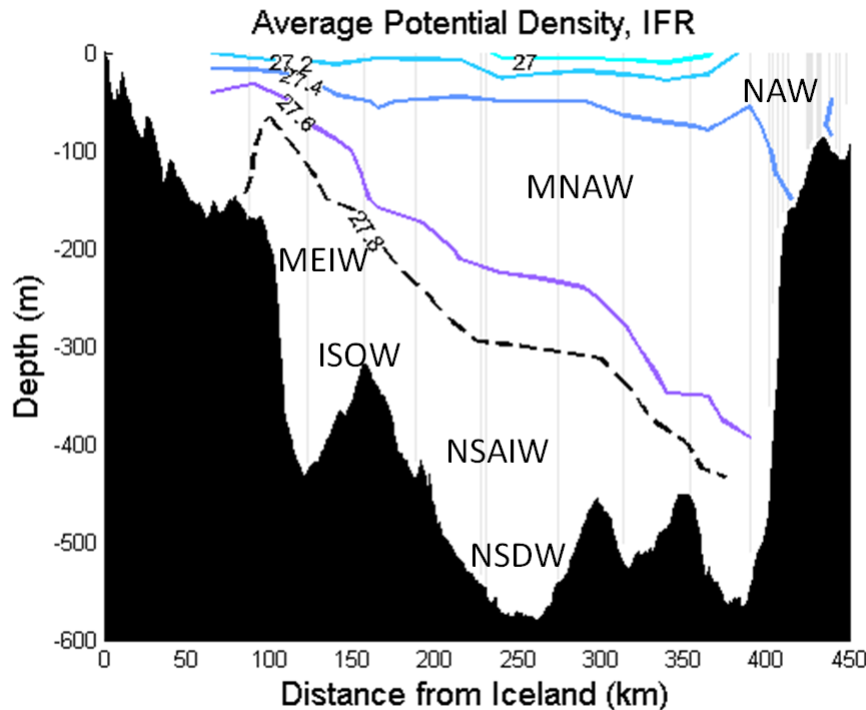
Figure 1.3: Average density and water masses along the Norröna's IFR transect. Density values are based on ICES hydrographic data and described in greater detail in Chapter 2.

1.3 Observational Data Collection and Processing

1.3.1 Shipboard ADCP data

This dissertation focuses on directly observed velocities observed from March 2008 through June 2012 (Figure 1.4). Data were collected by a hull mounted 75kHz RD Instruments Ocean Survey ADCP on the M/F Norröna, a high speed (21 kts) ferry operated by Smyril Lines, during its weekly circuit between Seydisfjordur, Iceland and Denmark (Figure 1.5). This dataset is unique for several reasons: firstly its collection and retrieval is completed remotely through the AutoADCP program; secondly, the spatial resolution is higher than the moored ADCPs currently used to monitor the long-term circulation through the FSC and over the IFR; and thirdly, the repeated

sections offer insight into the stability and temporal variability of the upper branch of the Atlantic Meridional Overturning Circulation.
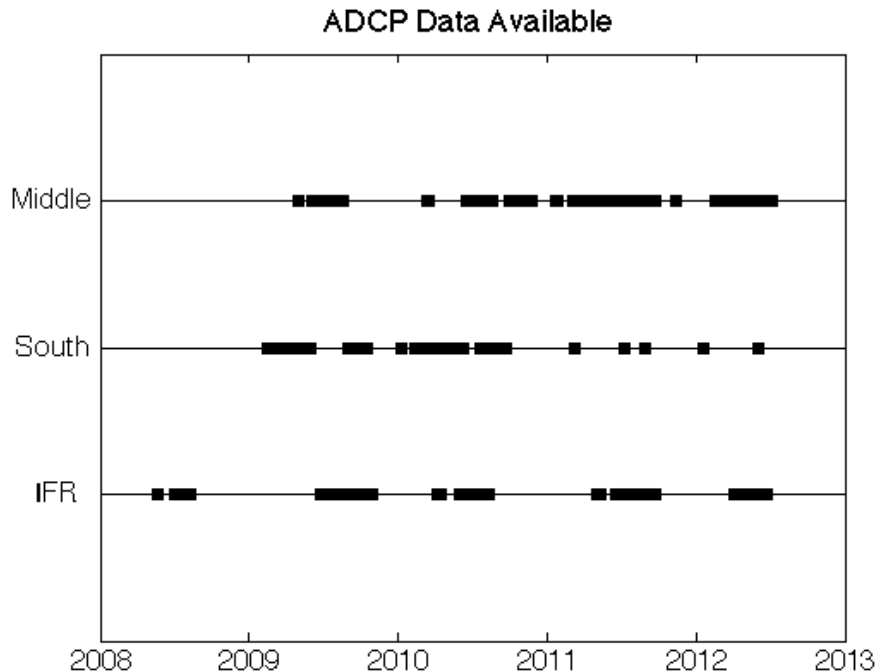
Figure 1.4: Date of data collection along each track.

Once collected, the raw files are processed using the UHDAS/CODAS program allowing for the correction of errors such as below-bottom data collection or heading offsets. The single-ping data are averaged into 3 minute temporal bins by 20 m depth. The 75 kHz ADCP consistently captures the upper 500 m of the water column and on occasion has a full depth range of up to 600 m. This more than adequately covers the surface Atlantic Water inflows, capturing the entirety of the water column over the IFR and the upper half of the deepest portions of the FSC. Over the shallow IFR, where the seafloor is within range of the ADCP, a bottom interference distance of approximately 20-40 m is removed.

Limitations to data collection occurred on many occasions due to the sweep down of bubbles due the Norröna's large bow thrusters. The flat bottom cause bubbles to become trapped beneath the ship in periods of poor weather (which are frequent in this region), leading to a complete blanking
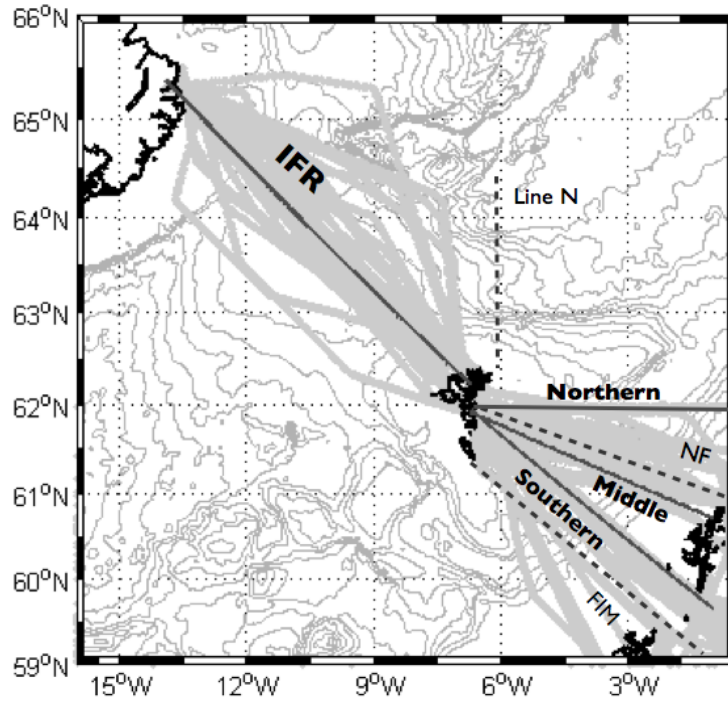
Figure 1.5: Map of Norröna crossings (gray dots) and mean locations of each transect (dark gray lines). Dotted lines are the Nolsa Flugga (NF) line, Fair Isle Munken (FIM) line, and Line N, maintained by the Scottish Marine Fisheries Services and Faroes Fisheries Lab. Bathymetry contours are from 250 m - 3000 m in increments of 250 m.

out of ADCP data collection. After a camera study, several stages of bubble fairing development, and movement of both the bubble fairing and the ADCP, the rate of data coverage increased considerably. Bubbles are still a source of interference, especially over the IFR where an open connection to the

Figure 1.6: Norröna system from po.msrc.sunysb.edu/Norrona. Additional information on the installation and maintenance of the system, as well as a full description of the bubble sweep-down interference can also be found on the website.

Atlantic increases the potential for high seas, limiting the temporal coverage of that section to the calmer summer months. Additionally gaps in the data have come from electrical issues addressed during a dry dock in January 2014 and failures of the beam former board.

1.3.2 XBT Program

In September 2013 an Autonomous eXpendable Instrument System (AXIS) was installed onboard the Norröna. The AXIS launches eXpendable BathyThermographs (XBTs) at predetermined times and locations while the ship is underway, allowing for the collection of near complete temperature profiles without the necessity of an onboard rider. Twelve XBTs are deployed for each section (FSC and IFR) each month (sample data from the first crossing shown in Figure 1.7). Resulting vertical profiles offer insight into water mass structure of each section and show the high degree of temporal variability associated with passing eddies. The recent failure of the ADCP has prevented the concurrent collection of temperature and velocity profiles, however this combination will be a powerful mechanism in the estimation and monitoring of heat flux over the ridge system.
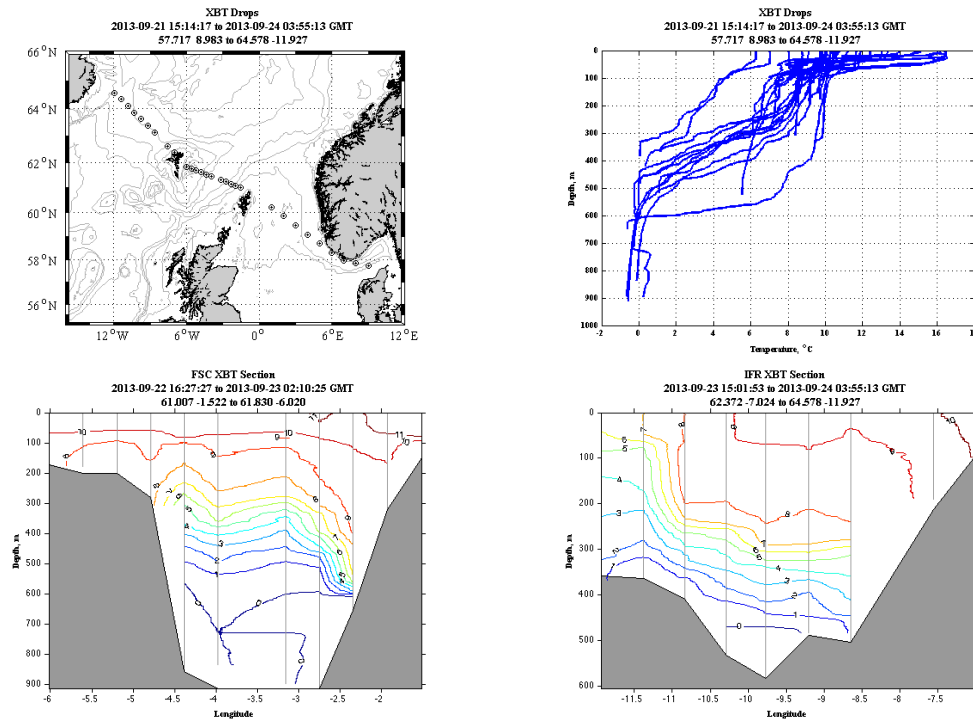
Figure 1.7: Sample XBT section from September 2013 showing drop locations (upper left), temperature profiles (upper right), FSC interpolated temperature section (lower left), the IFR interpolate temperature section (lower right).

1.4 Objectives

This dissertation aims to describe the mean circulation and transport across the Iceland Faroes Shetland Ridge. It begins with an observational analysis based on the first 4.5 years of ADCP data collected by Norröna program in Chapter 2, addressing the mean transports and pathways of flow crossing through the FSC and over the IFR. In Chapter 3 the spatial coverage is extended southward using a historical velocity dataset from an ADCP equipped ship of opportunity, the M/V Nuka Arctica, operating along several routes between Greenland and Denmark. This analysis uses volume conservation arguments to construct the regional circulation pattern approaching and crossing Faroes Shetland Ridge and establishes consistent transport estimates across the multiple observational sections. Through use of hourly results

11

from a data assimilating run of the MITgcm in Chapter 4, we increase the fine scale spatial and temporal resolution. This section addresses the mean circulation of the FSC north and south of the observational sections and considers the effect of mesoscale eddies. In Chapter 5, the same numerical simulations are used to establish connectivity between the observed inflows, by way of the recirculation flow east of the Faroes. In this chapter stream-lines are used to predict the flow path between the observational transects and to link the southern flow on the Faroe shelf and slope to the IFR and FSC inflows. Finally the thesis concludes with a brief summary and outlook in Chapter 6.

Chapter 2

Directly Observed Volume Flux between Iceland and the Shetland Islands

Abstract

Atlantic Waters flowing northward into the Nordic Seas are important for their role as an early indicator of changes to North Atlantic Deep Water formation. As such this requires a fundamental understanding of the pathways and volume fluxes through the primary passageways from the Atlantic into the Nordic Seas. Mean annual volume transports of 5.7 - 6.3 Sv were observed flowing in above the σ_t=27.8 isopycnal (a proxy for the lower limit of Atlantic Water depth), through the Faroe Shetland Channel (FSC) and over the Iceland Faroes Ridge (IFR) from March 2008 through June 2012, using repeat velocity sections obtained from a vessel mounted Acoustic Doppler Current Profiler (ADCP). A new vessel route has expanded the spatial coverage of FSC observations and reveals a difference in average inflow transport, which most likely results from an interannual variation in the total transport through the FSC, which in turn is tied to a weakening of the southerly flow over the western slope of the channel. This interannual variability has increased the mean transport through the FSC from 0.9 Sv observed over the first two years (Rossby and Flagg, 2012) to a 4.5 year mean of 1.7 Sv, which is closer to other published results (Sherwin et al., 2008; Berx et al., 2013; Hughes et al., 2006) and emphasizes the importance of knowing the

flow along the Faroese shelf. Interannual fluctuations in transport observed over the IFR are related to the width of the inflow over the Faroese half of the ridge. Despite large short term variability, results from each section indicate relative consistency of the inflows through the FSC and over the IFR for the full period of observations

2.1 Introduction

The primary Atlantic Water inflows to the Arctic Mediterranean occur through the Faroe Shetland Channel and over the Iceland Faroes Ridge. These waters enter the northern North Atlantic as part of the North Atlantic Current, and ultimately source the dense water production in the Nordic Seas. A description of the mean current structure and northward flux through the Shetland-Faroe-Iceland opening towards the Norwegian Sea has been developed using nearly 4.5 years of observational velocity data collected by the M/F Norröna. This report expands upon the first summary paper (Rossby and Flagg, 2012) including data from the two most recent years (2011 and 2012), as well as a comparison with transports across the two FSC routes now in use by the ship (Figure 1.5).

Historic observations of the FSC and IFR region date back as far as the maps of Olanus Magnus in the 16th century and circulation observations by Helland-Hansen and Nansen in the late 19th and early 20th centuries (Helland-Hansen and Nansen, 1909). Regular hydrographic observations have been collected since the 1970s (Coachman and Aagaard, 1974), and recent descriptions of the transport through the FSC and IFR rely heavily on moored ADCPs and hydrographic data along the Fair Isle Munken (FIM) line, south of the Norröna's southern track and line N, north of the Faroes (Hansen et al., 2003, 2008; Sherwin et al., 2006b, 2008; Hansen et al., 2010). The Faroes Fisheries Lab and Fisheries Research Services, Abderdeen have monitored standard hydrographic locations along the FIM line since 1994 (Sherwin et al., 2008), which are supplemented by ADCP deployments originally as part of the Nordic-WOCE project and later incorporated into the VEINs and MAIA projects (Hughes et al., 2006). For almost twenty years, five to seven moored, upward looking ADCPs have been in use along the line from the 300 m isobath on the western Faroese slope to the Shetland Shelf (Hughes et al., 2006). The westernmost ADCP was removed a few years into the study due to the low transport observed at that particular location

(Hughes et al., 2006). Most of the published results from the FIM section use the location of this ADCP as the western point of transport integration, in an effort to exclude the southerly flow on the Faroese side, and report FSC transports of 2.7±0.5 Sv (Berx et al., 2013), 3.5 Sv (Sherwin et al., 2008) and 3.9 Sv (Hughes et al., 2006). Similar methods along line N show inflow of Atlantic Water (AW) across the IFR to be 3.5±0.5 Sv (Hansen et al., 2003, 2010).

The Norröna velocity data approaches the estimation of transport from a different perspective. The use of vessel mounted, rather than moored ADCP data, significantly improves the horizontal resolution and increases coverage in the shallow regions of the FSC. Direct observations of velocity across both sections also eliminate any dependence on geostrophic estimates between stations. In particular a more robust image emerges for the IFR transport by sampling across the entire section and removing the need to account for other incoming eastward flows along the Iceland Faroes Front, which cross Line N along with the AW inflows (Hansen et al., 2003, 2010).

Waters moving from the Atlantic toward the Nordic Seas flow over the eastern (right in the figures) halves of both the FSC and IFR sections as the wedge shaped Shetland Slope Current (SSC) in the FSC and a less structured flow over the IFR (Figures 2.1 and 2.2; [Rossby and Flagg, 2012; Berx et al., 2013; Hughes et al., 2006; Sherwin et al., 2008]). Adopting the terminology of Hansen et al. (2003), we will refer to currents crossing the Iceland-Faroes-Scotland Ridge from the Atlantic toward the Nordic Seas and Arctic Ocean as "inflows" and waters going from the Nordic Seas toward the Atlantic as "outflows." In Rossby and Flagg (2012). 5.9 Sv of inflow was measured over the full depth of the southeastern half of the IFR and -1.5 Sv of outflow over the northwest. Through the FSC 4.1 Sv of inflow was reported and -3.2 Sv of surface outflow entered the north Atlantic above the σ_t=27.8 isopycnal. Of particular note in the Rossby and Flagg (2012) paper is the presence of the stronger than anticipated southward outflow through the western FSC, reducing the total mean inflow through the channel. The authors postulated roughly half of this flow to be the result of tidally rectified AW entering over the IFR and circling anticyclonically around the Faroes into the FSC. They further hypothesized that the other half of the southward flow may join the northeasterly Shetland Slope Current as evidenced by the width of the northward velocities extending farther west than the high salinity wedge Rossby and Flagg (2012). Subsequent data collection by the Norröna along a second route across the FSC allows us to explore questions about temporal

15

and spatial variability, a major objective of this study.

Short term variability in this region makes capturing a true "mean" image difficult and subject to velocity changes over a variety of timescales. An active eddy field, strong tidal oscillations, and interactions with steep and irregular topography impose further challenges. The results presented here show that even one additional year of data (compared to Rossby and Flagg (2012)) can have an impact on the overall description of velocity and transport in this region. A complete picture may only be possible after data has been collected over a full cycle of the AMO (Häkkinen et al., 2013) or NAO (Sherwin et al., 2008), which has been shown to influence the strength of currents in the Nordic Seas and Iceland Basin (Jakobsen et al., 2003) and the development of persistent eddies in the FSC, in turn adjusting the mean path of the SSC (Chafik, 2012). In addition, drifter analyses by Valdimarsson and Malmberg (1999) found drifter behavior between Iceland and the Faroes to alter in conjunction with the phase of the NAO, which has been in a low phase for the majority (2009-2012) of data collection by the Norröna. However, the relatively consistent pattern of flow over the IFR and good agreement between coincident periods across the two FSC routes suggest that the velocities and transports presented here are a good approximation of the average long term surface inflows from the Atlantic to the Nordic Seas. This is further supported by observations by Jakobsen et al. (2003) that the changing velocity magnitudes of circulation features north and south of the Iceland-Faroes-Scotland Ridge may not exert significant influence on the magnitude of transport across the IFR. This paper will first summarize the mean velocities and transports through the FSC and IFR then consider the temporal and structural variability in relation to previous studies of the region.
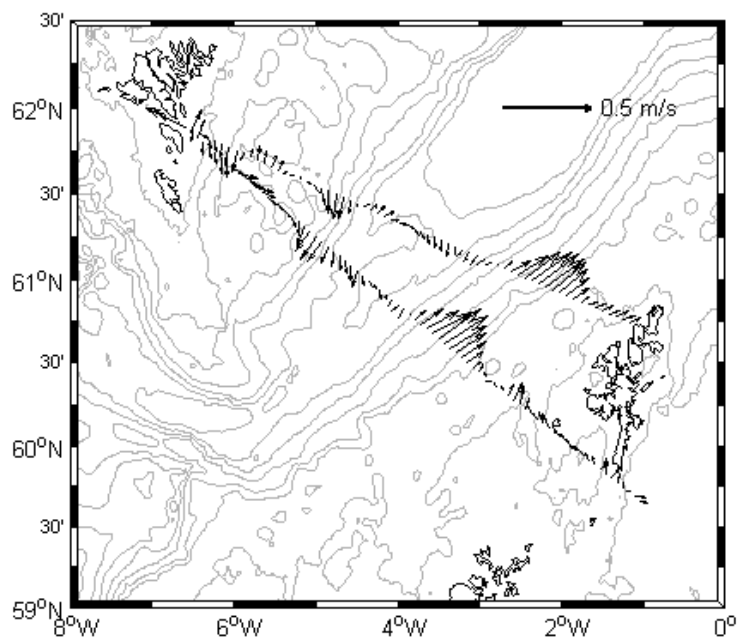
Figure 2.1: Map of surface FSC surface velocities (mean of upper 200 m) and local topography from 100 m - 1300 m in increments of 200 m.
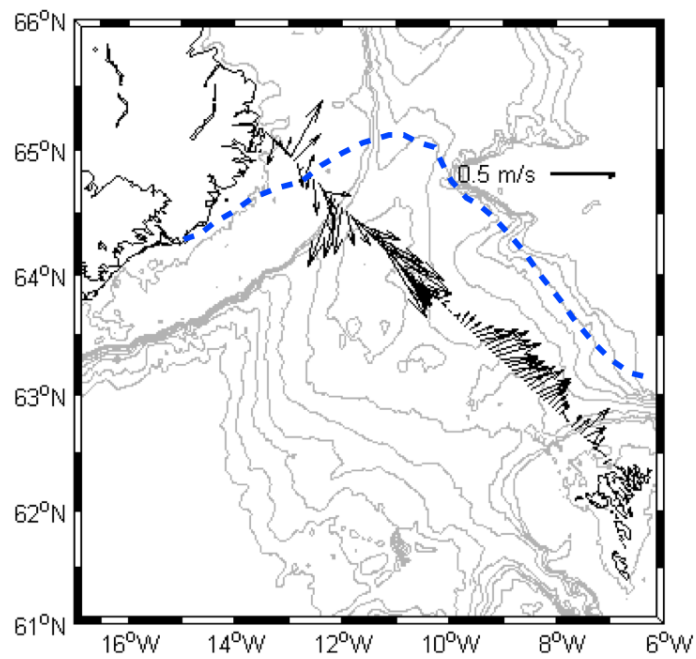
Figure 2.2: Map of surface IFR surface velocities (mean of upper 200 m) and local topography from 100 m - 1500 m in increments of 200 m. The blue dotted line indicates the mean position of the Iceland Faroes Front.

2.2 Data and Methods

The data set is built up of direct velocity observations from a vessel mounted 75 kHz RDI Ocean Surveyor ADCP run in narrow-band mode to reach depths of up to 600 m. Vessel heading is provided by a Thales ADU-5 once per second, which in addition to errors in the single ping accuracy from the ADCP results in a total uncertainty of 0.025 m/s (Rossby and Flagg, 2012) The Norröna travels weekly from Denmark to Iceland and back along three primary routes: (1) from Seydisfjördur, Iceland to Tórshavn along the Iceland Faroes Ridge; (2) from Tórshavn to Bergen, hereafter referred to as the "Northern Track"; (3) from Tórshavn to Hirtshals, Denmark via a route north of the Shetland Islands, the "Middle Track"; (4) from Torshavn to Hirtshals, Hantsholm or Esbjerg, Denmark via a route south of the Shetland Islands, the "Southern Track" (Figure 1.5). An expedited schedule during the summer shortens the round trip travel time and provides the opportunity for more than 50 round trip crossings per transect each year. Over the course of this study the Northern route has been abandoned. Bubbles underneath the vessel prevent data collection in conditions of high sea swell due to the heaving of the bow and breaching of the large bow-thruster openings. These scoop large volumes of air that are subducted and entrained into the flow along the hull, disrupting data collection during the winter and spring. Following the final adjustments during a January 2009 dry docking the data return over the IFR doubled from full coverage during 6 transect crossings in 2008 to 12 in 2009 (Figure 1.4). This level of data return has continued, with 10-14 successful observations of the IFR section per year. Presently the ADCP sits about 1/3 of the way back from the bow in a streamlined fairing that extends 0.2 m below the hull. Individual pings are averaged into 3-minute ensembles, then further averaged into bins of 5 km in the horizontal and 20 m vertically.

Several water masses move through the FSC and over the IFR, making an accurate estimate of the local temperature and salinity structure important in determining the volume of AW entering the Nordic Seas. To help define the water masses, hydrographic data are taken from the ICES database using the online data portal. All available temperature and salinity measurements collected from March 2008 through June 2012 and within 50 km of each transect were used to construct mean temperature, salinity, and density profiles for each section (Figures 2.3 - 2.6). In the FSC, most hydrographic data comes from regular monitoring of the FIM and Nulsa Flugga lines just north

and south of the Norröna transects. Each three-month season (DJF, MAM, JJA, SON) has at least 50 available stations except for DJF 2011, which has 44. Similar to the ADCP data, the hydrography is also slightly biased toward the summer and fall, when a greater number of sections are available. Hydrography over the IFR is more limited both spatially and temporally. Figure S2 shows the location of available temperature and salinity profiles, which are largely concentrated near the Faroe shelf and slope.
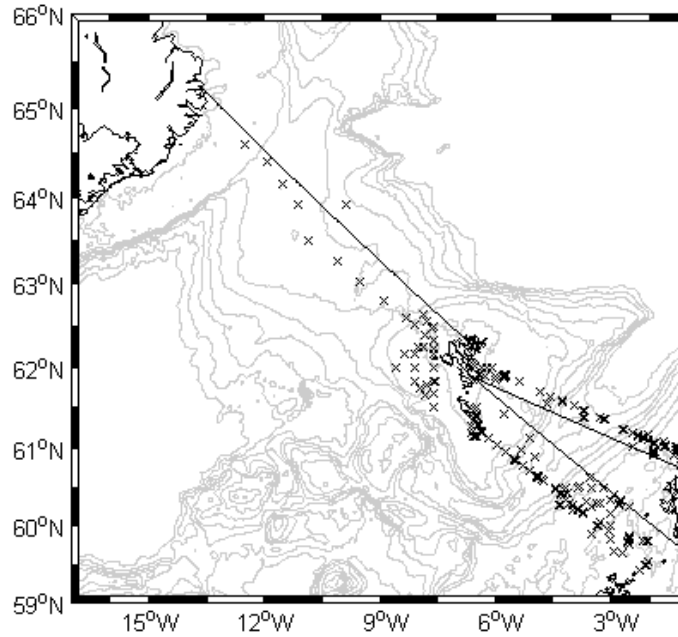
Figure 2.3: Collection location for all ICES hydrographic data used for the calculation of AW depth. Lines represent the mean path of each Norröna transect, x's are individual temperature and salinity observation locations, and contours show bathymetry for every 200 m from 100-1500 m depth.

Here we refer to waters with potential densities less than σ_t=27.8 as AW, which is consistent with previous studies by von Appen et al. (2014); Våge et al. (2013); Rossby and Flagg (2012). Complementary AW definitions in recent analyses of the region using the average depths of the 35.05 psu isohaline (Hansen et al., 2010) and 5^oC isotherm (Berx et al., 2013), fall within 60 m of the isopycnal determination across both FSC sections (Figures
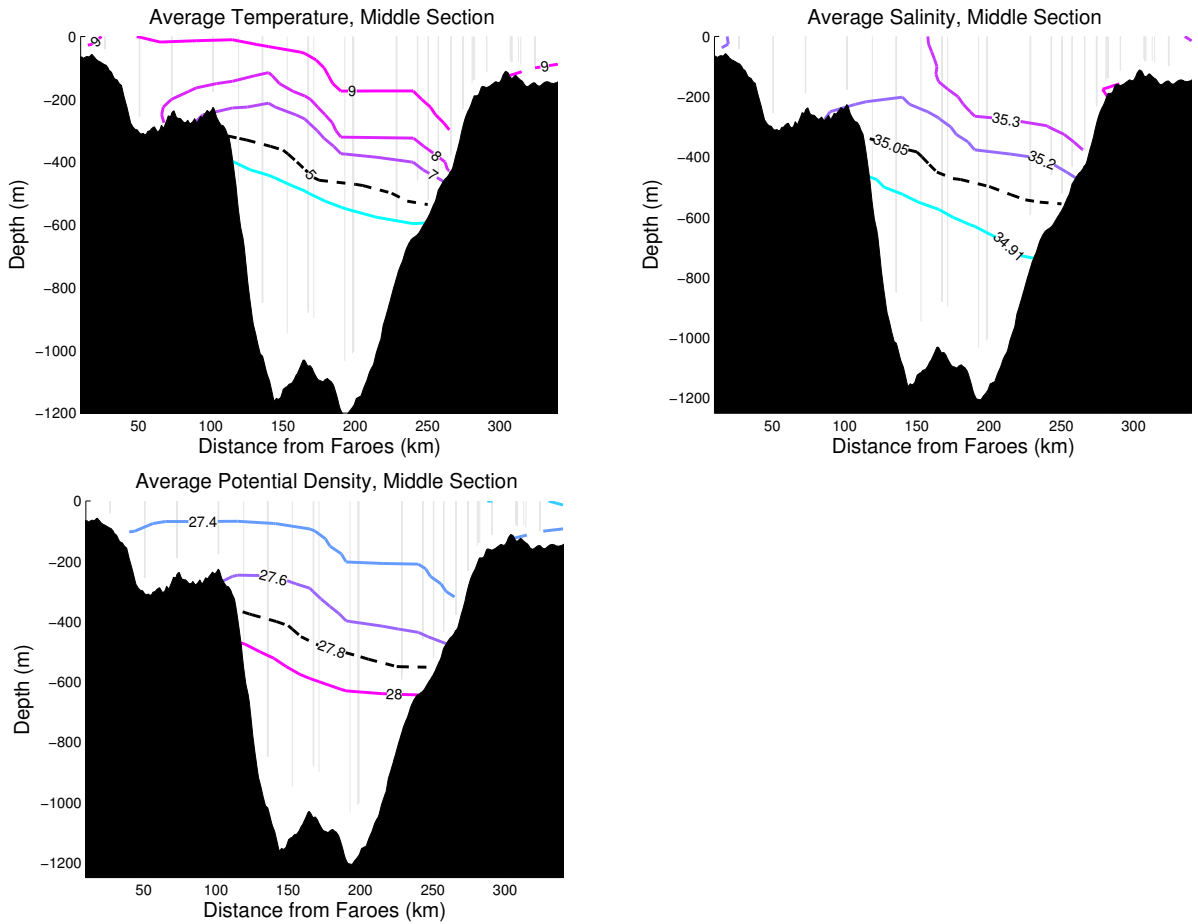
Figure 2.4: Mean temperature, salinity, and potential density from all available hydrographic data within 50 km of the FSC Middle Route. Observations were first averaged into 25 km lateral by 20 m vertical bins, and then averaged over time to produce contours. Grey lines show the observation locations used for the interpolation along each transect. Black dotted lines show AW depth references for each parameter.
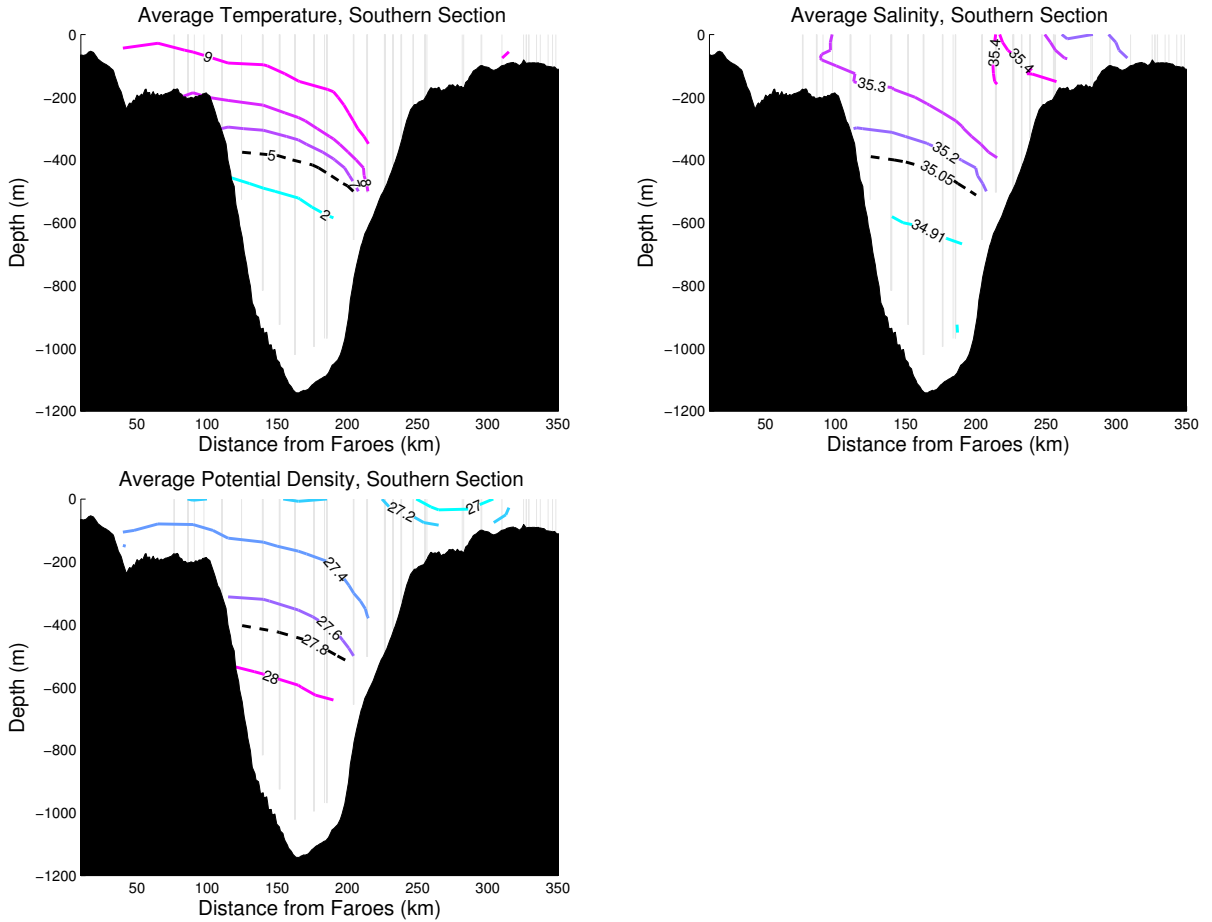
Figure 2.5: Mean temperature, salinity, and potential density from all available hydrographic data within 50 km of the FSC Southern Route. Observations were first averaged into 25 km lateral by 20 m vertical bins, and then averaged over time to produce contours. Grey lines show the observation locations used for the interpolation along each transect. Black dotted lines show AW depth references for each parameter.
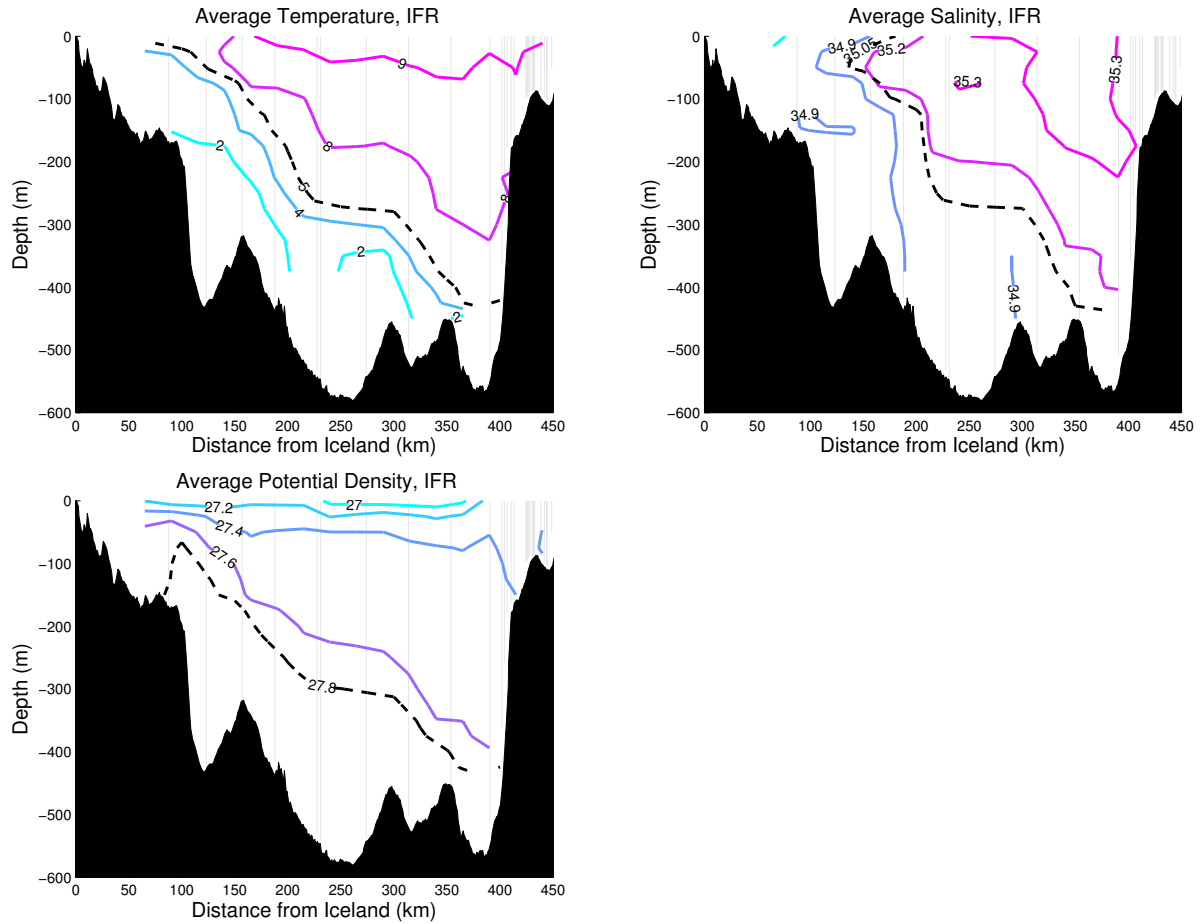
Figure 2.6: Mean temperature, salinity, and potential density from all available hydrographic data within 50 km of the IFR Route. Observations were first averaged into 25 km lateral by 20 m vertical bins, and then averaged over time to produce contours. Grey lines show the observation locations used for the interpolation along each transect. Variations in the bathymetry along the transect (as compared to the Norröna section) are due to the southerly position of the hydrographic observations, relative to the Norröna route.

2.4 - 2.6). Significant changes in seasonal stratification exist in this region (Larsen et al., 2008; Borenäs et al., 2001; Gaard and Hansen, 2000), however observations of the depth of the σ_t=27.8 isopycnal for each FSC transect vary seasonally by less than 100 m. Without concurrent hydrographic sections available during each transect crossing, we use the mean isopycnal depth over the nearly 4.5 year collection period as an indicator of the vertical extent of AW. This assumption introduces an estimated error of 0.02 Sv for the Southern route and 0.01 Sv for the Middle route, associated with a 100 m vertical difference in the lower limit of transport integration.

The methods of ADCP data collection utilized in this analysis are not conducive to traditional procedures of tidal characterization due to the lack of simultaneous observations or temporally frequent data at any given location. A method using least squares fitting to a distribution of interpolation knots (Dunn, 2002; Wang et al., 2004) is used to separate and characterize the tides appearing in the observations. With this method, the spatial dependence of the tidal velocity components in the upper 100 m of the water column are represented by Gaussian basis functions permitting estimation of the tides at the irregularly spaced observation locations [Wang et al., 2004]. The resulting tidal amplitudes compare favorably in amplitude and phase to a numerical model produced by the Earth and Space Research (ESR) Institute in collaboration with Oregon State University (Egbert and Erofeeva, 2002), and to published tidal ellipses from moored ADCP data on the Faroes shelf (Larsen et al., 2000).

The detided, bin-averaged velocity data set forms the basis for all subsequent analyses, including the computation of the across track volume flux or transport in Sverdrups (1 Sv=$10^6 m^3/s$) through each bin as

$$Q = A_{bin} \times u_{bin} \qquad (2.1)$$

where A_{bin} is the area of each bin and u_{bin} is the velocity normal to it. All available data falling within each geographical bin is used to compute the mean along and across track velocity for that particular bin. This method results in some bins having a greater number of samples when spatial coverage over a transect is incomplete. The total transports for each section are obtained by summing the bin transports along each transect over the depths associated with inflowing Atlantic Water (above the σ_t =27.8 isopycnal, Figures 2.7 and 2.8). Velocity uncertainties were calculated using the observed standard deviation in across section velocity to determine the total

single section uncertainty for each transect crossing. Velocity and transport uncertainties are the standard error of the mean, with the degrees of freedom equal to the number of transect crossings, assuming that the individual crossings separated by one to four days represent independent observations.

Steep and variable bathymetry, such as in this region, influence mesoscale flows by guiding them along isobaths and inducing nonlinear interactions. For the consideration of along topography flow, we use bathymetry for the region from NASA's ETOPO2 topographical dataset (U.S. Department of Commerce and Atmospheric Administration, 2006). The resolution is 2 minutes of both latitude and longitude (approximately 4 km and 2 km, respectively over the domain under study) and 1 m in the vertical (U.S. Department of Commerce and Atmospheric Administration, 2006). A range of frequently sampled velocity bins were selected for comparison to the direction of nearby $f/$H contours, computed using the ETOPO2 bathymetry. Although not without temporal gaps, the time series of velocity vector orientation at nearby locations serves as an indicator for topographic steering strength.

2.3 Results

Results from the FSC will be discussed first, followed by the IFR. The FSC analysis will be broken into an examination of the Shetland Slope Current structure and variability, followed by a consideration of the southward flow on the Faroese slope.

2.3.1 Flow through the Faroe Shetland Channel

Inflow through the FSC is dominated by the Shetland Slope Current flowing along the steepest portion of the Scottish slope, and a southward outflow along the Faroese slope. In late 2010 a shift in data collection occurred from more frequent use of the Southern Route to a favored use of the Middle Route. From 2008 - 2012, 132 crossings (88 via the Middle route and 44 using the Southern) have contributed to the overall coverage of the FSC, and in general the velocity structure is similar for both routes. The best data returns occur near the surface, with the number of samples dropping roughly in half below 500 m and halved again below 600 m for both tracks. Standard errors in the channel range from 1 - 5.7 cm/s per bin, and integrated transect uncertainties of the surface inflow (σ_t<27.8) are 0.17 Sv for the Middle route

and 0.23 Sv for the Southern. Velocity uncertainties were calculated using the observed standard deviation in across section velocity to determine the total single section uncertainty for each transect crossing.

The mean inflow through the FSC east of 200 km from the Faroes and above the σ_t=27.8 isopycnal is 3.4±0.17 Sv (Middle section) and 4.0±0.23 Sv (Southern section) primarily attributable to the Shetland Slope Current (surface inflows east of 200 km from the Faroes). The Slope Current dominates the eastern shelf region along both transects with the middle track showing a slightly weaker core (Figures 2.7 and 2.8). Interannual variations in the Shetland Slope Current transport across both FSC sections range from 3.1 Sv at its weakest in 2009 to 3.7 Sv at its strongest in 2011. The vertical structure of the upper water column of both FSC routes is largely depth-independent. Cross-transect transports are negligible in the upper 100 m and gradually increase with increasing integration depth (Figures 2.7 and 2.8).

Velocities within the SSC are largely depth independent, with vertical shears in the northeastward velocities over the top 400 m of the SSC less than 0.001 sec^{-1} for each route. This is consistent with the description of barotropic, geostrophic flow along isobaths. These conditions are modified in the ocean by the presence of stratification, viscosity, and nonlinear effects (Lagerloef, 1983). The local Rossby and Burger numbers illustrate the relative influence of topographic steering and stratification. The Rossby number, defined as

$$Ro = \frac{U}{\Omega L} \qquad (2.2)$$

where, U is the mean flow, Ω is the rotation rate of the Earth, and L is the characteristic length scale of the velocity, in this case the width of the SSC, must be small for geostrophic flows (Lagerloef, 1983). This is case for the core of the SSC where the Rossby number is 0.06, consistent with topographically steered, geostrophic flow. The internal Froude number,

$$Fr = \frac{U}{NH} \qquad (2.3)$$

where N is the Brunt Vaisala frequency and H is the water column height, is an indication of the inertial forces versus stratification. A small Froude number indicates that the flow will tend to follow isobaths. Here Fr ∼0.15 on the Southern track and ∼0.15 $for the Middle track. The ratio of the two, the Burger Number,$

Figure 2.7: Mean ~NE velocities normal to the FSC middle track (top) and cumulative across track transport (bottom). The black solid line includes all available data over the full AW depth from March 2008 - June 2012, a total of 88 sections.

$$B = \left(\frac{Ro}{Fr}\right)^2 = \left(\frac{NH}{fL}\right)^2 \tag{2.4}$$

illustrates the relative contributions of each regime. Within the SSC the Burger number is less than 0.16 for the Southern track and less than 0.27 for the Middle route, indicative of the predominant impact of the bathymetry in guiding the current. This is in contrast to the central FSC, where stratification is more pronounced and the Burger number values are larger for all seasons.

The alteration in preferential route from more frequent usage of the southern to middle transect introduced a puzzling discrepancy in transport estimates (Figure 2.9). The Norröna sampled the Southern section heavily from

27

Figure 2.8: Mean ~NE velocities normal to the FSC southern track (top) and cumulative across track transport (bottom). The black solid line includes all available data over the full AW depth from March 2008 - June 2012, a total of 44 sections.

March 2008 through August 2010 (87% of the total Southern transects) and the Middle track from June 2010 through June 2012 (71% of the total Middle transects). Despite a closed channel between the two sections the observed magnitude of the average northeast transport was higher through the middle route. However, when considering only the few early sections from the middle track, the mean transport estimate agrees relatively well with the southern track data, to within 0.8 Sv, over approximately the same time period. Only after the inclusion of the last year and a half of data does the total transport increase by almost a full Sv to 1.7 Sv through the middle section, suggesting a temporal change in flow through the channel as the source for the transect differences. During periods of roughly coincident coverage, such as during the summer of 2010 as well as isolated crossings in 2009, 2011, and 2012 (Figure 1.4), when the ship sampled along both routes over a short

time span (less than two weeks), the structure and net transport agrees well across both sections, despite the influence of local eddy activity in the channel. Using the likeness of temporally similar crossings of each track as an indicator for consistency in the FSC, it is reasonable to combine the full set of FSC observations for the analysis of interannual fluctuations.
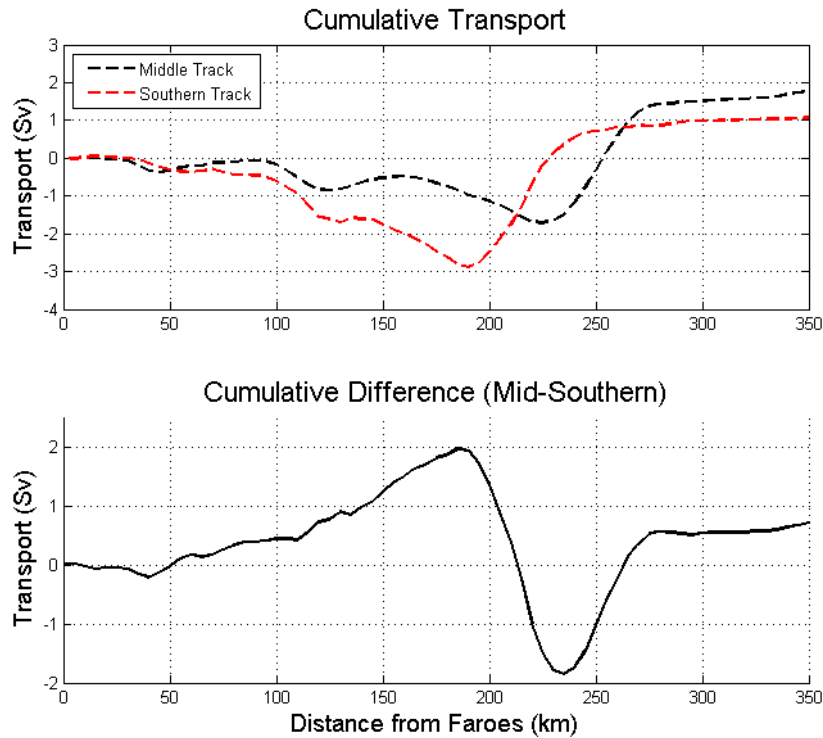
Figure 2.9: Cumulative transport for each track (upper) and their cumulative difference (Middle - Southern track) with distance along the FSC.

The combined time series for the FSC has a lower standard error (0.19 Sv) and improves the temporal and spatial coverage of the surface outflow on the Faroese Shelf and Slope. Opposite the Shetland Slope current a $\sim$30 km band of southerly flow along the Faroese slope comprises most of the surface outflows, which account for -1.0 Sv on average of transport towards the Atlantic above the σ_t=27.8 isopycnal (Table 1). The largely depth independent outflow shows an interannual variability of up to half of its average magnitude. It peaks from 2008 - 2010, weakens considerably in 2011, and

partially rebounds in 2012.

Temperature and salinity profiles show a clear distinction between the warmer and saltier inflow waters of the SSC and the relatively cooler and fresher surface outflows over the Faroese Shelf and Slope (Figures 2.4 - 2.5). The high salinity wedge associated with the SSC extends much farther westward than the core of observed inflow velocities. This may be due to recirculating waters, which originate north of the Faroe Plateau and mix with NAW south of the Norröna's southern route, after traversing southward along the western edge of the FSC. This is particularly likely for the surface outflows over the Faroese Slope, which unlike those on the Shelf, are unlikely to be forced by tidal rectification around the plateau (Larsen et al., 2008).

2.3.2 Flow across the Iceland Faroes Ridge

Largely depth independent inflows appear over the southeastern half of the IFR section with outflows confined to the Iceland side (Figure 2.10). Outflow transports are bottom intensified, with almost no measurable outflowing volume flux within the upper 100 m of the western IFR. To the east, inflow transport gradually increases with integration depth. Sampling over the IFR is least reliable on the western side of the section (eastern slope of Iceland), but most of the top 300 m has been observed on more than 25 separate occasions. Means over the IFR are the composite of 54 individual transect crossings and resulting standard errors range from 0.7 - 5.8 cm/s per bin. Highest error values exist on the Icelandic shelf, where observations are limited, and the Faroese shelf where the velocities are more variable. The resultant integrated transport error over all the full depth range of the IFR section is 0.46 Sv.

High short term variability and eddy activity over the ridge region introduce fluctuations over a large range of timescales, thus the similarity in the average annual northeast velocity profiles for the years 2010 through 2012 is striking (Figure 2.11). Annual means are heavily weighted toward the summer months when data collection is most successful, introducing additional uncertainty to the annual averages. However, little seasonal variation in transport has been observed over the IFR by others (Hansen et al., 2008), despite the observation of increased crossings of the IFR by drifters in the summer by Valdimarsson and Malmberg (1999).

Annual averages from years 2010 through 2012 are comprised of at least 10 transect crossings each and have strong similarities in structure. Namely,
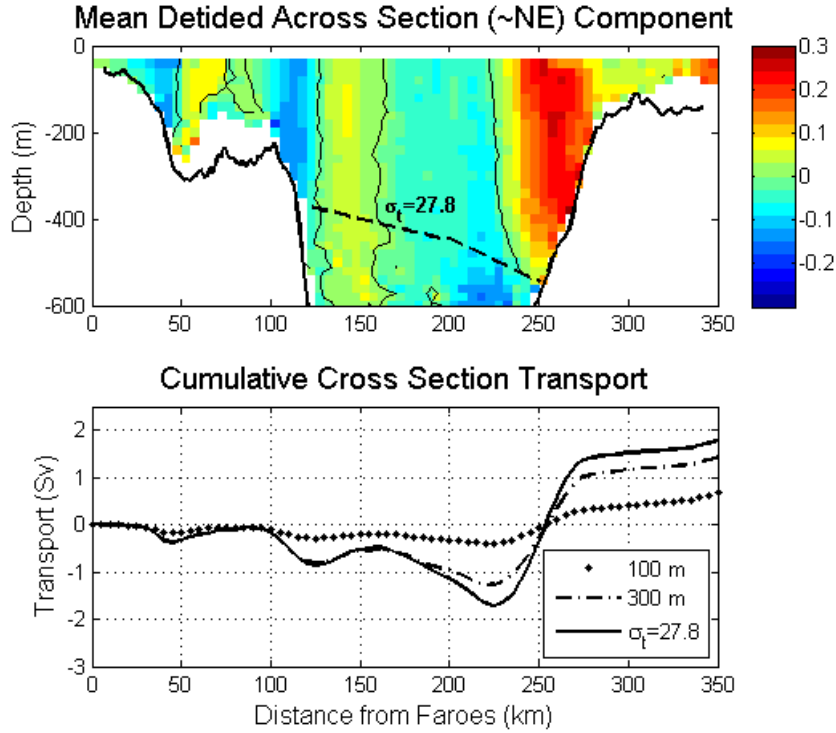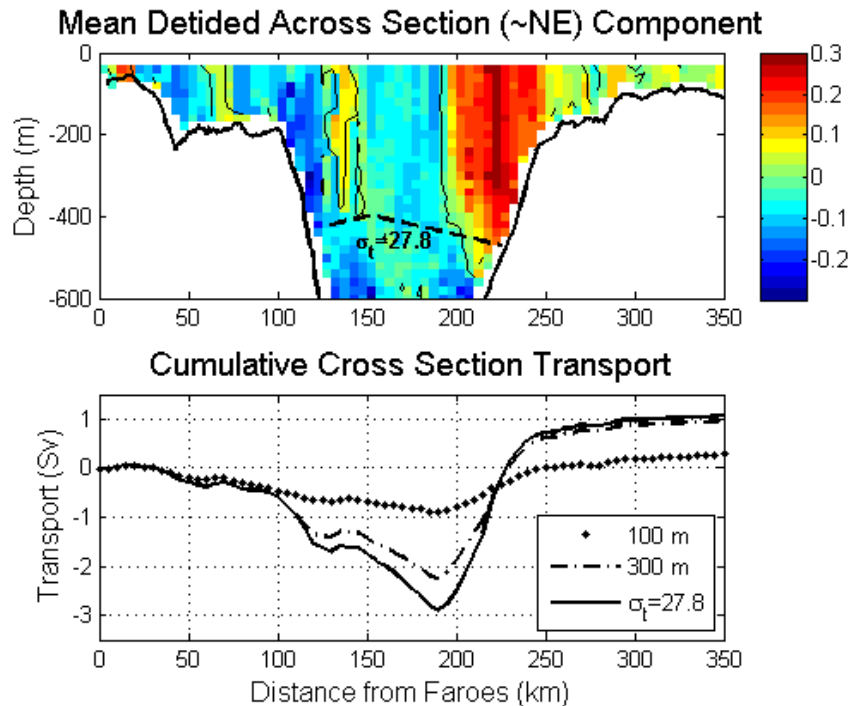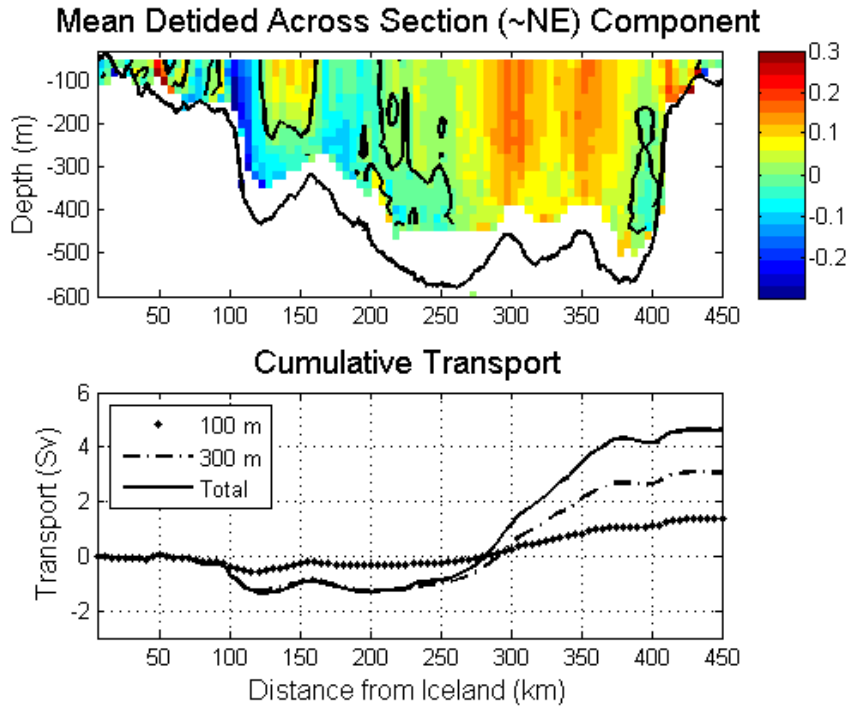
Figure 2.10: Mean ∼NE velocities normal to the IFR track (top) and cumulative across track transport (bottom). The black solid line includes all available data from March 2008 - June 2012, a total of 54 transects.

a strong inflow appears over the eastern half of the channel and other than a narrow band of inflow from 100 - 150 km east of Iceland, limited northeasterly flow exists over the western half of the channel. The lateral position of the zero velocity contour in the central channel and the depth of the inflow to the Nordic Seas on the Iceland side vary interannually. Since the magnitude of the inflow shows little temporal variation, the average annual width of the inflow is logically related to the northeast transport for that year. Wider inflows such as in 2010 and 2012, carry on the order of 9 Sv of Atlantic Water over the ridge, while in 2011, when the inflow narrows to ∼150 km, the volume flux drops to around 5 Sv. The average flow over the IFR from March 2008 - June 2012, incorporating the outflows on the Icelandic side, is 4.6±0.46 Sv, split into 5.9 Sv of inflow and 1.3 Sv of outflow (Table 1).

31
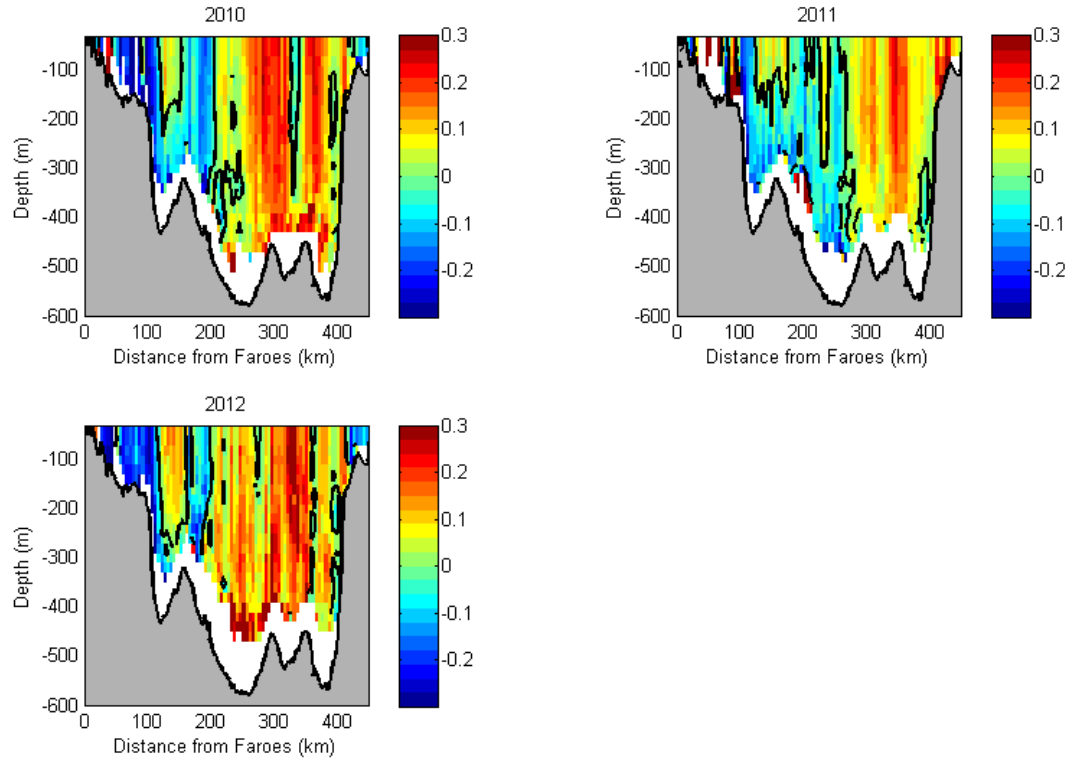
Figure 2.11: Mean northeast velocities over the IFR by year from 2010 - 2012.

2.4 Discussion

Both the FSC and IFR are subject to fluctuations over a wide range of timescales, and understanding the locations and magnitude of the variations in velocity and hydrographic properties are a critical step in monitoring the AW flux into the Nordic Seas. Mesoscale processes can significantly alter the position of inflows, as evidenced by the ADCP velocities and more recently by XBT deployments taken monthly across each section (Figure 2.12). These profiles show that even the strong Shetland Slope Current and inflows over the western Faroese Slope change both position and depth over a one month period. However, constraining this movement and visibly adjusting the flow (for instance the location of the cold overflow in the IFR sections) is the

strong influence of topography. We consider here the temporal and spatial characteristics of the FSC and IFR separately, as well as their relation to previous observations of the ridge system.

2.4.1 Temporal and Spatial Characteristics of the FSC

Temporal variations in the week-to-week sections are large, but 3-6 month averages quickly recover the familiar mean structure of the FSC circulation. This is illustrated in Figure 2.13, which is a composite of each section crossing of either FSC transect with greater than 80% spatial coverage over the upper 200 m (gray dots) and a 6 month running mean of all sections. Velocity structure and magnitude through the FSC are similar to previously reported values and are augmented by coverage of the Faroese shelf shallower than the 300 m isobath, often excluded from prior estimates. The discrepancy between total AW transports cited here and previous estimates are likely the result of the varying spatial coverage of observations. Using the location of the westernmost moored ADCP along the FIM line as the starting point for cross channel transport integration, as in most previous studies (Sherwin et al., 2008; Hughes et al., 2006), we find a net transport of 2.2±0.19 Sv toward the Nordic Seas, comparable to the 2.7 Sv observed by (Berx et al., 2013) and lower than the 3.5 Sv and 3.9 Sv reported by Sherwin et al. (2008) and Hughes et al. (2006), respectively. Since each estimate incorporates many years of ADCP, hydrographic, and in the case of Berx et al. (2013) altimetric, observations we expect that time variability is not the source of the discrepancy. Instead it may be attributable to finescale structure over the central channel that can be resolved more accurately with the vessel mounted ADCP, or related to the varying definitions used to determine the bottom boundary of Atlantic Water depth, which were defined using a 3-point mixing model (Hughes et al., 2006) and 500 m depth (Sherwin et al., 2008). Older estimates by Tait (1957) and Dooley and Meincke (1981) which relied on geostrophic calculation over an upper layer, defined as above 550 m and with salinity less than 35 psu, are 2.3 Sv and 2.0 Sv, respectively, closer to the average transports across the Norröna sections. Additional a discrepancy may be attributable to an incomplete capturing of the full seasonal cycle by the Norrna data. A lack of winter data prevents an accurate estimation of the annual cycle, however, based on three seasons of observations we find a seasonal cycle of 0.8 Sv with a maximum in February. This is not inconsistent with recent findings by (Berx et al., 2013) of seasonal fluctuations of 0.7 Sv
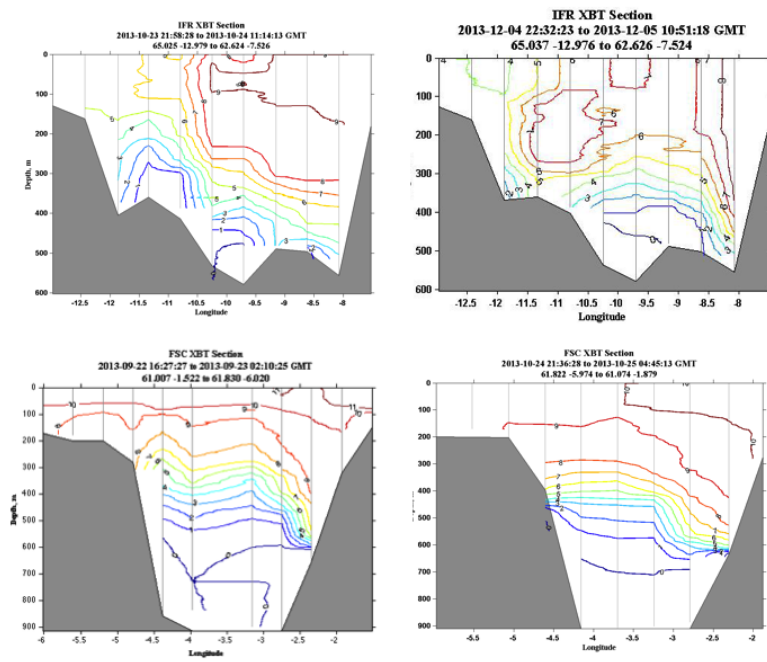
Figure 2.12: XBT sections taken over the IFR in October (top left) and November (top right) and across the FSC in September (bottom left) and October (bottom right). Temperature contours are in degrees Celsius and inconsistencies in the topography are due to slight variations in the ship's track with each crossing.

with a winter maximum.
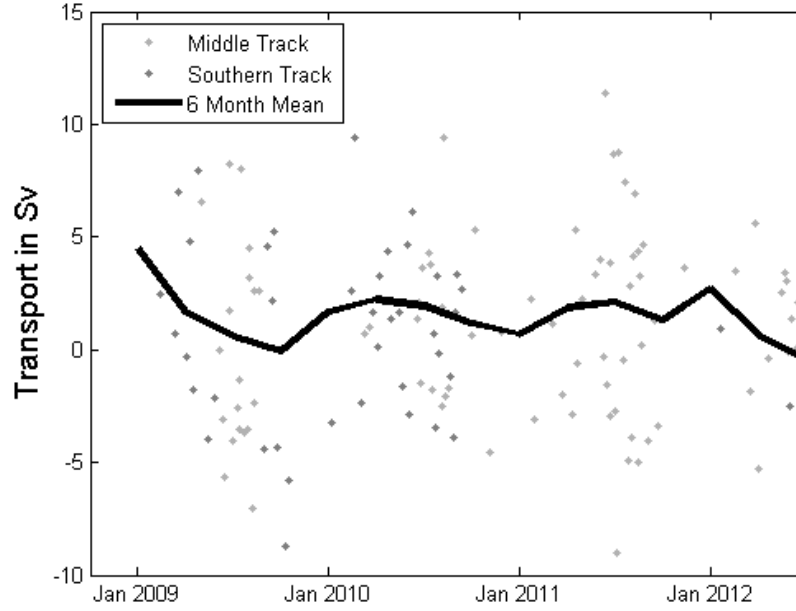
Figure 2.13: Time series of FSC section averages (gray dots) and 6 month running mean. Spatial gaps in data collection were filled using a linear interpolation, which increases the average uncertainty. The standard error from the mean for all available FSC sections (including both the Middle and Southern routes) is 0.35 Sv.

Using the 300 m isobath as the western integration boundary, previous literature for this region have failed to capture the persistent, depth-independent southward flow on the Faroese Shelf. This appears over the middle track from approximately 125 - 245 km from the Faroes and in the southern track from 125 - 175 km from the Faroes with a magnitude ranging from -0.4 to - 1.9 Sv annually. Temporal variations in the outflow transport exist, with the current appearing in 67% of middle track transect crossings and 74% of southern transect measurements. Of the remaining periods of data collection, a widening of northeastward flows in the central channel partially or fully mask the outflow. Hydrographic factors may be largely ruled out as the source of discrepancy between the two FSC tracks, since

the σ_t=27.8 isoline remains at a similar depth between the FSC transects, and large stationary eddies such as those described by Chafik (2012) are too large to account for changes over such a short distance. This leaves temporal variations in this southerly flow over the Faroese Shelf as the most likely cause of the difference in transport through the FSC sections. The magnitude of interannual transport variations in the southward outflow are larger than those in the Shetland Slope Current and may significantly affect observations of total transport across the Iceland Faroes Shetland ridge.

Present throughout this analysis are the implications of topography and the steering of flows by the bathymetry. This is evident in the tendency of the Shetland Slope Current to hug the eastern slope of the FSC over the region of steepest topography and the increased variability over the deeper and more stratified central channel. This can be quantitatively expressed by correlating a time series of velocities to nearby f/H contours. The tight relationship between topography and the largely depth independent flows over the shelves and slopes of both sections is not surprising. Following this line of reasoning, and noting the similarity in tidal excursion and characteristic current length scale, tidal rectification is expected (Zimmerman, 1978, 1981; Robinson, 1981) and in fact has been observed by Larsen et al. (2008) following the shelf bathymetry around the Faroes in water shallower than 200 m. It is possible that the strong southward flow we observe farther east, along the outer edges of the Faroese shelf may be related to a similar process, but it is more likely that the deeper and more eastern slope flows are tied to inflows over the IFR that may circulate east then south into the FSC before bending northward and joining the Shetland Slope Current. The precise behavior and magnitude of recirculating flow should become more evident with increased coverage by the XBT program and the ability to separate recent Atlantic Water inflows from those exposed to mixing with water from the Nordic Seas.

2.4.2 Temporal and Spatial Characteristics of the IFR

Similar to the FSC, the weekly and monthly variations in IFR section transport are large (Figure 2.14), but despite large short term fluctuations, the spatial characteristics of the northeastward current over the IFR are consistent for most years. This is especially true for the latter years of observation (2010-2012) when there was an increase in IFR data coverage, both spatially and temporally. The lateral width of the inflowing velocities over the east-

36

ern half of the section vary by up to 50 km and may be associated with the strength of the inflow, with the inflow expanding westward during years when the magnitude of the northeast velocity is greatest. The presence of a small, surface intensified inflow over the upward slope of the seamount 100 km east of Iceland, Figure 2.10, is suggestive of the influence of flows along the IFF and its tendency to meander along the Norröna's IFR transect.
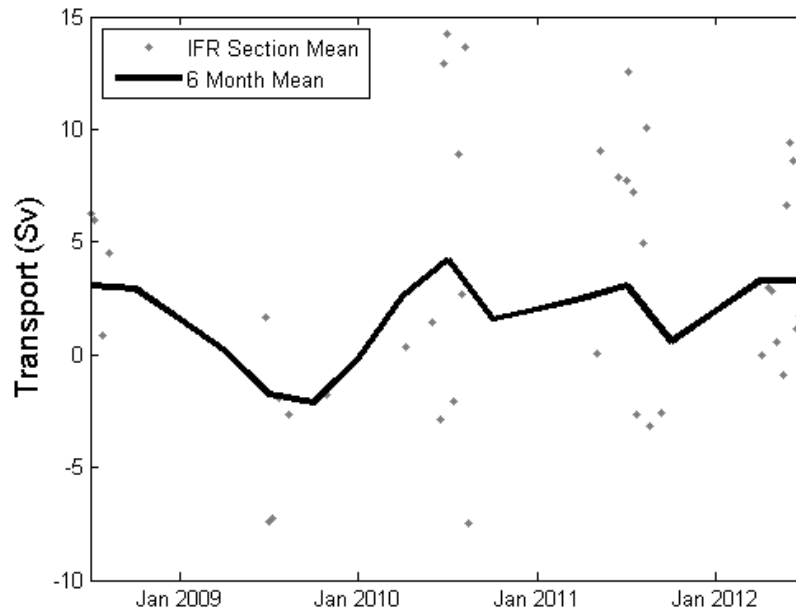
Figure 2.14: Time series of IFR section averages (gray dots) and 6 month running mean. Spatial gaps in data collection were filled using a linear interpolation, increasing the average uncertainty. The standard error from the mean for all available IFR sections is 0.80 Sv.

The observed large fluxes of Atlantic Water across the IFR are worth noting here. These estimates may even be under-represenative of the full inflow. Summing the average transport through the bottom-most bin and extending these values to the seafloor over the eastern (inflowing) half of the section increases the mean flow across the IFR by 0.9 Sv. The inclusion of surface outflows on the western edge of this section in to the average surface transport may also cause the average IFR inflow to be an underes-

Table 2.1: Average transport above σ_t=27.8 across each transect in Sv.

	Net	North(east)	South(west)
FSC Middle	1.7±0.2	3.4	-1.7
FSC Southern	1.1±0.2	4.0	-2.9
IFR	4.6±0.5	5.9	-1.3

timation of the total AW flux, since western outflows are not AW, but are instead related to the East Icelandic Current (Malmberg and Kristmannsson, 1992). The 5.9 Sv mean inflow value appears high compared to the 3.5±0.5 Sv reported by Hansen et al. (2003, 2010), using line N observations of temperature, salinity, and moored velocity profiles along a section extending directly north of the Faroes. Those papers defined the mean depth of the 35.05 isohaline as the southern most boundary for inflowing AW. Historical hydrographic data available from ICES over a similar temporal and spatial section, shows salinity values close to or slightly below 35 psu over the deeper and western edges of the observed IFR inflow. We consider here that as the Atlantic Water crosses the IFR it is prone to mixing with cooler and fresher Nordic Sea waters. This mixing may change the hydrographic character of the flow considerably, reducing its salinity to below 35.05 psu and resulting in an apparent "disappearance" of Atlantic Water between the Norröna's IFR transect and the observations along line N. This is particularly true for the deeper waters at depths greater than 500 m, and during periods when the width of the inflow has extended westward, potentially entraining some of the less saline water on the Icelandic side and resulting in a loss of the characteristic high salinity of NAW. A detailed analysis of the effect of mixing on the hydrography of the IFF and IFR region can be found in Beaird (2013) and is beyond the scope of this analysis, but significant differences in the inflows reported here as compared to those found in Hansen et al. (2003, 2010) may be attributable to differing definitions of the lower bounds of IFR inflows. In addition, contributions from seasonal effects not resolved by the Norröna observations over the IFR may exist.

2.5   Summary

Repeated observations along standard sections in the IFR and FSC offer an accurate estimate of volume flux into the Nordic Seas. In total, approxi-

mately 6.1 ±0.31 Sv of directly observed surface transport crosses the Iceland Faroes Scotland Ridge, with 4.6 Sv entering over the full depth of the IFR and 1.5 Sv above the σ_t=27.8 isopycnal, through the FSC. This shows an overall increase from earlier observations of the FSC by this program due to a weakening of along isobath southward flows on the western slope of the FSC, and emphasizes the importance of long term observations in this region. A difference in the average transport through the two FSC sections also highlights the temporal variability and spatial consistency of current structure through the channel. Similarly, when averaged over periods long enough to remove short term eddy processes, flows over the IFR maintain their basic structure over all years of data collection with variations in northeast transport related to the width of inflow.

As expected, the surface flows are tightly coupled to the bathymetry of each section, especially over the steep slopes and shallow shelves. The ability of the topography to influence the relatively fine scale structure of the currents in this region is particularly evident in this method of data collection, which is of higher spatial resolution than satellite or moored current meter observations of the region. The addition of an XBT program earlier this year will improve estimates of heat flux across the ridge and offer a clearer image of the water mass structure and variability.

Chapter 3

Observed Pathways of Atlantic Water from 59.5^{O}N to the Iceland Faroes Shetland Ridge

Abstract

Direct measurements are used here to infer the mean pathways and volume fluxes of Atlantic Water east of the Reykjanes Ridge (RR) from 59.5^{o}N to their transit across the Iceland-Faroes-Shetland Ridge. The topography of the Hatton and Rockall Banks south of the Faroe Plateau splits the northward flowing water into more than 12 Sv, which cross the Iceland Basin toward the Iceland Faroes Ridge (IFR), and approximately 4 Sv headed through the shallow regions on the Scotland side. Upon reaching the IFR, $\sim$5 Sv of AW crosses into the Nordic Seas, while the rest of the western waters confined to the Iceland Basin recirculate west then southward along the RR. The waters in the shallow eastern region almost all cross the ridge either as part of the well defined Shetland Slope Current or as a topographically steered flow, which follows the topography anticyclonically around the Faroe Plateau.

3.1 Introduction

With the advent of new and repeated observations of the North Atlantic system, a more robust description is emerging of the structure and variability of Atlantic Water (AW) entering the Nordic Seas. The North Atlantic Current bifurcates at the southeastern end of the Reykjanes Ridge (RR), flowing poleward on either side, traversing the Irminger Sea and Iceland Basin before crossing the Greenland-Iceland-Faroes Ridge (Orvik and Niiler, 2002). Flows to the west of the RR are ultimately bound for the Labrador Sea, where they contribute to the intermediate depth Labrador Sea water. East of the RR, the poleward flows continue toward the Nordic Seas either over the IFR or via the Shetland Slope Current along the Scottish coast, later contributing to the Norwegian Atlantic Current (Orvik and Niiler, 2002). By combining the high resolution (5 km), repeated observations from two commercial vessels in regular traffic, we offer a more detailed representation of the major pathways of Atlantic Water between 59.5ºN and the Nordic Seas.

The M/F Norröna, a high-speed ferry operated by Smyril Lines, that makes weekly crossings from Iceland to the Shetlands via the Faroe Islands, operates a hull-mounted 75 kHz ADCP that can reach to about 500-600 m depth. This operation has been underway since March 2008. A complete description of the data collection, methods, and early results can be found in Rossby and Flagg (2012). The other vessel, the Royal Arctic Lines M/V Nuka Arctica operates on a three week schedule between Greenland and Scotland with occasional stops in Iceland. The data used here come from a hull-mounted 150 kHz ADCP. Velocity data were collected by the Nuka Arctica between 1999-2002 using methods summarized in Knutsen et al. (2005) and Chafik et al. (2014).

The Nuka Arctica data can be organized into three groups: a constant latitude (C) route, a great circle (G) route, and a diagonal (D) route to Iceland (Figure 3.1). Chafik et al. (2014) use the Nuka Arctica C route ADCP data and satellite altimetry to describe the spatial and temporal characteristics of poleward flows between Greenland and Scotland over the top 400 m. Of particular note is the strong role of the RR in separating topographically bound flows toward the Nordic and Labrador Seas. The variable bathymetry of the region organizes the velocities over these sections into a series of northward flowing currents parallel to the RR, especially on its western side.

We focus here on the 8.0±1.6 Sv flow east of the RR (Chafik et al., 2014), as the most likely source for transport across the Iceland-Faroes-Shetland
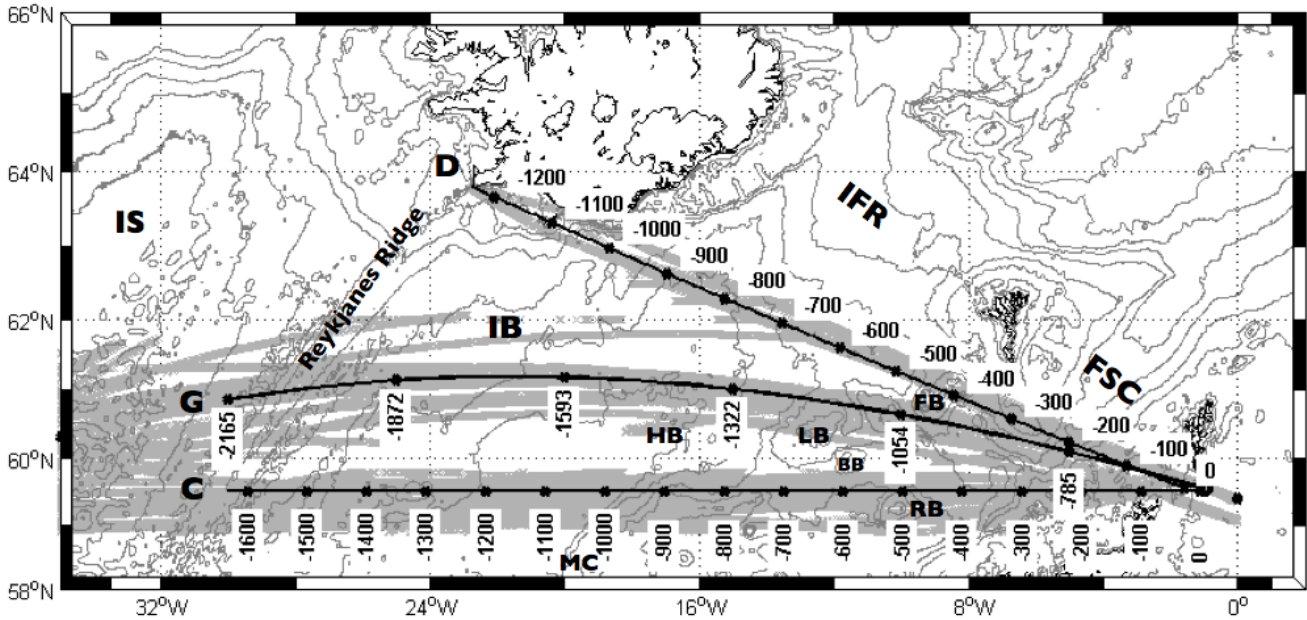
Figure 3.1: Map of Nuka Arctica crossings (gray) and mean location of the constant latitude (C), great circle (G), and diagonal (D) tracks. Additional abbreviations are the Iceland Faroe Ridge (IFR), Faroe Scotland Channel (FSC), Lousy Bank (LB), Rockall Bank (RB), Maury Channel (MC), Hatton Bank (HB), Bligh Bank (BB), Faroe Bank (FB), Irminger Sea (IS), and Iceland Basin (IB). Distances are measured from the location where the three transects cross near Scotland.

Ridge. The total transport across the C and G routes can be decomposed into three primary flows, from west to east, they are a 4.5 Sv flow over the

Maury Channel, a 1.2 Sv flow just east of Bligh Bank, and 1.7 Sv flow along the Scottish slope (Chafik et al., 2014). The authors propose that these two latter currents cross the ridge between Iceland and Scotland, reaching the Nordic Seas, along with most of the westernmost, Maury Channel flow. The remaining Maury Channel transport turns south, following the RR.

Expanding upon the findings of Chafik et al. (2014) we include the Nuka Arctica data along its diagonal (D) route, to the north and east of the C and G transects, and use this section as a way of linking the structure and temporal variability of the southern sections to the observations of cross ridge flow along the Norröna line between Iceland and the Shetlands. We will first describe the data and methods in Section 3.2 followed by a consideration of the Atlantic Water mass and its depth boundaries. We then describe the spatial structure of the currents and their transport across the Nuka Arctica diagonal track in Section 3.3. Our discussion in Section 3.4, is split into descriptions of the eastern and western portions of the transect delineated by the shallow ridge and bank system extending south and west of the Faroe Plateau. This leads to a direct comparison between each section and its counterpart from the Norröna observational program. Finally, we present a brief summary of our findings in Section 3.5

3.2   Data and Methods

Data for this study relies on ADCP velocities obtained by two ships of opportunity in the North Atlantic: the M/F Norröna, a ferry operated by Smyril Lines between Iceland and Denmark, and the M/V Nuka Arctica, a Royal Arctic Line vessel following several routes between Greenland, Iceland, and Denmark. Full descriptions of data collection and processing can be found in Chafik et al. (2014); Knutsen et al. (2005) and Rossby and Flagg (2012). Here the 3 second ping ensembles are averaged into 5 km lateral by 8 m depth bins for the Nuka Arctica sections and 5 km lateral by 20 m depth bins along the two Norröna transects. Average density along each transect is calculated using CTD temperature and salinity profiles obtained from the ICES database. For the estimation of full AW transport, the average density deeper than 200 m is used to determine the mean vertical shear in the across transect velocities through the thermal wind equations,

$$-f\frac{\partial v}{\partial z} = \frac{g}{\rho}\frac{\partial \rho}{\partial x} \tag{3.1}$$

$$f\frac{\partial u}{\partial z} = \frac{g}{\rho}\frac{\partial \rho}{\partial y} \tag{3.2}$$

where u and v are the zonal and meridional velocities, z is depth, f is the Coriolis frequency, and ρ is the density. The average shears are integrated from the across transect velocities at 400 m to the full AW depth.

3.3   Results

3.3.1   Definition of Atlantic Water

A detailed description of the major water masses and hydrographic structure along and south of the Greenland-Iceland-Scotland Ridge can be found in Hansen et al. (2008); Sarafanov et al. (2012, 2007) and Yashayaev et al. (2008). Here we are primarily concerned with the pathways and fate of Atlantic Water (AW), which crosses the ridge system between Iceland and Scotland and ultimately cools to form Intermediate and Deep Water in the Arctic Mediterranean. Along its northward journey this water mass is subject to mixinsg with intermediate and surface waters from the cooler and fresher Nordic and Labrador Seas, modifying its hydrographic properties. As such, it is often difficult to characterize and isolate AW along its full passage across the ridge. We use the σ_t=27.8 isopycnal as a definition for the bottom boundary of AW, when it is available, which has been shown to be a robust demarcation between inflowing Atlantic surface currents and outflowing deep and intermediate waters (von Appen et al., 2014; Våge et al., 2013; Rossby and Flagg, 2012). The mean depth of all available ICES hydrographic observations of this isopleth fall between 400 and 600 m near the Faroes, sloping up toward the shallow bank at approximately 300 km from Scotland. In the Iceland Basin the σ_t=27.8 is considerably deeper approaching 1500 m over the western end of the Nuka Arctica's diagonal track. To the south, along the C and G routes AW is observed at depths of up to 2000 m, consistent with the AW depth observed by Sarafanov et al. (2007) in the Iceland Basin at the same latitude.

3.3.2 Current Structure and Transport

At the southeastern end of the region traversed by the Nuka Arctica, the topography divides the circulation between a shallow shelf and bank region to the east and the deep Iceland Basin to the west. The severity of this separation increases to the north eventually guiding AW flows either to the east or west of the Faroe Plateau. The transports across each transect both along the Nuka Arctica and Norröna lines are defined here as the volume flux in Sverdrups (1 Sv=$10^6 m^3/s$) normal to the transect and can be represented as

$$Q = A_{bin} \times u_{bin}, \tag{3.3}$$

where A_{bin} is the area of each bin and u_{bin} is the velocity normal to it. The bins are integrated to the maximum depth of accurate data collection (400 m in the case of the Nuka Arctica and 500-600 m for the Norröna) to obtain the total transport across each transect and further extrapolated to the depth of the σ_t=27.8 isopycnal as a proxy for the full AW transport.

The transport estimates are most robust on the eastern end, where the degrees of freedom are greater than 60, due to the overlapping of several Nuka Arctica routes. This confidence decreases towards the western end, with only 10 transect crossings reaching Iceland. The net transports are subject to a heading drift for distances greater than 100 km, introducing an uncertainty of up to 0.01 m/s (see Appendix A in Chafik et al. (2014) for more details). Integrating this instrumental uncertainty over the upper 400 m and across the full distance of each section introduces an error of 0.88 Sv, 1.58 Sv, and 1.46 Sv for the C, G, and D routes, respectively. Integrating the standard error of the mean for each route, with a single crossing counted as one degree of freedom, results in an additional 0.76 Sv, 1.18 Sv, and 1.19 Sv error for each section. Together the cumulative uncertainties are 15%, 16%, and 35% of the total mean transport for each route. The infrequent crossing of the D route, increases its uncertainty relative to the other sections.

Beginning at the intersection point of the three routes near Scotland and moving westward to Iceland, several circulation features are discernible across all three Nuka Arctica tracks. A depth independent northward flux leaning against the steep Shetland slope crosses the C route at approximately 300 km west of Scotland (Figure 3.2) and at -300 km along the G route (Figure 3.3). Downstream at the D route, this develops into the surface intensified ∼3 Sv Shetland Slope Current (Figure 3.4), which continues through the
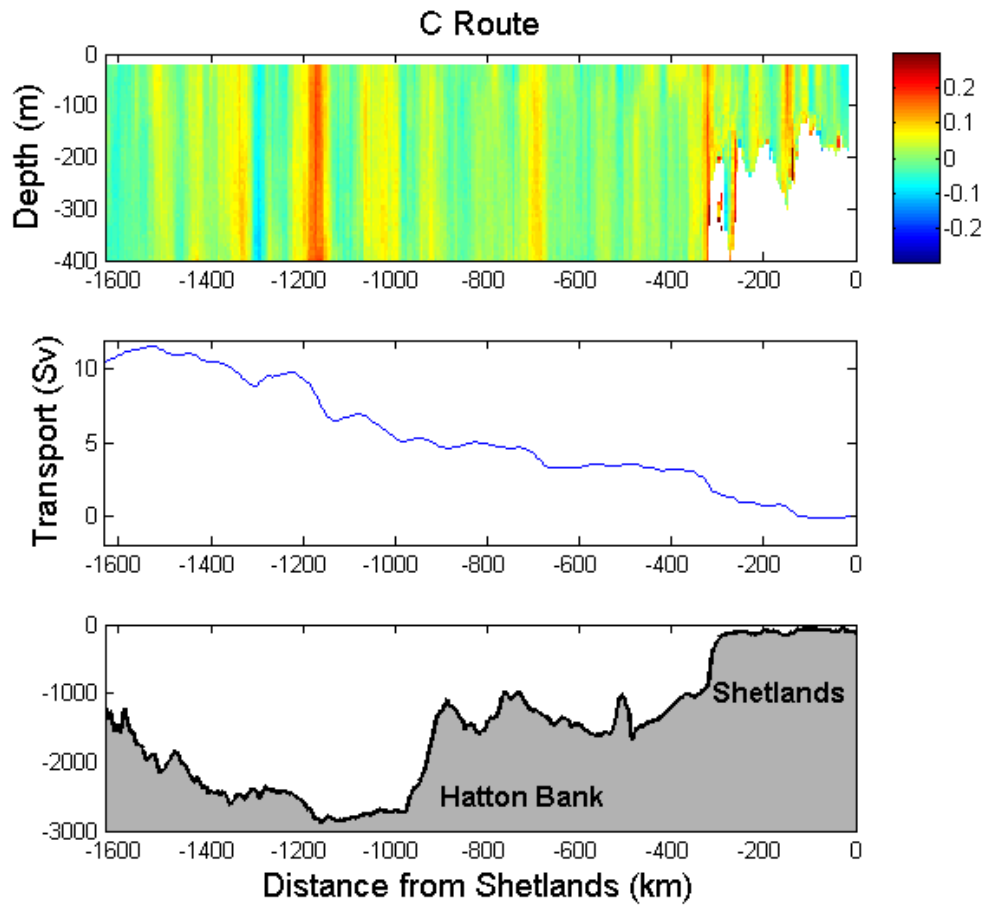
Figure 3.2: Mean cross transect velocity in m/s (top), cumulative transport (middle) and topography (bottom) with distance from Scotland for the Constant Latitude Nuka Arctica route.
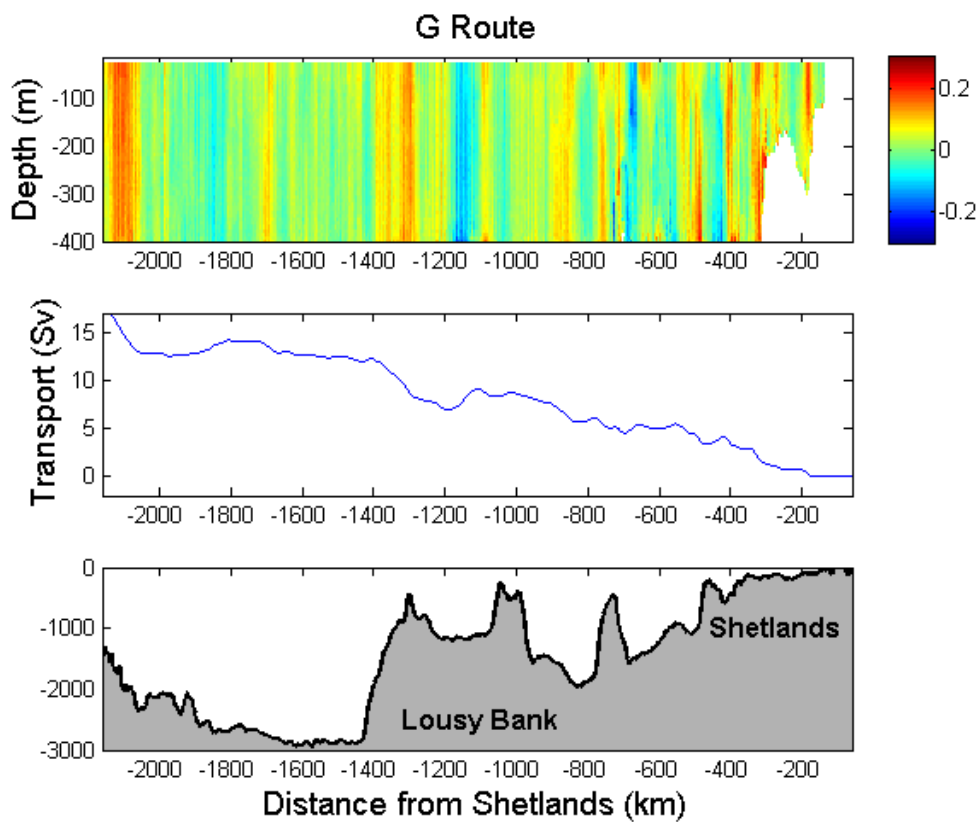
Figure 3.3: Mean cross transect velocity in m/s (top), cumulative transport (middle) and topography (bottom) with distance from Scotland for the Great Circle Nuka Arctica route.

47
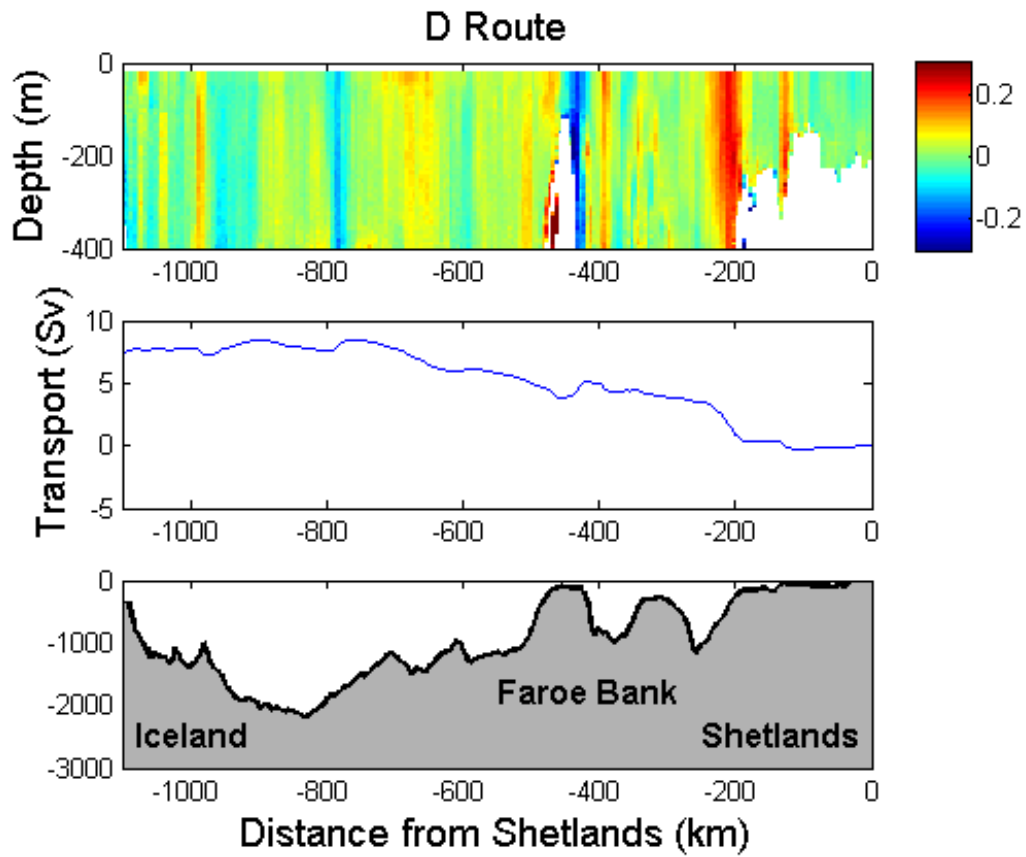
Figure 3.4: Mean cross transect velocity in m/s (top), cumulative transport (middle) and topography (bottom) with distance from Scotland for the Diagonal Nuka Arctica route.

FSC (Figure 3.5) leading to the Norwegian Atlantic Slope Current. Moving westward, additional northward currents flow past the C route at roughly 700 and 1200 km west of Scotland, widening and moving northeastward across the G route at nearly 900 km and 1300 km west of Scotland before reaching the D route as broad cross ridge flows from -500 to -800 km. Some of this water crosses the shallow IFR to enter the Nordic Seas (Figure 3.5). Crossing much of the remaining width of the transects are weak southerly and southeasterly flows, except in the case of the D route, where a particularly shallow topographic feature at -450 km is surrounded by an anticyclonic circulation. This illustrates the importance of topography in guiding much of the current structure in this region, where the ratio of mean along topography (across track) kinetic energy to across topography (along track) kinetic energy can approach 50:1 in the areas of steep bathymetry.
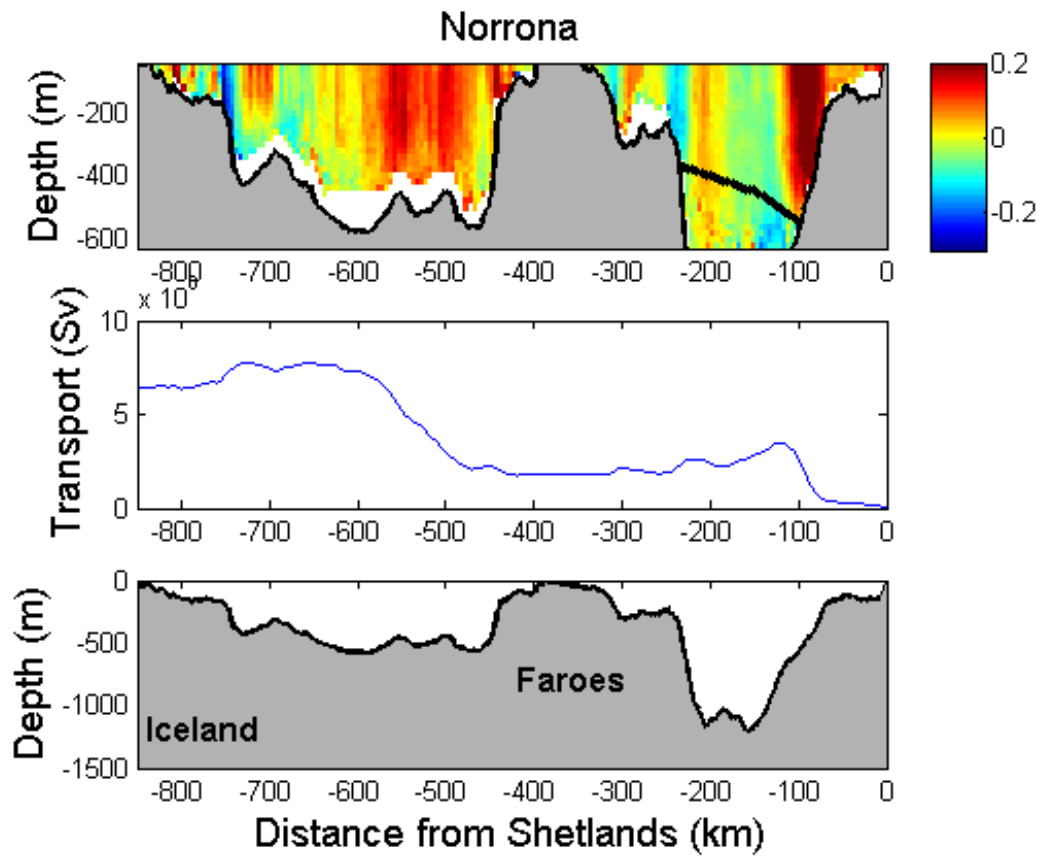
Figure 3.5: Mean across transect velocity in m/s above the σ_t=27.8 isopycnal along the Norröna route (top), cumulative transport (middle), and along route topography (bottom).

3.4 Discussion

3.4.1 Banks Region Flow

Of the 8±1.6 Sv observed by Chafik et al. (2014) to flow poleward in the top 400 m east of the RR, roughly half is expected to flow east of Hatton Bank. These waters traverse the variable channels and banks on a northeasterly route toward the FSC. At the latitudes of the C and G lines, the northward fluxes are split into roughly equal parts, one following the steep Scotland slope and another between Hatton and Bligh Banks. Upon reaching the D route, the topography has funneled the flow into two channels, the westernmost one with weakly northeastward fluxes across its full width and the eastern channel with the now well-defined Shetland Slope Current along its eastern slope. To obtain a more complete picture of the rates and transport of AW, we extend the measured velocities from the deepest 100 m of the C and D routes to the depth of the σ_t=27.8 isopycnal using the thermal wind equations. This extension of the depth of the C and D sections using the average density along each route, increases the total transport uncertainty for each by expanding the vertical integration distance of both the instrument and oceanic uncertainties. The resulting instrument errors for each route increase to 2.47 Sv and 1.79 Sv for the C and D sections. The oceanic uncertainties increase to 2.13 Sv and 1.46 Sv, assuming the same average eddy deviation from the mean over the extended depths. The concurrent increase in transport from the interpolation generally preserves the percentage error in transport at 13% for the C route and 32% for the D route.

As a result of the vertical extrapolation, more than 15 and 5.8 Sv of north(east)ward flow cross the C and D routes, respectively, east of the Iceland Basin, where AW occupies most of the water column (Figure 3.6). By the latitude of the D route most of the northeasterly flowing Atlantic Water is within range of the ADCP, with the σ_t=27.8 isopycnal sloping downward from Faroe Bank to approximately 500 m depth to the west and east (Figure 3.7). The ∼5.9 Sv of surface layer transport is dominated by the >3 Sv Shetland Slope Current with smaller contributions from a northward flux around 400 km west of Scotland and weak, more uniform inflows across the rest of the section. With the Faroe Plateau just north of this route, it is possible that some of the inflows over the western portion of this section are steered westward around the plateau and across the IFR, rather than towards the FSC. Surface outflows across this track are weak and vertically uniform, with

the exception of the likely circulatory flow around the Faroe Bank at 500 km from Scotland.

Despite the temporal gap in the data from the Nuka Arctica and Norröna, the Shetland Slope Current is of remarkably similar magnitude and structure along both the Nuka Arctica's D line and the Norröna's FSC route. In both cases, the current transports more than 3 Sv toward the Nordic Seas as a wedge shaped flow hugging the Scottish slope. West of the current, the Norröna FSC observations show weak outflows and a more intense along slope southward flow that reduces the net transport through the channel. Alternatively, the Nuka Arctica D line has some weak outflows, but also a greater distribution of weak inflows across the section, producing a higher northeastward volume flux.

3.4.2 Flow within and across the Iceland Basin

The surface waters of the Iceland Basin have been observed to follow a northward route from the North Atlantic Current toward the Iceland Faroes Ridge where most of upper layer transport is deflected west and south along the RR (Pollard et al., 2004; Bower et al., 2002). From the Nuka Arctica data we estimate that approximately 11 Sv cross the extended velocity and transport profiles of the C transect toward the north. This is similar to the 12 Sv observed by Pollard et al. (2004) in the same vicinity, along a diagonal transect from Iceland to Lousy Bank. This northward flux is surface intensified and strongest over the eastern half of the Iceland Basin. To the west, especially deeper than 1000 m, the flows tend to follow the topography southward. Along the D route, where the AW depths are shallower, roughly 13.9 Sv of northeastward and 8.4 Sv of southwestward transport occurs above the σ_t=27.8 isopycnal in the basin. Between the two transects, the bathymetry shoals by more than 500 m to even shallower than the AW depth over the C route. This likely contributes to a redirection of upper layer transport toward the west, which is supported by stronger southeasterly fluxes visible along the D route (Figure 3.7).

Just to the north and east of the D route, the AW crosses the Norröna's Iceland to Faroes transect, which follows the shallow crests of the IFR. The topography brings the full depth range of AW within range of the ADCP, providing a robust estimate of the northeasterly flux across the full length of the ridge. Similar to the FSC, a striking correspondence exists between the Nuka Arctica's D route and the Norröna's IFR transect. A 5.9 Sv mean

Figure 3.6: Nuka Arctica velocities interpolated down to the σ_t=27.8 isopycnal for the Constant Latitude route (top) and cumulative transport (bottom). Across transect velocities below 400 m are extrapolated based on the average density and thermal wind equations.
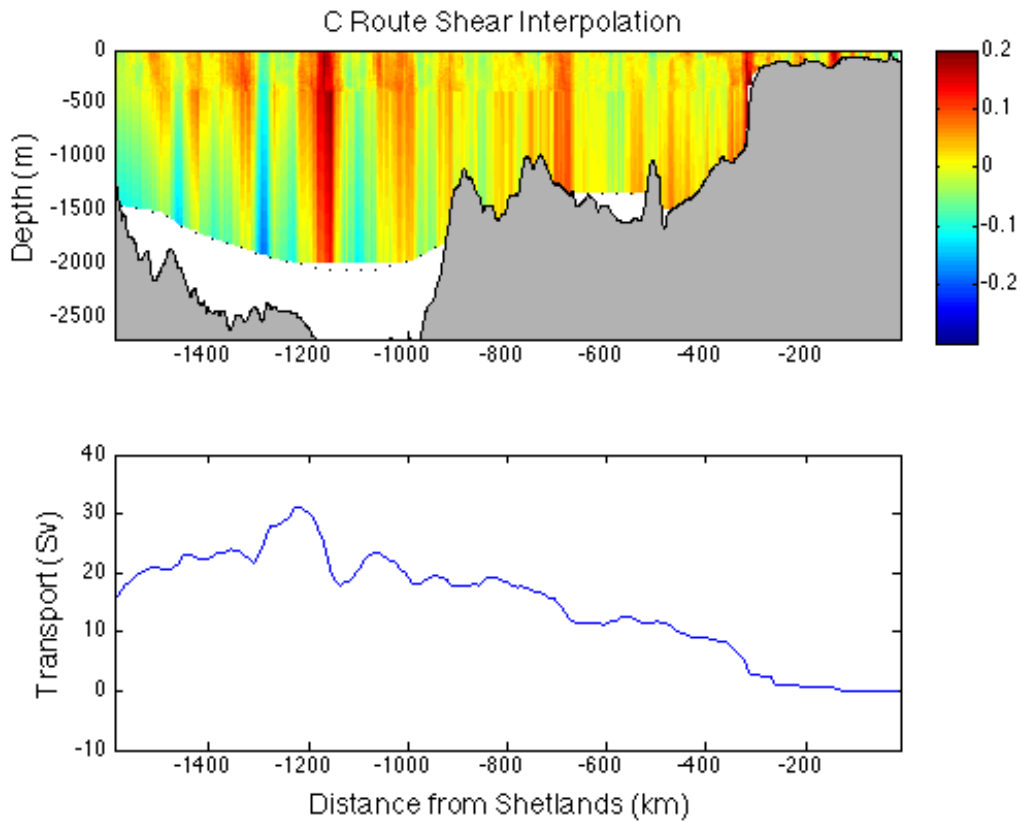
Figure 3.7: Nuka Arctica velocities interpolated down to the σ_t=27.8 isopycnal for the Diagonal route (top) and cumulative transport (bottom). Across transect velocities below 400 m are extrapolated based on the average density and thermal wind equations.
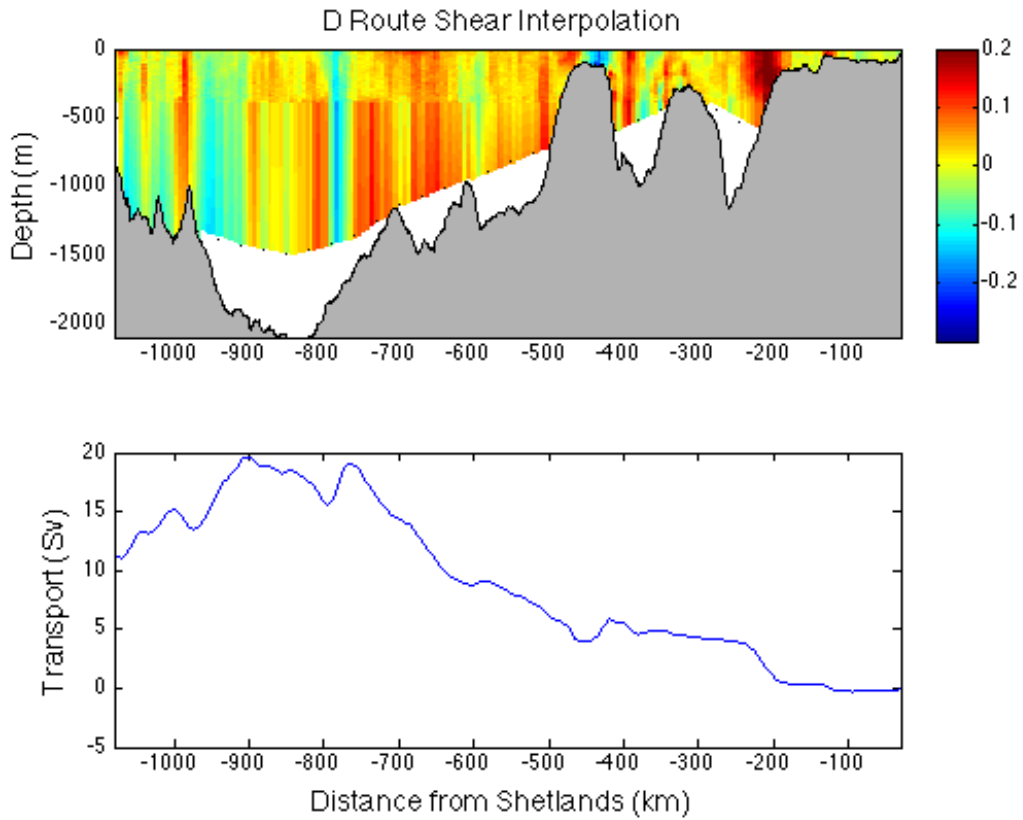
northeastward flux of Atlantic Water crossed the Norröna's IFR transect between 2008-2012. A southward flow over the western end of the section reduces the net northeastward flow to 4.6 ± 0.46 Sv, but the source of up to 1.5 Sv of the return flow is questionable and may not be of AW origin. Instead the outflow could be partially overflow waters moving southward along Iceland's coast with contributions of modified water related to the nearby Iceland Faroes Front. Assuming a consistent flow structure over the nearly decade gap between the observation periods of the two programs, this would suggest that most of the AW mass approaching the steep incline of the IFR from the south is deflected west and south prior to the D route, and that waters reaching that latitude are squeezed into a shallow northeastward flow over the Faroese half of the IFR.

3.5   Summary

By incorporating contributions from two ships of opportunity we are able to expand upon the analysis of Chafik et al. (2014) and establish the mean path of AW between 59.5°N and the Iceland-Faroe-Shetland Ridge. AW approaches the ridge system in bands of largely depth independent flow split almost equally between the Iceland Basin and the shallow regions east of Hatton and Rockall Banks. The flows to the east of the Iceland Basin, through and over the Banks region are separated into a wider band along Bligh Bank and a narrower, but stronger contribution along the Scottish Slope. The Scottish Slope flow is clearly defined as the >3 Sv Shetland Slope Current by its transit across the Nuka Arctica's D route at 60°N and continues as such over the eastern side of the FSC. The George Bligh Bank flow encounters complex topography just south of the Faroe Plateau and is likely steered anticyclonically along the bathymetry toward the IFR. The Iceland Basin portion is concentrated mostly over the Maury Channel trough and follows the topography of the eastern slope northward toward the IFR. The extreme depth of AW (compared to east of Hatton Bank) means that most of the AW approaching the ridge is unable to cross over the much shallower IFR, along its eastern (Faroese) side and is instead deflected west then south along the RR.
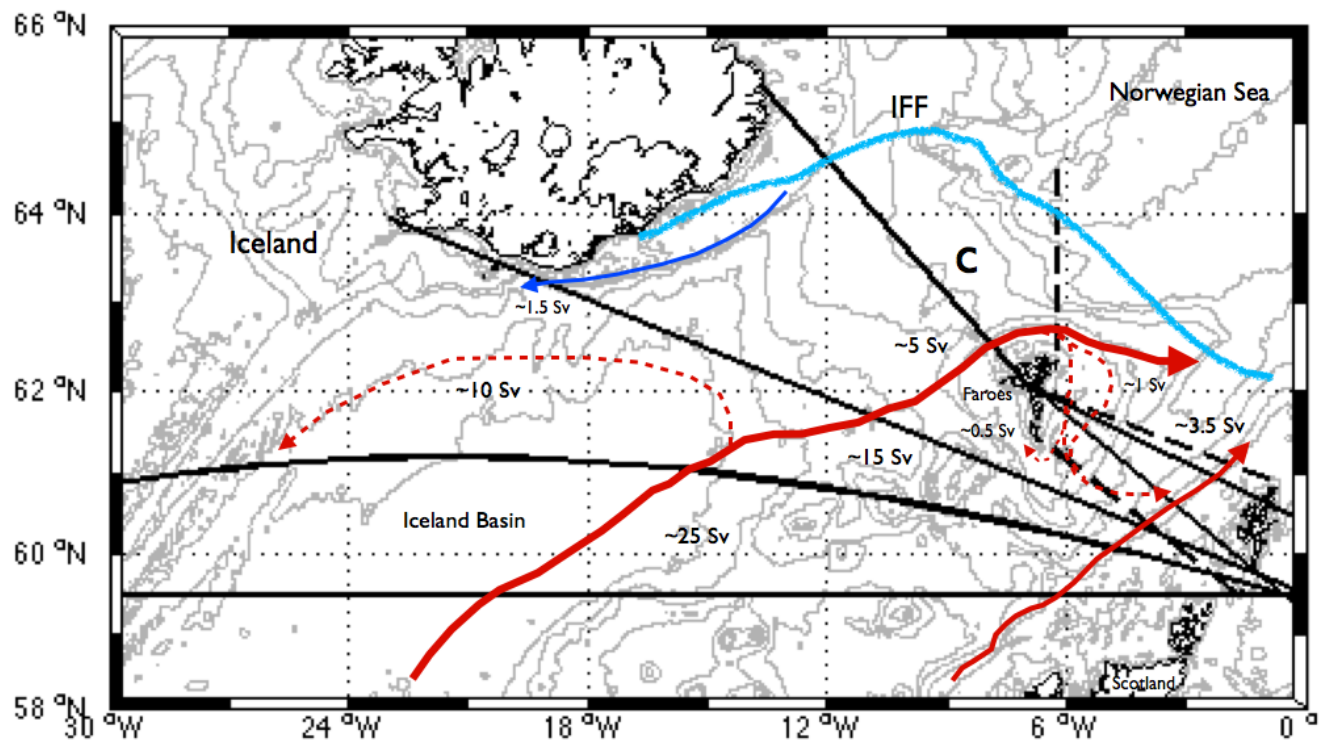
Figure 3.8: Simplified cartoon of the major currents observed by the Nuka Arctica and Norröna programs.

Chapter 4

Numerical Simulations of the Faroe Shetland Channel

Abstract

The mean and time varying circulation of the Faroe Shetland Channel (FSC) are explored using two months of high resolution ($1/12^o$) output from the ECCO2 configuration of the MITgcm. Basic circulation structure and temporal variability corresponds well with direct observations and is used to investigate the mean circulation of the southward Faroe Shelf flows as well as mesoscale fluctuations within the central channel. The Faroe Shelf is shown to play a large role in both eddy development and surface fluxes of volume and heat southward. The strong southerly Faroe Shelf flows observed over the northern FSC by the Norröna program diverge in the model output north of 61^oN and between 6-7^oW into a westward component which follows the bathymetry around the Faroes Plateau, and a larger eastward component, which flows south then east to join the Shetland Slope Current (SSC). Numerically simulated eddies are similar to the observations by Sherwin et al. (1999); Williams and Sherwin (2002), and Sherwin et al. (2006a,b) of transitory ($\sim$1 week) features originating along the temperature front at the northeast corner of the Faroe Plateau and due to instabilities in the SSC. These are in contrast to the lingering eddies observed by Chafik (2012), which can remain within the FSC for months and are not present in the model output. Simulated eddies from either FSC source are 30-50 km in diameter with deep vertical temperature signatures. They remain within the FSC, slowly

propagating away from their source region for approximately 5-7 days before dissipating in the central channel or being re-entrained by the SSC.

4.1 Introduction

The Faroe Shetland Channel (FSC) is a narrow passageway through which warm water branching off from the North Atlantic Current flows northeastward toward the Nordic Seas. Waters entering the channel first must cross through a region of banks and shallow channels before being funneled through the opening between the Faroes and Scotland. Here the North Atlantic Water (NAW) encounters cooler Modified North Atlantic Water (MNAW) moving southward along the Faroese coast from the Iceland Faroes Front (IFF). This mid channel temperature front and the rapidly changing topography with downstream movement creates an environment particularly conducive to the development of eddies and meanders. Not surprisingly, transport and velocity fluctuations have been observed in this region over a wide range of time scales from mixing due to breaking internal waves (Gordon and Huthnance, 1987) to interannual and decadal responses to the NAO and climate change (Sherwin et al., 2008; Chafik, 2012).

The most persistent features within the channel are the strong Shetland Slope Current (SSC) carrying warm, salty NAW along the bathymetry of the Scottish coast and eventually contributing to the Norwegian Atlantic Slope Current, and a southward flow of MNAW from north of the Faroe Islands toward the southern end of the channel. Upon reaching the southern tip of the Faroe shelf, this flow either continues to follow the bathymetry around toward the west and north, or is routed eastward across the channel upon encountering the temperature front where the inflowing NAW and MNAW meet (Sherwin et al., 2008). Within the central channel, little net transport occurs and eddies dominate the variability in heat and volume flux (Sherwin et al., 2008).

Several studies have noted the presence of mesoscale eddies within the FSC and described their potential sources, pathways, and preferential locations (Otto and Van Aken, 1996; Oey, 1997; Sherwin et al., 1999; Turrell et al., 1999; Williams and Sherwin, 2002; Sherwin et al., 2006a,b, 2008). Otto and Van Aken (1996) noted in their RAFOS float analysis that one drifter encountered a ∼30 km cyclonically rotating eddy within the FSC, transporting it out of the SSC and into the deeper mid channel waters. In Turrell

et al. (1999) nearly a century of historical hydrographic observations were compiled, including numerous examples of mesoscale eddies disrupting the mean circulation of the FSC. Sherwin et al. (1999) describe the passage of a 42 km cyclonic eddy through the central FSC northward, altering the path of the SSC. Interestingly, the eddy was larger subsurface, extending 57 km laterally at 300 m depth, which they note to be more than 10 times the internal Rossby radius associated with flow along the Scottish slope. The eddy was first hypothesized to have originated along the front at the southern end of the FSC, rather than from the IFF to the north, but this was later amended in Williams and Sherwin (2002), during a more detailed exploration of the development and decay of mesoscale meanders in the SSC. The Sherwin et al. (1999) eddy is estimated to have transported up to 1 Sv of MNAW within its boundaries. Sherwin et al. (2006b) provide a more detailed description of the observed eddy activity within the channel using drifters, noting that the greatest speeds in the FSC occur not within the core of the SSC, but along anticyclonic meanders that form at its western edge and around eddies occupying the central channel. The drifters were affected by meanders ranging in size from approximately 60 km to upwards of 80 km, growing from two primary locations (60.6ºN, 4.5ºW and 60.5ºN, 2.6ºW) and breaking off into cyclonic eddies (Sherwin et al., 2006b). The authors observed that some eddies moved slowly or only over short distances, postulating that the deep water outflow at the base of the central channel diminishes the group speed of surface disturbances and prevents the eddies from moving at the background flow rate associated with the SSC (Sherwin et al., 2006b). The authors also associated the observed cooling of the SSC along its route north with the mixing of MNAW and NAW by the meanders and absorption of mesoscale eddies of the type first characterized in Sherwin et al. (1999).

In addition to the propagation of detached frontal meanders from the SSC, mesoscale eddies of another sort were described by Chafik (2012) to occupy the central FSC during extreme low phases of the NAO. Using gridded altimetric SSH data, cyclonic eddies were seen to move southward into the channel from the IFF, occasionally acquiring a counter rotating partner from the SSC and remaining trapped for months by small topographic ridges. Such large scale and long term features deformed the pathway of the SSC and shoaled the halocline. The northerly source (and accompanying cold water signature) differentiate these eddies from those considered by Sherwin et al. (1999, 2006b, 2008), which are sourced within or very near to the channel and comprised of MNAW and NAW (Chafik, 2012). However, both types of

mesoscale eddies have a marked effect on the position and strength of the SSC as well as the deeper hydrographic properties of the along channel flow.

Williams and Sherwin (2002) and Sherwin et al. (2006a) considered the frequency and time variability of mesoscale meanders and eddies using moored ADCPs, drifters, and hydrographic profiles. Transient, rotating features, the signature of both SSC meanders and mesoscale rings, took approximately 10 days to pass over each ADCP and often occupied much of the upper 400 m of the water column (Williams and Sherwin, 2002). The meanders grew to ~50-60 km in amplitude and wavelength, with speeds up to 75 cm/s along their outer bounds and moved toward the northeast with a phase speed of 10 cm/s (Williams and Sherwin, 2002). Drifter tracks and AVHRR imagery suggest that the development of a meander in the SSC requires about 6-10 days before breaking, often shedding a cyclonic eddy in the process (Sherwin et al., 2006a). The hydrographic structure of the water column and fractional depth of the SSC directed Williams and Sherwin (2002) to conclude that baroclinic instabilities drive the meander development along the Scottish slope, likely tied to flow over the downstream Wyville Thompson Ridge. In addition both Williams and Sherwin (2002) and Sherwin et al. (2006a) noted the presence of eddies of a similar size but a more northerly source, postulating that eddies originating from the northwestern corner of the Faroes shelf could carry more than 2 Sv of MNAW into the FSC.

Oey (1997) made an early effort to model the meanders and eddy development characteristic of the FSC. He noted the failure of a 20 km grid to produce observed mesoscale features, despite its ability to accurately resolve the mean geostrophic field. Using a nested model (with $\frac{10}{3}$, $\frac{10}{5}$, and $\frac{10}{7}$ km resolutions), 20 km meanders developed within the SSC over periods of 5-10 days, accompanied by a change in the cross-slope gradient of the Ertel potential vorticity (Oey, 1997). The associated velocities were not well correlated with local winds or internal wave development. Recent very high resolution global runs allow for a reexamination of the modeled behavior of observed meanders and eddies in this region.

Here we aim to better describe both the mean circulation and its response to passing eddies through the use of high resolution ($1/12^o$), eddy resolving output from the ECCO2 configuration of the MITgcm, to elucidate further details regarding the observed flow regimes within the channel. The impetus for utilizing numerical simulations is to gain a greater understanding of the spatial and temporal patterns in the region not currently resolved by observational data. The high resolution model output covers only a short

time period (approximately two month) and recreates the fine structure and temporally brief circulation features of the region, such as the development and dissipation of eddies. Keeping this in mind, we employ the model results to aid in a further knowledge of the following observed features of the FSC:

- the magnitude of across channel fluxes and eddy transports determining the fate of the southward current along the Faroese slope;

- the creation and dissipation of eddies and meanders along the temperature front dividing the FSC;

- and the passage of eddies through the FSC entering from the fronts to the north and south of the channel.

Prior to such explorations an explanation of the simulation methods and a clear validation of the model's ability to represent the observed features and variability of the region must be established. This description is found in Sections 4.2 and 4.3, followed in Section 4.4 by an overview of the mean state of circulation and hydrography within the FSC, with particular attention paid to the southward transport over the Faroese slope. Section 4.5 considers the time varying components of the flow and the effects of mesoscale meanders and eddies within the channel. The chapter concludes with a short summary in Section 4.6.

4.2 Model Description and Methods

Results from this analysis are based on output from a high-resolution run of the ECCO2 (Estimating the Circulation and Climate of the Ocean, phase II) data assimilating configuration of the Massachusetts Institute of Technology Global Climate Model (MITgcm), formed as part of the World Ocean Circulation Experiment (WOCE) in 1992 and maintained by NASA's Jet Propulsion Laboratory (Menemenlis et al., 2008). Data from altimetry products such as the NASA Goddard Space Flight Center's TOPEX colinear SSH; temperature measurements such as XBT profiles from the Tropical Atmosphere Ocean array, Hawaii Ocean Time Series, Bermuda Ocean Time Series, and PALACE floats; as well as drifter, hydrography, and sea-ice observations are first adjusted for instrument errors and tidal fluctuations, then incorporated into the ECCO2 initial and surface conditions through least squares

fitting or regression to prevent discontinuities near the source of observations (Menemenlis et al., 2005, 2008).
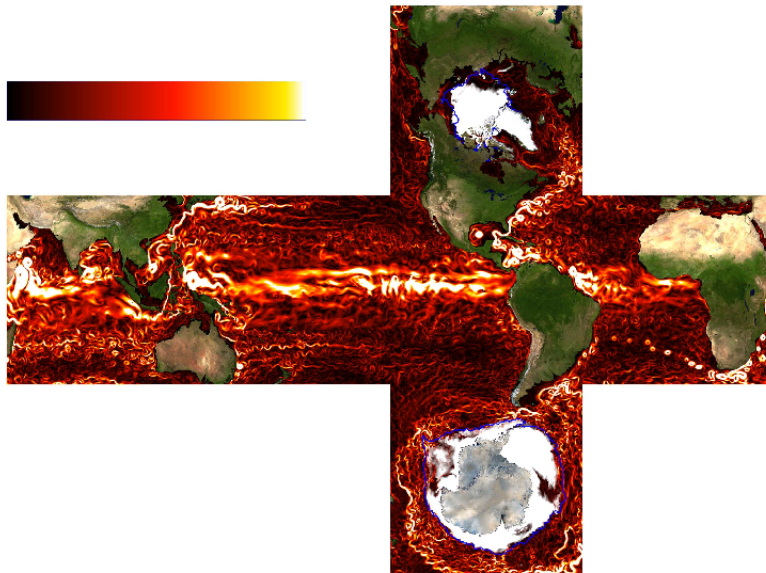
Figure 4.1: Cube-sphere domain of the ECCO2 model configuration from Menemenlis et al. (2008). Ocean current speed and sea ice cover at 15 m depth is shown.

Model output used here is from a $1/12^o$ cube-sphere configuration (Figure 4.1). Sub grid scale processes rely on coefficients representing mixing and diffusion rates (Menemenlis et al., 2005). Boundary conditions include a free surface boundary, a free-slip lateral boundary, and a no-slip bottom, which are described in further detail in Menemenlis et al. (2005). Surface forcing includes 12 hourly wind stress as well as daily heat and fresh water fluxes from the National Center for Environmental Prediction (NCEP) Reanalysis, with minor adjustments also outlined in Menemenlis et al. (2005). This particular run uses an adjoint-method, which allows for adjustment of the initial and boundary conditions simultaneously, and is optimized by a Green's functions method (Menemenlis et al., 2005, 2008). Output used for this

chapter is from a run initiated on January 1, 2010 with the addition of tides and atmospheric analysis at 90s intervals after one year (Menemenlis, personal communication). The full temporal period of the $1/12^o$ global run spans only two months, from February 9 - April 8, 2012 (yearday 40-99). The entire temporal output over a domain extending from just north to just south of the FSC and from the western edge of the Faroes to the eastern coast of the Shetlands (Figure 4.2) is used in this chapter to consider circulation processes with period of 2 months or less. At this latitude the meridional grid resolution is ~4.8 km. Vertically, the water column is divided over roughly 60 layers z layers, with less along the shallower edges of the FSC.
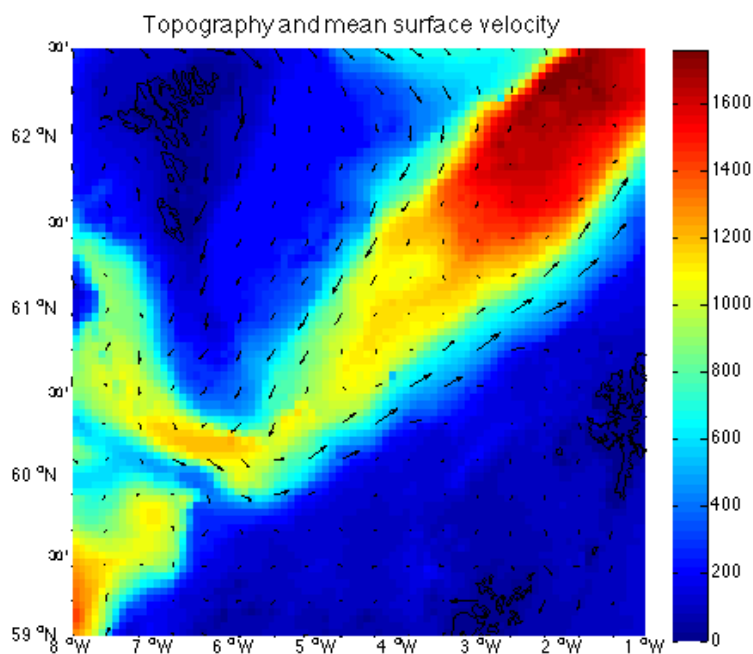

Figure 4.2: Depth (m) and average surface (upper 200 m) velocity over entire model period (yearday 40-100).

4.3 Model Validation

Validation of the relative location and magnitude of the large scale circulation features is ideally obtained through comparison of daily model output to velocity observations collected by the Norröna project over a concurrent time period and along the same transect. However, due to the low data returns by the Norröna observational program during the winter (the period of this numerical simulation) a further comparison to the average cross transect velocities over the full period of Norröna observations proved more fruitful. Tidal influences were removed from both the numerical simulations and observations using a method of least squares fitting to knot locations (Wang et al., 2004; Dunn, 2002). Similar mean structural features exist both in the model output and observations, such as a 40-50 cm/s northeasterly SSC and intermittent southward flow of up to 30 cm/s along the Faroese slope. However an exaggerated horizontal extension of these features by the model leads to an overestimation of both the southward flow on the Faroese side and the SSC (Figure 4.3). The mean transport of the Faroe Shelf and Slope flow is large, with nearly -4 Sv of southward transport simulated compared to the -0.9 Sv observed. The increased SSC flux (approximately 5 Sv, compared to 3.5 Sv observed) does not fully compensate for the overestimated southward transport, which along with a small ($<$0.5 Sv) difference in mid channel southward flow, produces a modeled mean AW (σ_t<27.8) transport of -0.3 Sv versus 1.7 Sv observed. The southward flux on the Faroese side is of considerable interest, and its presence in the model output is encouraging. The large amplitude in the simulation data may be due to unresolved circulation features or particular to the time period of the output, since it is close to Sherwin et al. (2008)'s spring maximum and within the upper range of the southward flux observed by the Norröna. Since the overall structure and primary current features of the FSC are similar between the model output and observations, we will proceed by focusing the discussion on relative rather than absolute transports across particular transects.

To compare deviations from the mean circulation in the model output and observations we consider the variance (Figure 4.4) and EKE (Figure 4.5) of each. The variance in both the model output and observations is greatest along the direction of isobaths in the shallower regions near the Faroes and Shetlands, with more circular variance ellipses in the central channel. Magnitudes of the major and minor axes are similar, although slightly larger in the observations, especially near the Faroes. Both the observations and
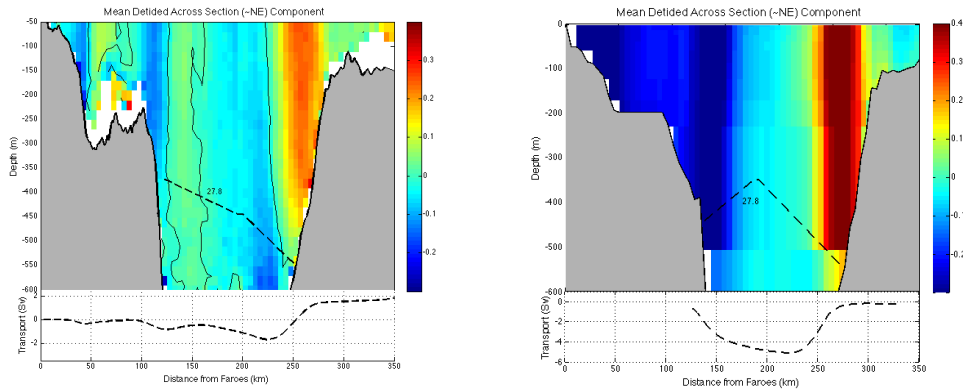
Figure 4.3: Observed (left) and model (right) detided across section, ∼northeastward velocity and cumulative transport. Observed velocities are averaged over the full observational period of the Norröna program, while model velocities are for numerical simulations form February 9 - April 1, 2012. Dotted line indicates the depth of the σ_t=27.8 isopycnal, a proxy for Atlantic Water depth.
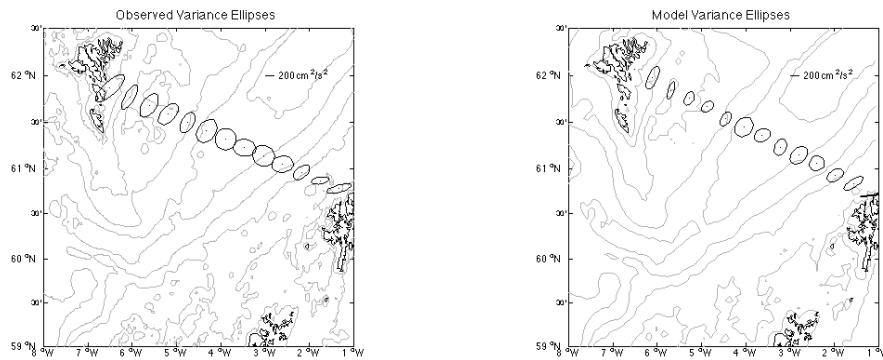
Figure 4.4: Observed (left) and model (right) detided variance ellipses vertically averaged over 20 - 200 m depth and shown in 25 km steps. Bathymetry contours at 50, 100, 200, 500, then every 500 m.

numerical simulations also indicate greater cross bathymetry transport on the slope of the Shetland side of the FSC than Faroese side. Eddy kinetic energy extends the variability analysis to the full upper water column (Fig-

65

ure 4.5). Highest EKE values occur at the surface for both the observations and simulations, especially over the central channel. These values decrease considerably below 200 m depth and are negligible below 400 m. Differences between the simulations and observations include slightly weaker EKE values at the surface in the simulations and much weaker EKE over the Faroese shelf.
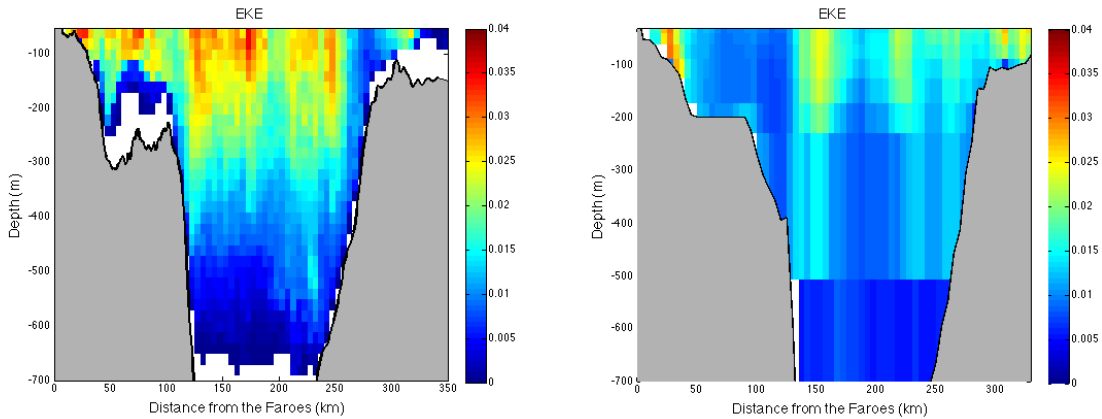
Figure 4.5: Observed (left) and model (right) eddy kinetic energy in m^2/s^2.

4.4 Mean State

Temperature and salinity transects in the FSC region strongly influence the position and extent of circulation features. A composite AVHRR satellite image from February 2012 (Figure 4.6) clearly shows the lateral gradients in sea surface temperature. Fronts between surface water masses are visible south and north of the FSC, as well as extending along a meandering line through the center of the channel. These same features are reflected in the model output. Vertical gradients in hydrographic properties separate a largely homogenous surface flow from a strong return flow at depth, while sharp lateral density gradients split the FSC between counter flowing slope currents. Temperature and salinity transects running north/south and east/west through the section are shown in Figure 4.7. The highest observed temperatures and salinities occur within the core of the SSC along the eastern edge of the FSC. Moving offshore from the current's core, salinity and temperature decrease,

suggesting incorporation of MNAW or the cooler and less saline central channel waters, along the outer boundary of the SSC. Surface MNAW is found over similar depths on the Faroese shelf and slope, and has a T-S signature that is distinct from the NAW of the SSC core. Intermediate water masses occupy the 400 - 600 m depth range, below which are the deep, cold overflow waters.

Figure 4.6: AVHRR composite image from February 2-8, 2012, courtesy of RSDAS. A distinct meander in the along channel MNAW/NAW front is visible near 61ºN,4ºW.

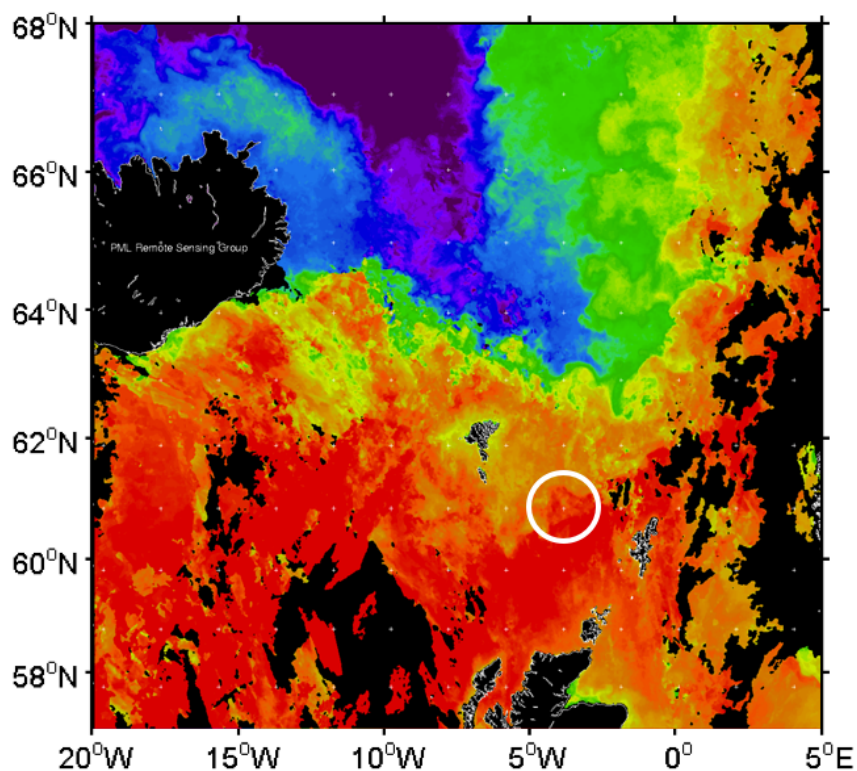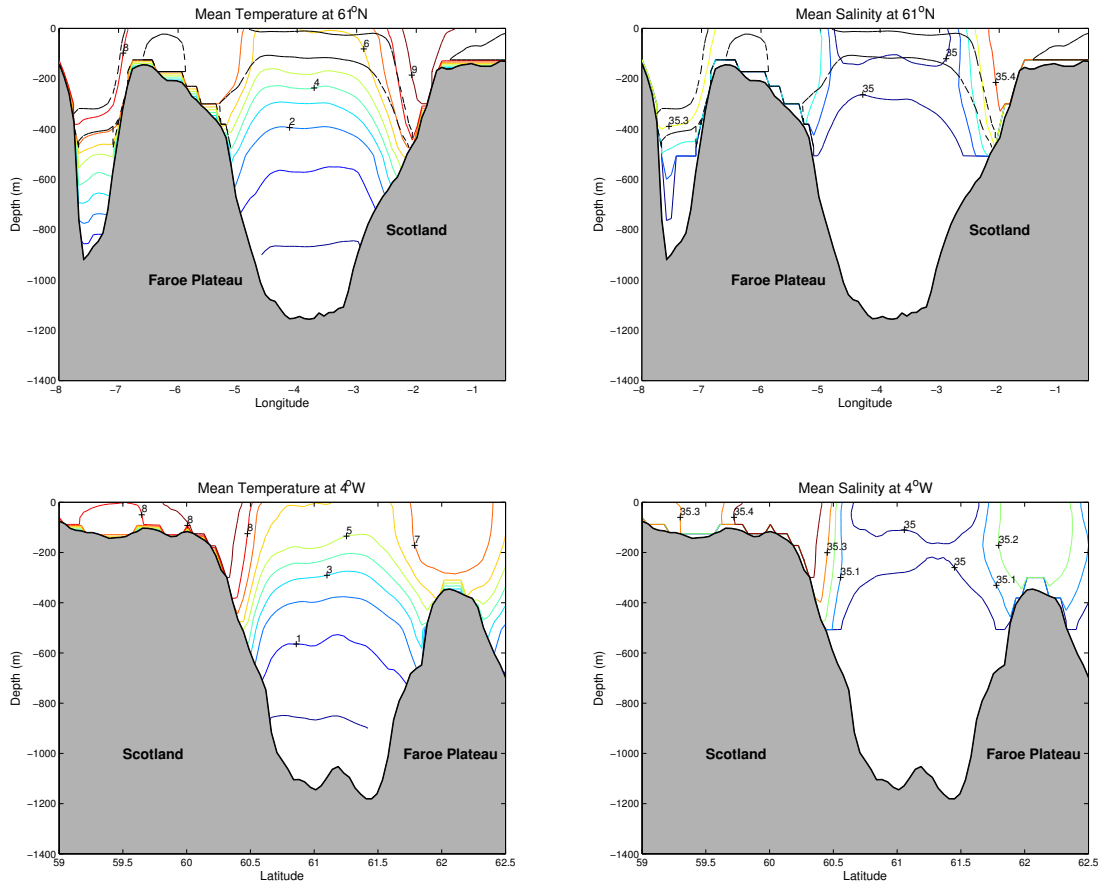Figure 4.7: Mean potential temperature and salinity profiles through the FSC along 61°N (upper) and 4°W (lower). The black dotted line in the upper panels indicate the depth of the σ_t=27.5, 27.6 potential density isopleths.

Time averaged circulation through the FSC from the model aligns well with the bathymetry and can be decomposed into the northeastward flowing SSC on the Scottish side and a southward flow along the Faroe Plateau (Figure 4.2). The central channel exhibits negligible velocities and cross channel flow is confined to the southern end of the FSC, where a sharp temperature front between the inflowing Atlantic Water blocks the southward flux of MNAW circulating around the Faroes. Mean vertical sections taken across the channel from both the model output and Norröna observations similarly reveal the importance of the SSC to the east and the southward flows over the shallower portions of the western channel (Figure 4.3).

The expected flow paths of water entering the channel from either side can also be inferred from the mean hydrostatic potential vorticity field, defined here as

$$PV = \frac{f}{g}N^2, \tag{4.1}$$

and shown in Figure 4.8 for 60 m depth. Potential vorticity contours largely follow the topography in the shallow regions near the Faroes and along the Scottish coast, helping to shape the northeastward SSC and southward Faroese slope flow. The opposing directions of currents along the two sides of the channel establish a strongly cyclonic (counterclockwise) flow in the central FSC. A sharp gradient in the potential vorticity exists along the SSC, with a cross slope change in the sign of the potential vorticity, conducive to the development of instabilities (Gill, 1982). Around the Faroes, closed contours do not circle the continental shelf where the bathymetry is deeper than 300 m, but rather turn back east toward the SSC. North of the FSC a cluster of smaller regions of both high and low PV extend into the channel from the IFF.

4.4.1   Faroe Shelf and Slope Flow

In Rossby and Flagg (2012) a strong southward flow along the Faroes side of the FSC was noted crossing the Norröna transect. This circulation feature has been previously observed (e.g. Sherwin et al. (1999); Turrell et al. (1999); Williams and Sherwin (2002); Sherwin et al. (2006a,b, 2008); Hansen et al. (2008)), but its fate at the southern end of the FSC is currently unknown. Rossby and Flagg (2012) postulated a downstream partitioning of this flow into a westward component, following the bathymetry around the Faroes, and an eastward recirculation at the southern end of the FSC resulting in

a contribution to the northeastward transport of the SSC. This important aspect of the FSC circulation is considered using the mean model output velocities. The relative separation of the flow and the location of recirculation are considered here by examining the transport crossing a series of transects (A-D) near the Faroes (Figure 4.9).
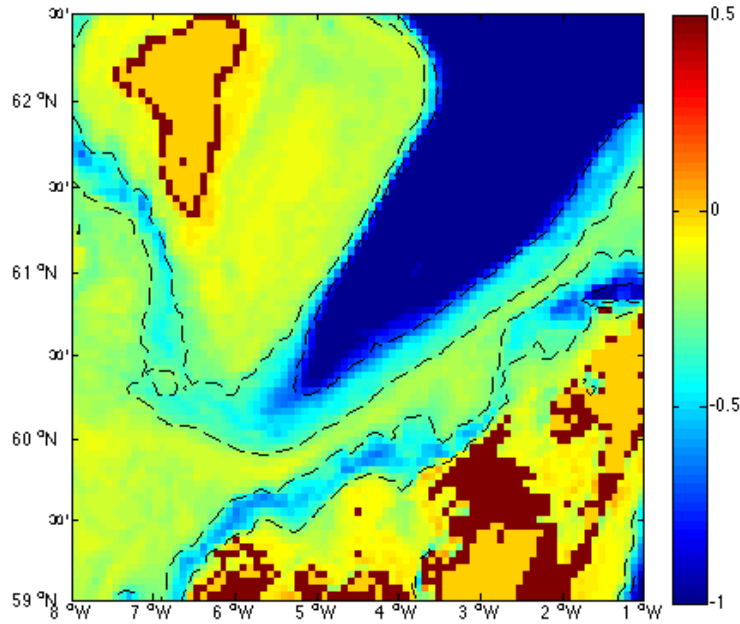
Figure 4.8: Average hydrostatic potential vorticity ($\times 10^{10}$) at 60 m depth. Black dotted lines show contours at -0.75 and -0.30.

The volume flux of MNAW crossing each transect acts as an indicator of the relative contributions of the southward flux to a circum-Faroes current and to the SSC. As described in Section 2, the absolute magnitude of the model velocities on the Faroes shelf and slope are considerably larger than direct observations at similar locations. For this reason, volume fluxes will be presented in terms of their magnitude relative to the southward transport of MNAW crossing Line A (Q_A). Line D is on the shallow western Faroes shelf, where only MNAW is present and transport is integrated over the full water column. However, along lines A, B, C, and E the volume flux is measured over AW depths (σ_t<27.8, T>5^oC, approximately 500 m for all sections).

The resulting mean southward transport over the 60-day simulation period across Line A is almost equal to the westward volume flux across Line B (Q_B=0.88Q_A). This suggests that little recirculation of surface waters occurs east of 6°W. Slightly west at 6.5^{o}W (not shown), the westward transport decreases to 82% of Q_A and by 7.0^{o}W the westward flux is only 34% of the southward transport at Line A. This isolates the area between 6.0-7.0^{o}W as the critical location where most of the southward flux along the Faroese shelf and slope either follows the mean PV contours (Figure 4.8) and joins the SSC or continues along the isobaths toward the north. North and west of this location, the flux is primarily southward (Line C) from 8°W to the Faroese Plateau, indicating that most water circulating around the Faroes turns west north of 61°N. The majority of the surface transport crosses Line D at 61.5^{o}N toward the north, with a small southward flow along the temperature front between NAW and MNAW at 7.5^{o}W. The average volume transport toward the north at Line D is 32% of Q_A.

Figure 4.9: Black lines show the location of the transects used to estimate the separation of southward flowing waters along the Faroese slope into a recirculating component joining the SSC and a bathymetry following flow around the Faroes Plateau. White diamonds indicate locations of spectral analysis and blue squares are the sampling locations for temperature and salinity in Figure 4.10. White arrows indicate the percentage of volume flux crossing each transect (see text). Mean velocities and SST are shown for reference.

Time series correlations link the temporal behavior of the filtered, hourly, across transect velocity at 50 m in the regions of highest flow (white diamonds in Figure 4.9) and full cross-transect averages. Since the upper water column velocities are largely depth independent, it is assumed that the 50 m level serves as an appropriate proxy for the behavior of the surface circulation at a given location. Correlations are weak (0.18-0.51) but statistically significant (p<0.02) for most of the transect lines around the Faroes. Negative correlation coefficients of 0.25 and 0.51 link the southward flux at Line A to the northward fluxes at Lines C and D. In comparison, each line has an r<0.10 or is not significantly correlated with the time series of the velocities at the Central FSC location. Only Line C shows any coherence with the behavior of the SSC, with an r=-0.47. This link is likely due to the NAW/MNAW

front along both lines, which causes the southward flows at Line D to increase concurrently with increasing speeds of the northeastward SSC (Line E). Lagging by 8 hours slightly increases the correlation coefficient between lines B and C, but delays do not have a large impact on the other correlation coefficients.

The mean hydrography along the SSC also points to entrainment of waters with lower salinity and temperature than the inflowing NAW. An abrupt decrease in both salinity and temperature occurs between 59.6^{o}N 6.85^{o}W, just south of the front between MNAW and NAW, and 60.0^{o}N 6.35^{o}W (Figure 4.10). A decreasing trend continues in temperatures over the upper 400 m of the water column along the SSC toward the north, likely due to both heat loss to the atmosphere and mixing with cooler and fresher waters from the central FSC, which are considered in greater detail in the following section.
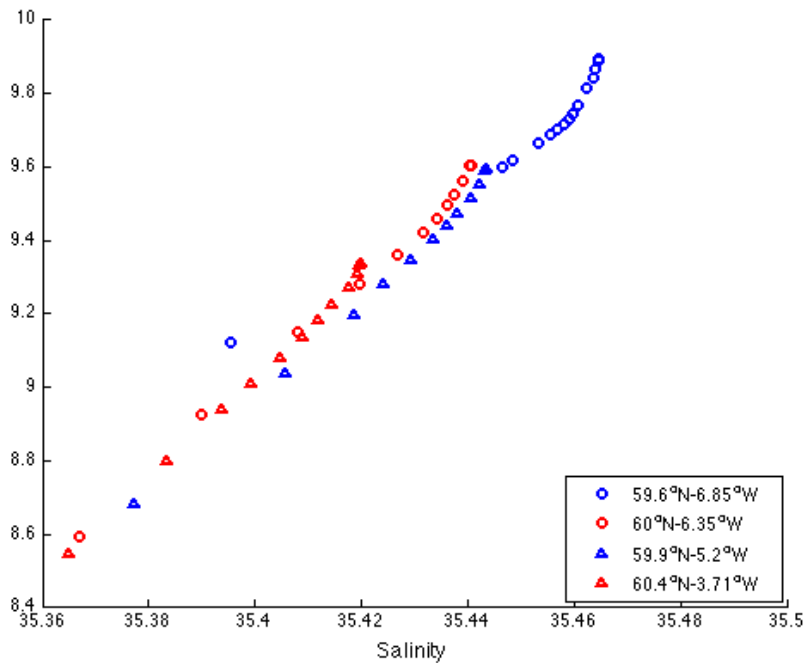

Figure 4.10: Temperature-salinity diagram over the upper 400 m for four locations along the SSC (blue square in Figure 4.9), starting just south and east of the Shetland slope and showing a progressive cooling toward the northeast.

72

4.5 Time Varying Circulation

The FSC is exposed to a plethora of sources of temporal variations to the mean circulation and hydrographic structure. The two-month numerical model output period draws our attention to higher frequency variations, from tidal periods through monthly variability. Topography and water depth determine the relative influence of tides in the FSC. Figure 4.11 (upper) shows the hourly north/south velocity at 50 m depth for four locations along the FSC over 60 days. At locations A and D, on the Faroese slope and shelf, the effect of tides is immediately evident. On the Shetland slope at location E, tidal effects are apparent but considerably smaller in magnitude, as is the case of the centrally located profile in the bottom panel. A pl33 (http://woodshole.er.usgs.gov/operations/sea-mat/bobstuff) low-pass filter using the weighted average of 66 data points (33 on each side) was used to remove the tidal influence from each velocity time series and the results are shown in Figure 4.11 (lower). The resulting filtered time series from within the two shelf currents (D and E) are greatest both in the magnitude and variability of their velocities.

A spectral analysis of all four locations illustrates the periods associated with the greatest energy density. As expected, peaks are evident at the frequencies of the major tidal constituents, with additional peaks at the higher frequencies of the over-tides (a sample for Line B is shown in Figure 4.12). Rotary spectra for each location further demonstrate the strong influence of the full range of tidal constituents with approximately equal energy density amongst the clockwise and counterclockwise components (sample for Line B shown in Figure 4.13). Peaks at the frequencies of the mixed and over tides, especially in locations along the Faroes shelf and slope, are suggestive of tidal rectification, which is in agreement with observations by Larsen et al. (2008). Coherence and rotary coefficient stability levels are high over the full frequency domain and especially for the lower frequency (longer period) fluctuations, indicating a high likelihood of a similar source. The low frequency coherence ellipses are strongly aligned with the topography at each location, except for the deep Central FSC position, where the u-v ellipse is approximately circular. Figure 4.14 depicts a summary of the energy density spectra of the across transect velocity at 53 m depth at the white diamonds on each line from Figure 4.9. The semi-diurnal tidal frequency is indistinguishable from the inertial period (T=14 hrs) at this latitude. Peaks are evident at the diurnal and over-tide frequencies for all locations.
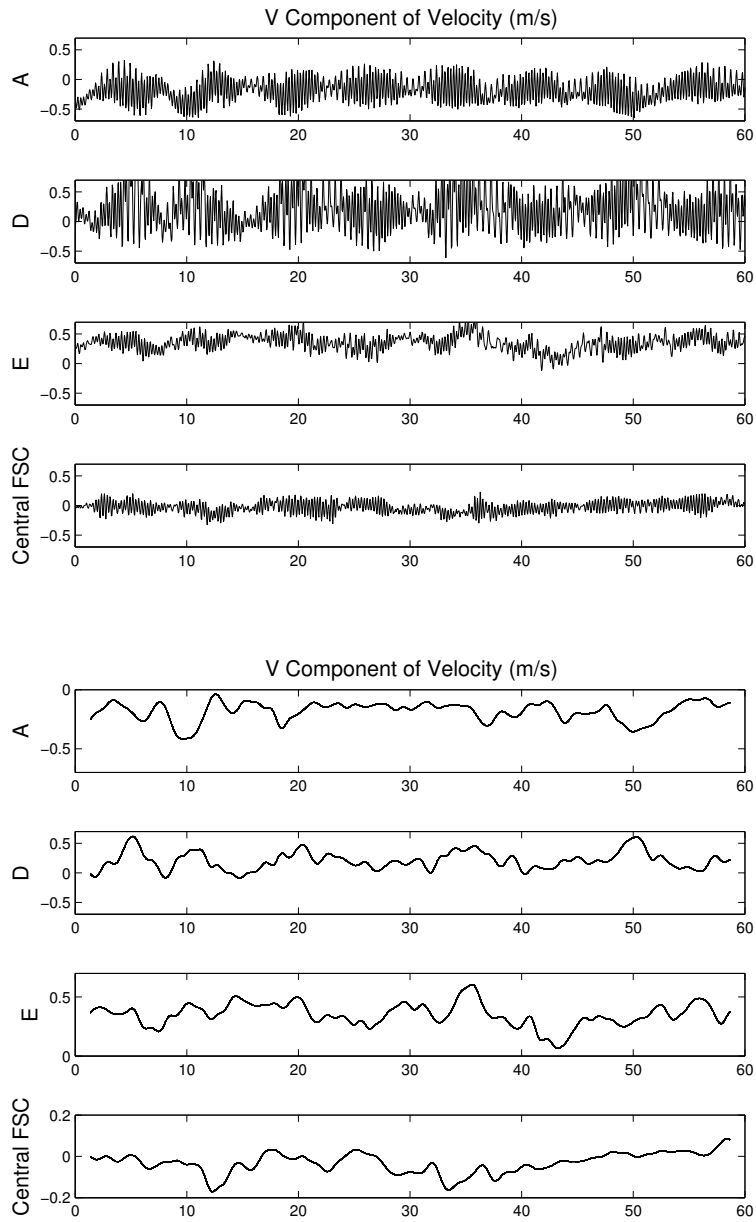
Figure 4.11: Time varying velocity at 53 m depth for several locations (shown as white diamonds in Figure 4.9) before (upper) and after (lower) application of a pl33 filter. Horizontal axis is days since February 9.
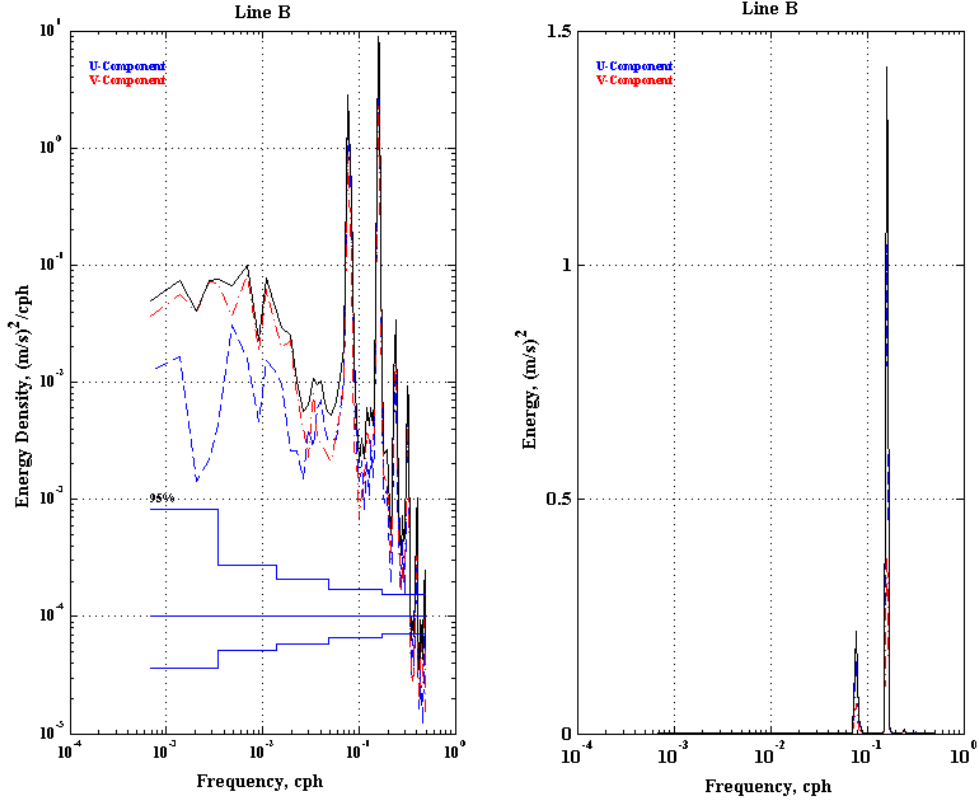
Figure 4.12: Sample energy density spectrum (left) and energy conserving variance plot (right) for hourly data at 53 m in the center of Line B (white diamond in Figure 4.9). The frequency peaks are associated with tides and described further in the text. Confidence limits are shown in blue and computed using a Hanning window with 50% overlap.

Between the low and high frequency spectral peaks we can define a period of "mesoscale variability" for the FSC. Within this frequency range, alterations to the mean flow often come in the form of 30-50 km wide eddies that separate from the along channel density front, or enter the FSC from fronts to the north and south. Eddies, manifested as largely depth independent vertical striping in the observed along channel velocities, are also present in the model output indicating a high degree of model fidelity (example in Figure 4.16). Eddies are usually present along the Norröna track and are visible
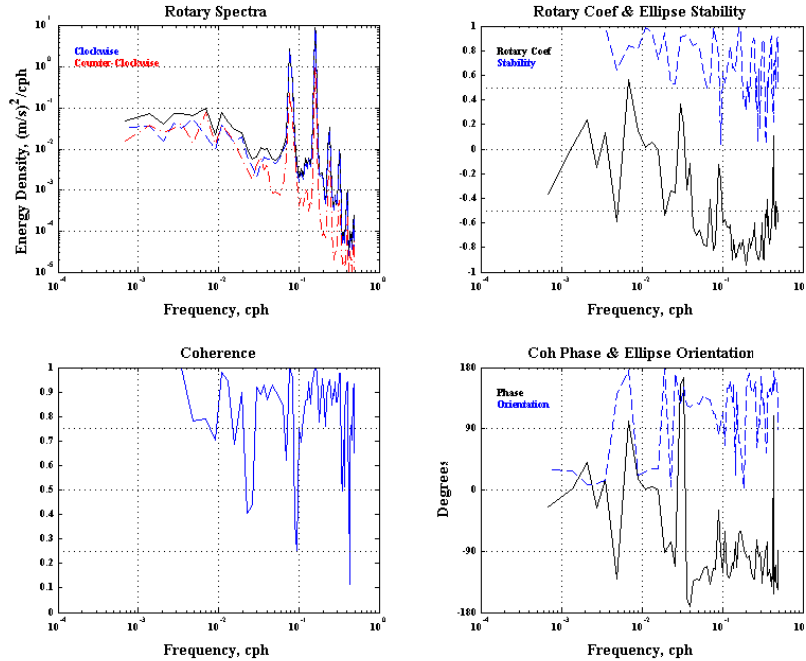
Figure 4.13: Sample rotary spectra for the central point of Line B. (white diamond in Figure 4.9). The coherence and rotary coefficient for all sampled locations are high for low frequency variations. The low frequency motions at each location are aligned closely to the topography.

in 63% of the FSC observations and 60% of the daily simulated velocities along the Norröna's FSC route. In addition, the surface temperatures and velocities from the model also suggest near ubiquitous eddies, providing a frequent alteration to the mean flow.

4.5.1 Mesoscale Eddy Field

Williams and Sherwin (2002) and Sherwin et al. (2006b) characterized the behavior and importance of mesoscale eddies and meanders in the SSC. Both studies identified the primary source regions for mesoscale eddies to be the northeast corner of the Faroese slope and meanders in the SSC, especially near 61ºN 4ºW (visible in Figure 4.6). The numerically simulated SST field also develops meanders and fluctuations along the frontal boundaries be-

76
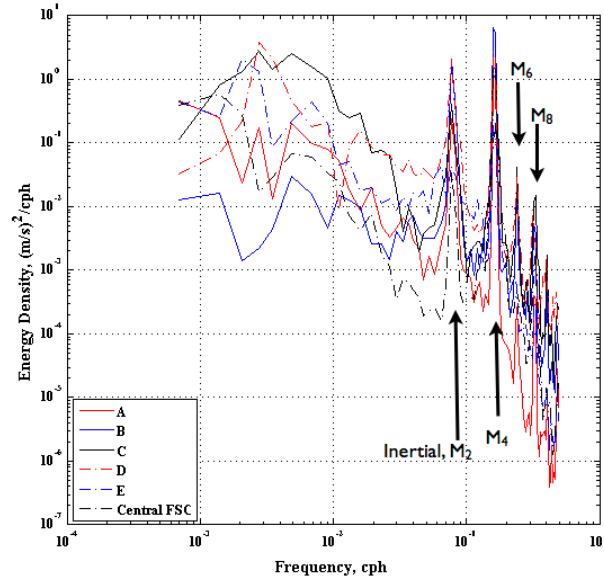
Figure 4.14: Composite image of energy density spectra of the cross transect, hourly velocity along each line shown in Figure 4.9 at 53 m depth.

tween the cooler central channel waters and the warmer MNAW and NAW to either side. Simulated meanders in the SSC occur in two primary locations: at approximately 60.5^{o}N 4.0^{o}W and 61°N 3°W, near Sherwin et al. (2006b)'s observed meander locations. An example of both source regions is shown in Figure 4.15 which depicts the interaction of a meander in the SSC and an eddy traveling south through the FSC on 8-23 March 2012 (yeardays 65-80). The eddy forms along the Faroese slope before breaking off into a cyclone with a diameter of approximately 30 km. As the cold water moves southward through the channel, its planetary vorticity decreases, increasing its cyclonic rotation (positive relative vorticity). As the eddy continues moving southward with the Faroe slope flow, it alters the SST on the Faroese

77

side of the FSC and begins to deflect the southward mean flow. Meanwhile a more than 50 km meander has been forming along SSC, which encounters the eddy on yearday 73, engulfing it into the SSC by yearday 81. Similar passages of eddies occurred throughout the modeled period, although often at a faster rate. Unlike the persistent features described by Chafik (2012) associated with extreme low NAO, or the topographically trapped mesoscale features observed by Sherwin et al. (2006b), most of the simulated eddies dissipate within 5-7 days, either due to re-entrainment into the shelf and slope flows, or through mixing with a(n) cyclone (anticyclone) counterpart in the central FSC. Since both the Norröna program and AVHRR composite satellite observations have sampling rates longer than one week, it is uncertain whether this period is characteristic of the region or a function of the model configuration.

The large fractional depth of the SSC to the total water column depth led Williams and Sherwin (2002) to identify baroclinic instabilities as the most likely source of SSC meanders, based on the rotating container experiments of Griffiths and Linden (1981). They hypothesized that upstream flows over the Wyville Thompson Ridge lead to downstream disturbances along the Scottish Slope. To determine the characteristic frequency and size of eddies within the FSC, and especially along the Scottish slope, Williams and Sherwin (2002) employed a 2 layer instability model from Killworth et al. (1984), previously used by Allen et al. (1994) over the IFR. Assuming a σ_t=27.85 separation between the surface and bottom layers and no lower layer motion, Williams and Sherwin (2002) found the wavelength and phase speed of the fastest growing mode to be 52.3 km and 10 cm/s, respectively. This corresponds well with both the size and duration of eddies in the model results, which are shown here to be approximately 1 longitudinal degree ($\sim$54 km) in diameter and last for 5 - 7 days before dissipation.

Important to the Sherwin et al. (2006b,a) studies was the idea of heat transport by mesoscale eddies and meanders. Eddies formed in the SSC often move into the central channel and lose heat to the surrounding waters, while MNAW eddies from the Faroese shelf carry cooler waters that are often entrained into the northeastward flowing SSC. The largely homogenous surface layer within the channel allows for the extension of surface eddies down nearly to the depth of deep overflow (Williams and Sherwin, 2002). This is consistent with hourly model output along a constant latitude section in the central channel, which shows the upward deflection of the thermocline between the deep, cold overflows and warm surface AW (above σ_t=27.8) as
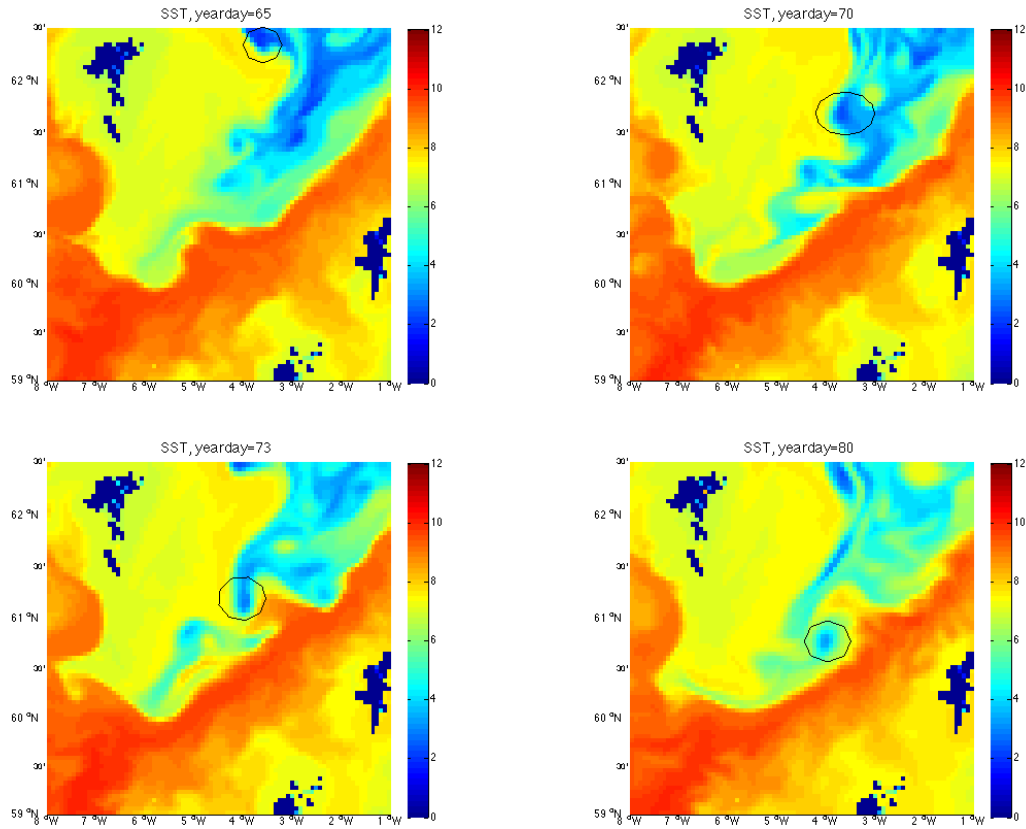
Figure 4.15: Progression of an eddy through the FSC from formation at the IFF to dissipation near the SSC.

a result of the passage of a cyclone (Figure 4.17). Similarly, vertical sections along the same line show a deepening of the 3°C isotherm while affected by a northward moving anticyclone. The same sections reveal an alteration of the lateral extent of both the northeasterly SSC and southward flows on the Faroese side while eddies are present within the FSC (visible as the width of the 8°C NAW on the eastern side and ∼7°C surface waters to the west in Figure 4.17). This phenomenon is also evident in the Norröna data, with complete disruptions of the flow path of the SSC rendering it unrecognizable in 9% of the observed sections, and the southward Faroese flow indistinguishable in 23% of the Norröna's northeastward velocity profiles. This has a brief but marked effect on the observed transport. An example is shown in Figure

79

4.16 for the same model output period as Figures 4.15 and 4.17. The left panel shows the model output cross transect velocities along the Norröna transect and the right is a sample Norröna section from 2009 with a similar structure. In this case the observed transport during the presumed passage of a mesoscale eddy decreased the magnitude of the southern transport to -0.61 Sv (mean is -0.9 Sv) on the Faroese side and to 0.5 Sv (mean is 3.7 Sv) on the Scottish slope, resulting in a net northeastward volume flux of -0.4 Sv, 2.1 Sv less than the mean across this section.

4.5.2   Potential Vorticity

The strong influence of topography is evident in the mean potential vorticity field (Figure 4.8), with the steep bathymetry forming almost closed PV contours in regions associated with eddy formation and trapping. As the mean PV field is perturbed, long filaments of anomalously low PV extend into the central FSC from the north along the western edge of the channel and the region of high PV intensifies over the western edge of the SSC. Oey (1997) finds that the decomposition of SSC meanders into eddies is always accompanied by an across slope change in sign of the PV gradient, such as in Figure 4.18. Oey (1997) suggests that this situation increases the likelihood of a baroclinic instability and encourages the breaking off of an eddy into the channel. The time period of progression is 4-5 days from the start of meander development to dissipation, corresponding well with the estimated meander growth period calculated by Sherwin et al. (2006a) for a first baroclinic mode instability. The temporally evolving PV field also illustrates a potential pathway for increased across channel exchanges of volume and heat through the extension of high PV filaments from the western edge of the Faroe Plateau toward the SSC, such as on year days 73-76. Also visible in Figure 4.18 is the formation and release of an eddy on yearday 76 at the northeastern corner of the Faroe Plateau.

Eddies just south of the Faroes may be partially attributable to cyclonic vorticity generation by the vertical movement of the density interface between the outflowing deep waters and surface inflows. This has been shown (Spall and Price, 1998) to produce an active cyclonic surface eddy field to the west in the Denmark Strait, through the production of cyclonic vorticity by the expansion (contraction) of the intermediate waters. The FSC conditions are not entirely analogous to those in the Denmark Strait, where the AIW layer is more pronounced and stretches by up to 100% during the passage of
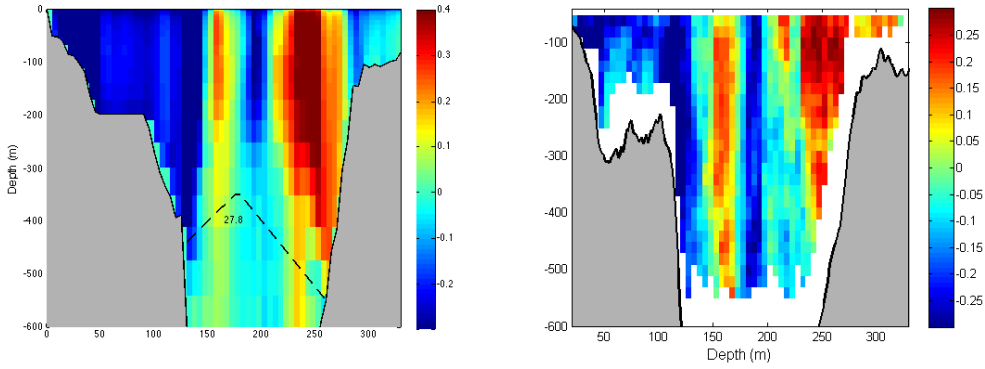
Figure 4.16: Vertical profile of northeastward velocity along the location of the Norröna transect at model yearday 73 during the passage of a cyclone/anticyclone pair (left). Norröna northeastward velocity showing a similar structure from a 2009 transect crossing (right) and associated cumulative transport across the channel.
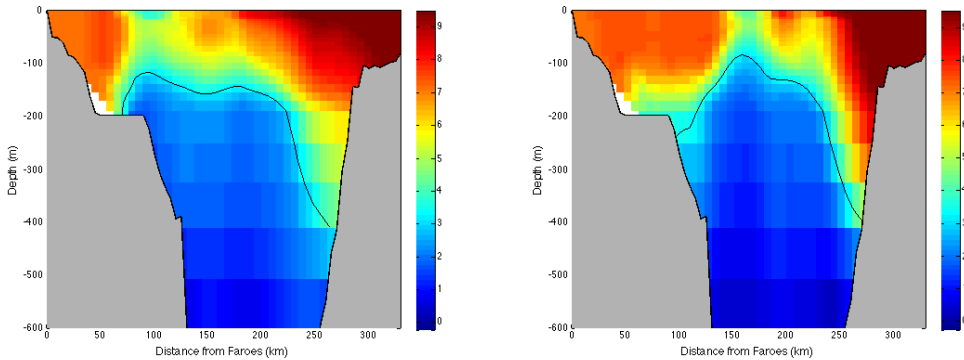
Figure 4.17: Vertical profile of temperature along a constant latitude section on yearday 72 (left) and 73 (right) of the model output showing the uplifted thermocline and cyclone/anticyclone pair seen in Figure 4.15. Black line indicates the depth of the 3^oC isotherm.
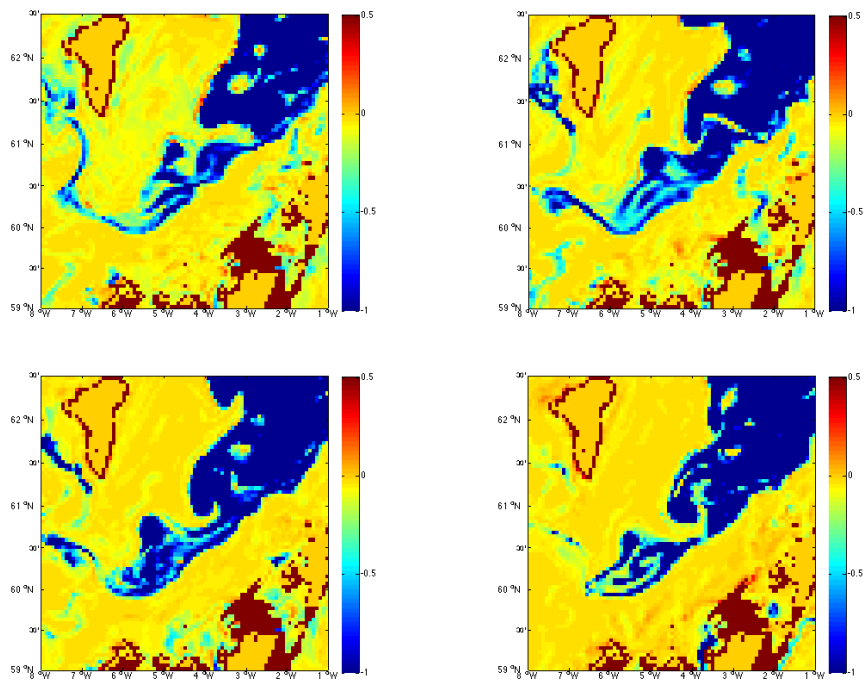
Figure 4.18: Potential Vorticity ($\times 10^{10}$) within the FSC for yeardays 73-76.

particularly strong bursts of dense outflows (Spall and Price, 1998). However, changes in the depth of the $\sigma_t<27.8$ isopleth in the FSC just south and west of the Faroes result in a vertical expansion (or contraction) of the upper water column, illustrated in Figure 4.19 by the enhanced vertical velocities on either side of the channel. By conservation of potential vorticity, this alteration in the vertical extent of the intermediate and upper water column along with negligible variations in f must necessarily accompany a change in relative vorticity.
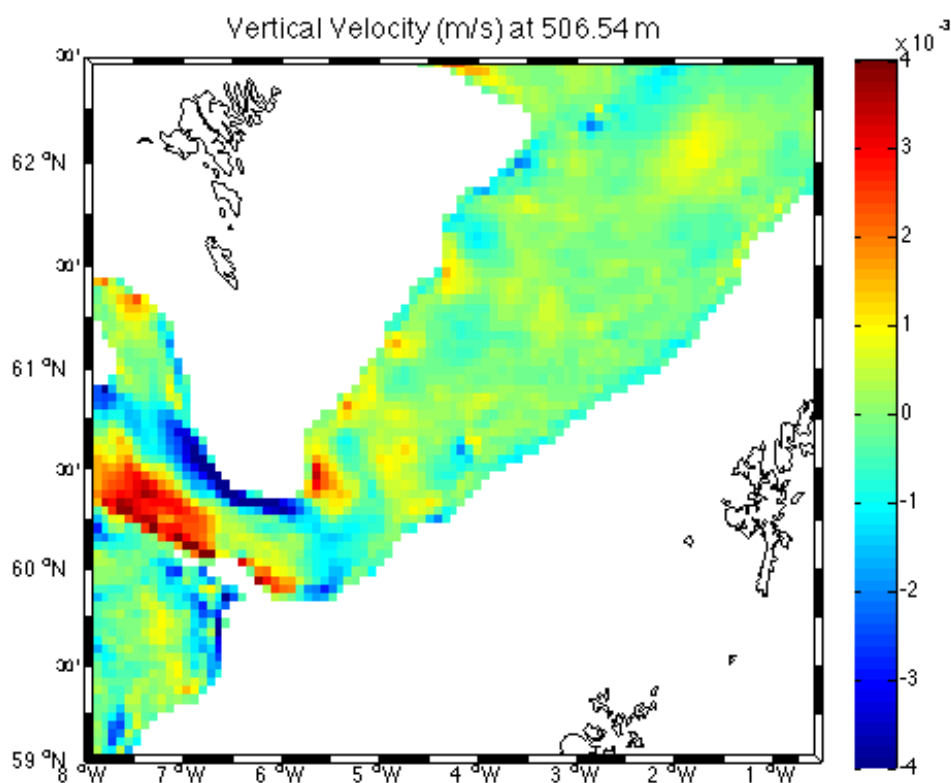
Figure 4.19: Average vertical velocity (in m/s) at 506 m depth, near the interface between the surface inflows and deep overflows for the full 60 day period. Enhanced vertical velocities are evident along either side of the deep channel southwest of the Faroes.

4.6 Summary

A description of the mean circulation, hydrography, and mesoscale fluctuations of the FSC has been presented using a high resolution, data assimilating configuration of the MITgcm. The model output correctly interprets the locations and magnitudes of the major circulation features in the region, but exaggerates their spatial structure, leading to an overestimation of volume flux. Relative transport estimates indicate that the southward transport originating north of the Faroes bifurcates north of 61ºN and between 6-7ºW into an westward component which follows the bathymetry around the Faroes Plateau, and a larger eastward component, which flows south then east to join the northeastward flowing SSC. The latter constituent has implications for the estimation of volume and heat transport across the Iceland Faroes Scotland Ridge, suggesting that calculations of volume and heat flux exclusively focused on the inflows may be overestimated.

Time varying components in the simulations with periods less than 2 months correspond well with direct observations and offer further insight into the formation, propagation, and dissipation of eddies and meanders in the channel. The size and frequency of both the SSC meanders and eddies agree with theoretical estimates for the given latitude range and hydrographic properties, as well as observations by drifter, satellite, and ADCP analyses. Meanders up to 60 km in both wavelength and amplitude are observed to form along the SSC, with a preferential formation region near 61ºN 4ºW. These meanders grow over approximately one week and move slowly toward the northeast before breaking, often shedding an eddy that moves northward through the FSC.

Eddies are almost omnipresent in the FSC, forming either due to an instability in the SSC or at the northeastern corner of the Faroes Shelf. Eddies forming from the SSC move first into the deeper FSC then slowly north and east. Faroes Shelf eddies move southward through the FSC, either dissipating in the central channel, or more frequently, being absorbed into the SSC around 61ºN. En route, the eddies disrupt the temperature gradients and circulation features on either side of the channel, briefly altering transports. Additionally the mesoscale rings in the channel alter heat transports, by drawing colder and fresher MNAW in to the channel and by often extending vertically below the surface AW layer (σ_t<27.8), possibly influencing deep outflows.

Chapter 5

The Sources and Pathways of the Southern Faroe Current

Abstract

In this chapter we connect the northward fluxes approaching the Iceland Faroes Scotland Ridge discussed in Chapter 3 with the observed (Chapter 2) and modeled (Chapter 4) cross ridge transports, through a closer examination of the around Faroes circulation. The southward flow oan the Faroe Shelf and Slope is a frequently observed feature of the FSC circulation, which has been attributed to both to tidal rectification around the Faroes (Larsen et al., 2008) and a recirculation of Faroe Current (FC) flows, ultimately joining the Shetland Slope Current (Sherwin et al., 2008) or some combination of the two (Rossby and Flagg, 2012). Here streamlines of velocity from the ECCO2 configuration of the MITgcm are used to predict the routes leading to the shelf and slope east of the Faroes, as well as the ultimate fate of the southward flux. Large short term fluctuations in velocities and passing features such as mesoscale eddies, exert significant influence over the streamline orientation and extent, especially west of the Faroes. The magnitude of flow (as indicated by the number of streamlines) reaching the Faroe Shelf and Slope from the Iceland Faroes Ridge (IFR) is shown to be negatively correlated (r=-.31) with the speed of the IFR inflow. No statistically significant correlation exists between the southward flow east of the Faroes and the FC strength. Streamlines originating over the Faroes Shelf and Slope generally turn eastward between the 200 - 500 m isobaths, likely joining the SSC. Flows

shallower than 100 m have a greater probability of turning westward at the southern end of the Faroe Plateau and circulating anticylonically.

5.1 Introduction

The Faroe Current (FC), which flows along the Iceland Faroe Front (IFF) and meanders across the ridge system between Iceland and the Faroe Plateau, before turning northward and forming the outer branch of the Norwegian Slope Current (NwSC), links the inflows across the Iceland Faroes Ridge (IFR) and Faroe Shetland Channel (FSC). In the 2nd chapter of this dissertation we used the Nuka Arctica observations to trace the mean transport path from 59.5^oN to the Iceland Faroes Shetland Ridge. There, we found that most of the North Atlantic Current traveling up the western edge of the Iceland Basin circulates cyclonically around the basin edge and along the Rekjanes Ridge toward the south. Only ~ 5 Sv crosses the ridge over the eastern half of the IFR. These IFR inflows (described in detail in Chapter 2) do not cross the ridge as a coherent current and are prone to large short term fluctuations. Once across the ridge, inflow waters encounter the IFF, a sharp temperature front between the inflowing Atlantic Water and cooler, fresher Nordic Seas water, and continue eastward along the front with the FC.

The FC transports Modified North Atlantic Water, a mixture of Atlantic Water (AW) and water of Arctic origin, which enters the region as part of the East Iceland Current (Swift and Aagaard, 1981), distinguishing it from the warmer and more saline AW inflows entering through the eastern FSC. East of the Faroes, a portion of the FC turns southward into the FSC along the Faroe Slope forming a surface outflow over the western FSC (Hátún, 2004; Sherwin et al., 2006b; Berx et al., 2013; Rossby and Flagg, 2012). This southward flux was clearly visible in both of the Norröna FSC sections (Figures 2.7 and 2.8) and is prone to interannual variations. Since there is little interannual change in the volume transported by the SSC, which crosses the three Nuka Arctica sections and the two Norröna routes with remarkably similar structure and volume flux (Figures 3.2 - 3.5), the southward flux over the western FSC contributes the greatest source of interannual variability in surface ($\sigma_t<28.5$) transport through the channel (Figure 2.9). Key to accurately estimating the mean transport across the Iceland Scotland Ridge is an understanding of the source and fate of this southward flux, including the relative contribution of recirculating IFR inflows and the proportion of

the flow entrained in the SSC.

The intrusion of MNAW into the FSC creates a distinct density front on the Faroe Shelf. The hydrographic properties of Faroe Shelf water are subject to seasonal variations, related to changing precipitation and rates of atmospheric cooling, which influence the severity of the front between the on-shelf water and the cooler, less saline waters of the central FSC (Larsen, 2009). Rather than strictly following the bathymetry of the Faroe Plateau, the frontal location is tied to the barotropic tide and mixed layer depth (Simonsen, 1999; Larsen et al., 2009) and its slope is geostrophically balanced (Larsen, 2009), but prone to disruption from episodic events such as the passage of mesoscale eddies (Sherwin et al., 2008). Rapid geostrophic responses to extreme high/low NAO phases also alter the water mass composition of the shelf, by changing the SSH gradient over the region and acting to sharpen/diminish the front north of the FSC, which influences the relative extension of the FC and MNAW into the channel (Chafik, 2012).

Upon reaching the southern end of the Faroe Shelf, the southerly MNAW flow, coined the Southern Faroe Current (SFC) by Larsen et al. (2008), splits into an eastward and westward component. Over the shallow shelf, ADCP observations indicate the presence of residual circulation due to the barotropic tide, which form an anticyclonic flow around the Faroes (Larsen et al., 2008). Drifter tracks suggest an eastern extension and entrainment of some of the FC deflection into the SSC (Hátún, 2004), but the relative magnitude of each and the location of bifurcation is unclear. Drifter observations by Sherwin et al. (2006b) estimate the average transport of the SFC to be 2.0 Sv southward, which is in relative agreement with the ∼2.5 Sv of southward flux observed by Rossby and Flagg (2012) and the 4.5 year average of 1.0 Sv reported in Chapter 2 of this dissertation. Farther south along the FIM line, Berx et al. (2013) observe only 0.8 Sv of southward flux and suggest that much of the retroflection may occur north of the line.

In the previous chapter, the use of the ECCO2 configuration of the MIT-gcm was shown to compare favorably with observations in the Faroe Shetland Channel and isolated 61ºN, 6-7ºW as the critical area for the divergence of the SFC. Here the model output is expanded to cover the full Faroe Plateau and used to look more closely at the behavior, fate, and source of the southward flux along the Faroe Shelf and Slope, and especially at its expected behavior along the observational sections considered throughout this dissertation. The model output is not expected to be a perfect representation of observed behavior and lacks the temporal coverage needed to explore the seasonal and

interannual fluctuations of the SFC, however it offers an interesting insight in to the circulation dynamics of the Faroe Shelf and Slope and the pathways of AW and MNAW between the observational routes.

5.2   Data and Methods

The analyses in this chapter are based on the same model output as Chapter 4, and therefore follow the same configuration and boundary conditions. Here we use streamlines based on daily velocity (to reduce the impacts of tides) as the method for interpreting the source and fate of Faroe Shelf and Slope flows. It is important to note that streamlines are a snapshot of the velocity for a given time and depth. This is in contrast to pathlines, which follow the flow of a particle through a time evolving velocity field. The choice of streamlines over path lines is primarily one of computational limitations, however because the velocity field changes gradually - usually over 2-3 days, the choice still offers insight in to the behavior of the system. Additionally, the focus here is on 3 depths (60 m, 125 m, and 300 m) over the eastern IFR and two isopycnal layers (σ_T=27.5, 27.6) through the FSC, and neglects vertical motion. This assumption is likely contradicted, especially in regions of intense mixing. However, it is justified by the comparatively small magnitude of vertical motions relative to lateral advection over the IFR, and the unlikelihood of a particle being mixed out of the mostly depth independent velocities over the upper several hundred meters of the water column over the course of one day. Within the FSC variations in depth due to vertical velocities are mitigated with the use of isopycnal surfaces.

Streamlines are initiated at a series of starting locations over the IFR, as well as the Faroe Shelf and Slope. The IFR streamlines begin at locations west of the Faroes, both north and south of the Ridge. For comparison, a complementary set of streamlines are constructed originating from the observational routes of the Nuka Arctica, Norröna, and the Line N observations (e.g. Hansen et. al [2003, 2010]). Over the FSC, streamlines start from a dense network of nodes spanning the width of the Faroe Shelf and Slope over every 0.5 degrees of latitude. For each daily velocity field, the number of streamlines entering each of 3 boxes is used to determine the location and magnitude of the diverging components of the southward flux. Each streamline is only counted once per box, per day (for instance if a streamline is trapped within an eddy and circulates through a given box twice in one day,

it is still only counted as one entry into that box), producing daily snapshots of the concentrations of flows throughout the region. The streamline integration interval is ∼0.48 km, 0.1 of a grid box for 1000 and 1150 steps for the eastern IFR and FSC, respectively. The associated time period is approximately 2 weeks, beyond the 2-3 days expected for the evolution of local velocities, however it is necessary to allow streamlines to span the distances associated with passage across the IFR and along the full channel length of the FSC.

5.3   Results

5.3.1   Flow paths from the IFR to the Faroe Shelf

The average velocity field (streamlines in Figure 5.1) for the full 60 day period, inclusive of tides, reflects the complicated system of pathways and meanders that occur near the IFR. The Norröna observations indicate inflows over the eastern half of the IFR, so we consider only model output from this domain (14^oW - 7^oW). The modeled velocities are generally directed across the ridge over this section, but with less coherent structure than the observations. This may be partially attributable to a difference in season between the observations (weighted toward summer months) and numerical simulations (spanning winter and early spring). The modeled streamlines extend north of 63^oN before veering east toward the Faroes. Just north of the ridge, the eastward Faroes Current (FC), flows along the Iceland Faroes Front (IFF). The observed meandering and instability formation along the edges of the FC (Beaird, 2013) are evident in the model output.

Starting nodes for streamlines span the eastern half of the IFR, both north and south of the ridge, offering insight into the relative impacts of the FC and inflow from the Atlantic. Snapshots of the streamlines originating from all nodes on each day of the model output at 125 m depth are used to determine the percentage of days (out of the 60 days of model output) that a streamline initiated at each node crosses the red box on the Faroe Shelf (Figure 5.2). As expected, streamlines originating from nodes far to the north and south of the Faroes do not reach the FSC, and those that begin close to or on the Faroe Plateau are most likely to circulate into the FSC. Streamlines initiated just west and north of the Faroes enter the box east of the Faroes on 10 - 30% of the model output days. The greater likelihood of streamlines originating at
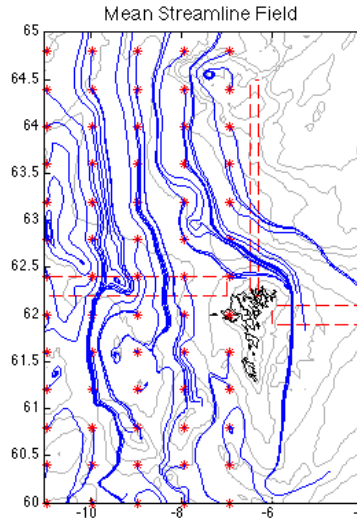
Figure 5.1: Streamlines based on the average velocities over the eastern IFR starting at the red star locations. The number of streamlines passing through each red box is used as an indicator of the magnitude and temporal variability of flow around the Faroes.

these nodes to cross through the box support the idea of an anticyclonic flow around the island group. In general the percentage of streamlines reaching the Faroe shelf from a given node decreases gradually with distance from the Faroes toward the north and west, and more rapidly toward the south.

Of particular interest to this dissertation is the similarity of the flow crossing each of the observational routes over the IFR, and the likelihood of the inflows measured across the Norröna, Nuka Arctica, and Line N sections to enter the FSC. The percentage of streamlines starting along each observational route to enter each of three boxes around the Faroe Plateau is shown for 125 m depth in Figure 5.3. It is worth emphasizing here that the daily streamline fields are snapshots, and the actual time required for a particle originating along each route to cross through Boxes 1 - 3 is more likely on the order of days. The spatially variable probabilities over the southernmost Nuka Arctica line illustrates the importance of topography in guiding flows toward and over the IFR. Moving from west to east around the Faroes, the percentage of streamlines reaching 62.5°N, Box 1, from the Nuka Arctica section generally increases with westward distance unless the
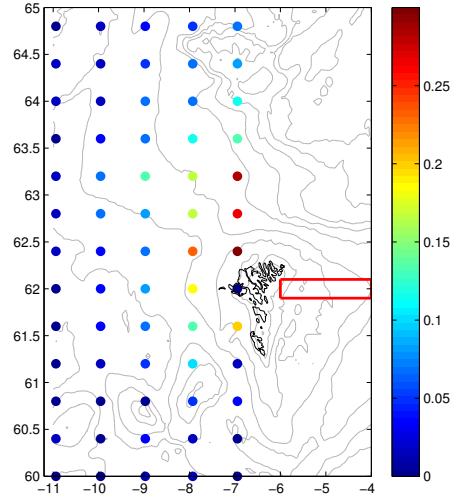
Figure 5.2: Percent of days during which a streamline originating at each node that passes through the red box east of the Faroes. Contours indicate bathymetry at 50 m, 100 m, 200 m, and every 500 m from 500-3000 m.

origination node is directly over a steep bathymetric feature, such as at 61°N 5°W. Overall, few streamlines from the Nuka Arctica line extend farther than Box 1 in each daily velocity field. This is unlike streamlines beginning along the Norröna section, especially close to the Faroe Plateau, which are divided almost equally between fluctuating around the crest of the IFR and crossing into Box 1, or continuing eastward along the bathymetry north of the Faroes. Line N streamlines show less variability and few flow reversals. Most streamlines south of 64°N extend eastward and those nearest the Faroes often turn southward into the FSC. While farther north on Line N, streamlines originating north of the 2000 m isobath continue toward the west.

Using 125 m depth as a reference, we consider daily snapshots of streamlines originating along the observational routes as examples of the range of streamline behavior (Figure 5.4). The highest streamline counts occur for Boxes 2 and 3 when a coherent eastward flux is present north of the Faroes with minimal disruption from mesoscale eddies, such as on Day 45. In comparison, greater eddy activity on Days 61 and 85 (not shown) coincides with a greater number of streamlines entering the FSC, and in the case of Day 83,
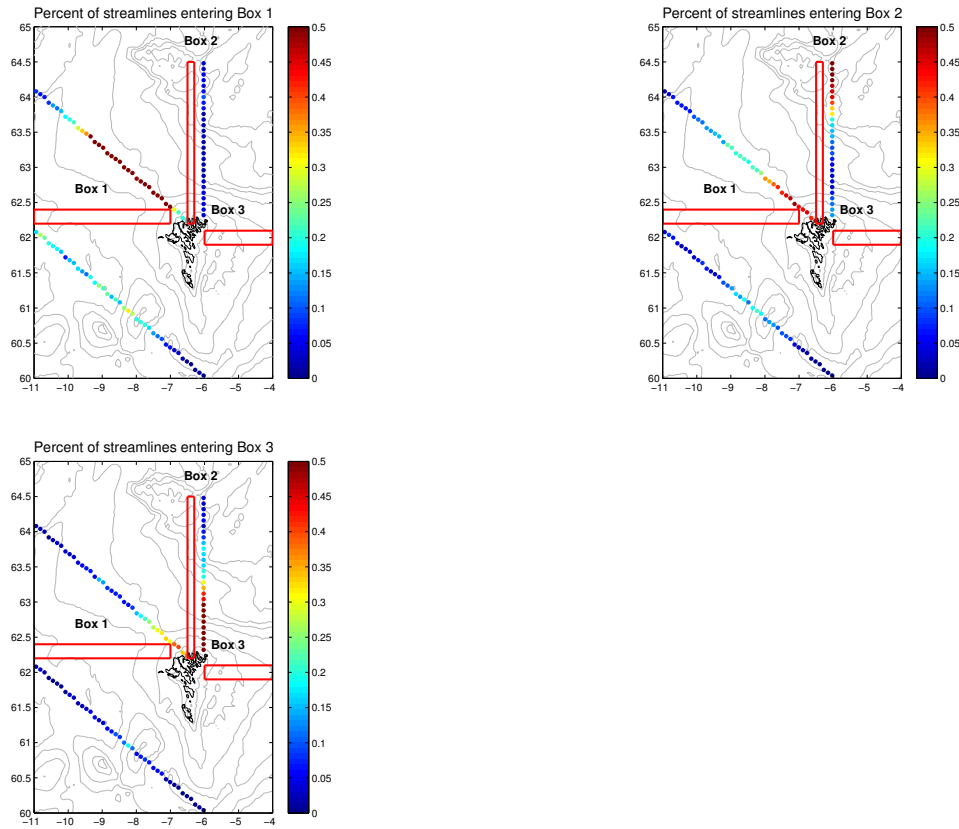
Figure 5.3: Percent of streamlines reaching each box based on origination node. Bathymetry contoured at 50 m, 100 m, 200 m, and every 500 m from 500-3000 m.

an increased inflow from south of the IFR. Anomalous streamline counts occur in all boxes on Day 72 (high in Box 1 and low in Boxes 2 and 3). A noted absence of the eastward flows north of the IFR and few mesoscale circulation features, suggest that a coherent FC is absent from the domain on that day. This coincides with streamlines originating from the Norröna and Nuka Arctica sections extending toward the southwest and those starting along Line N making a rare entrance into Box 2, before continuing southward into the FSC.
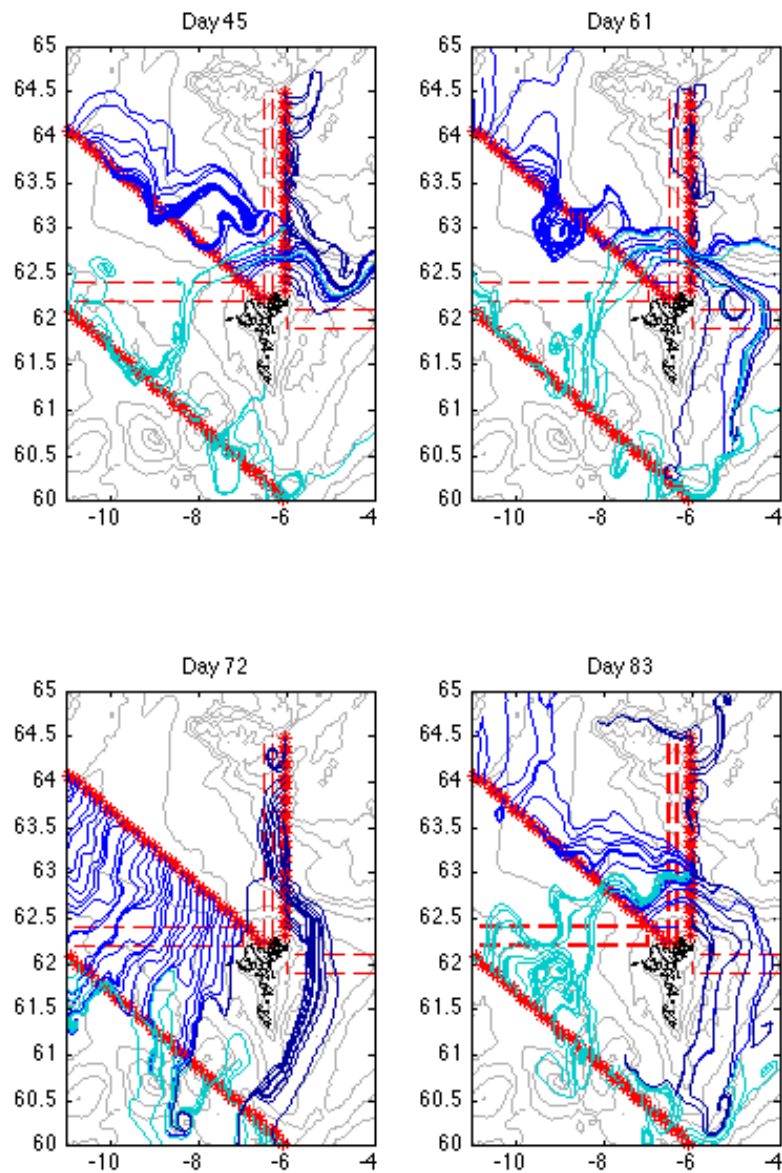
Figure 5.4: Daily streamlines originating from each node for a selection of dates. Bathymetry contoured at 50 m, 100 m, 200 m, and every 500 m from 500-3000 m.

5.3.2 Bifurcation of the Faroes Shelf and Slope Flow

Once within the FSC, waters may exit the channel through a variety of means. The most obvious are rapid entrainment into the SSC near the southern end of the Faroe Plateau, or circulation around the Faroese shelf toward the west and north. Alternatively, a particle released on the Faroese shelf may also be trapped by an eddy as it passes through the central channel or as part of an instability along the western edge of the SSC, prolonging its time within the FSC before it is likely entrained back in the inflow on the Shetland side. Particles may also exit the domain to the south, neither turning east with the SSC, nor circling the Faroe Plateau. Water following a route south of the Faroe Plateau likely mixes with the NAW south of the channel and returns later as part of the SSC inflow. Streamlines originating over the Faroe shelf and slope predict the division of Faroe Shelf water amongst these competing dynamics.

Unlike the eastern IFR, which is occupied almost exclusively by MNAW, current pathways in the FSC encounter several water masses. In particular, the substantial change in depth of isopycnals from the eastern to western sides of the FSC are expected to significantly impact the depth of streamlines. For this reason, FSC streamlines are presented on two isopycnal surfaces within the range of potential densities of MNAW, σ_t=27.5, 27.6 (visible as black dotted lines in the upper panels of Figure 4.7, since these extend across the full horizontal distance of the channel). These streamlines extend over 1150 steps of one tenth of a grid cell, corresponding to a total distance to approximately 544 km, equivalent to the along channel length. While this overestimates the time period any particle would be exposed to a given set of daily velocities, it does offer insight to the flow fields most conducive to circulatory or entrained flow at the southern end of the Faroe Plateau.

Streamlines resulting from the average velocity field on σ_t=27.5 (Figure 5.5) indicate that flows originating east of the Faroes preferentially move south and split into eastern and western components at approximately 60°N, 6-7°W, consistent with the transport comparison in Chapter 4. No streamlines circulate anticyclonically around the Faroes on this isopycnal layer, either due to its depth or the strong southward flux present in the average circulation.

Daily percentages indicate that 20 - 30% of streamlines initiated shallower than the 200 m isobath on the σ_t=27.5 surface reach the FAR box (Figure 5.6). Streamlines starting farther east are more likely to turn toward the SSC,
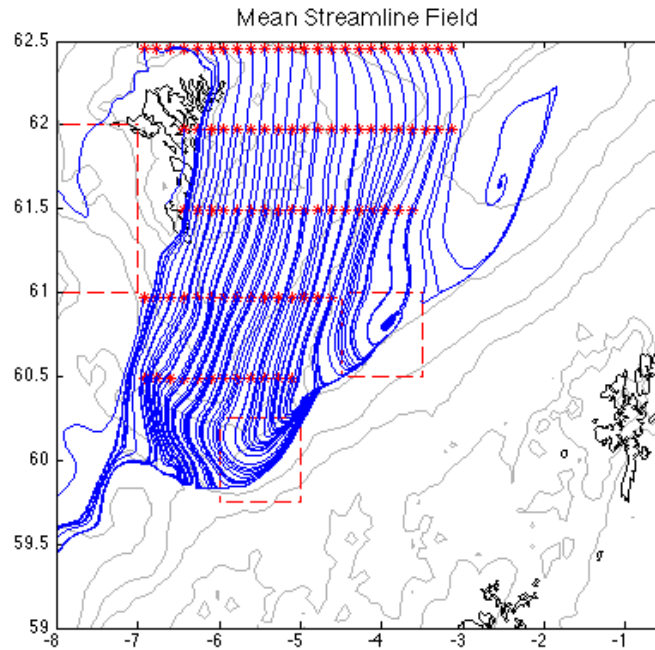
Figure 5.5: Locations of the streamline origination points in the FSC and streamlines of the average velocity on the σ_t=27.6 in the FSC. Red boxes indicate the FAR, SSC 1, and SSC 2 locations, which are monitored for streamline quantity.

resulting in more than 50% (30 days) of daily streamlines on the central shelf reaching SSC 1. Approximately half of those streamlines continued into SSC 2. Additionally >50% of the streamlines originating along the outer edges of the Faroe shelf also enter SSC 2.

The varied orientation of daily streamlines is illustrated in Figure 5.7 for the σ_t=27.5 isopycnal surface. In comparison to streamline activity west and north of the Faroes, greater coherence and structure is discernible in the Faroe Shelf and Slope circulation. Mesoscale eddies substantially alter the mean flow over the northeastern Faroe shelf (Figure 5.7, Day 67) as well as in the central FSC (Figure 5.7, Days 59, 67, 73, and 78), influencing the behavior of the eastward component of the Faroe Shelf/Slope bifurcation. Many streamlines wrap cyclonically within the SSC boxes, and are likely later entrained into the northeastward SSC flow. In some instances, such
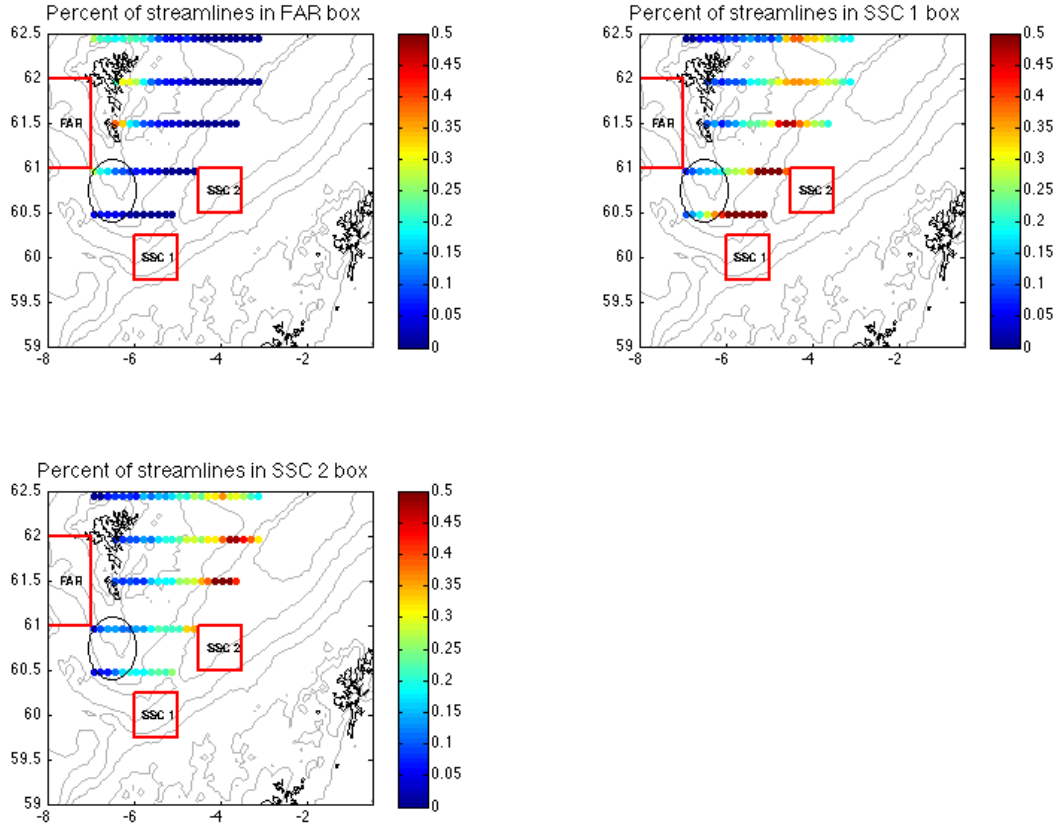
Figure 5.6: Percent of streamlines reaching each box on the σ_t=27.6 plane based on origination node. Bathymetry contoured at 50 m, 100 m, 200 m, and every 500 m from 500 - 3000 m.

as on Day 78 (Figure 5.7), the westward component turns northward to continue anticyclonically around the Faroes, but does not complete a full rotation within the allotted number of steps.
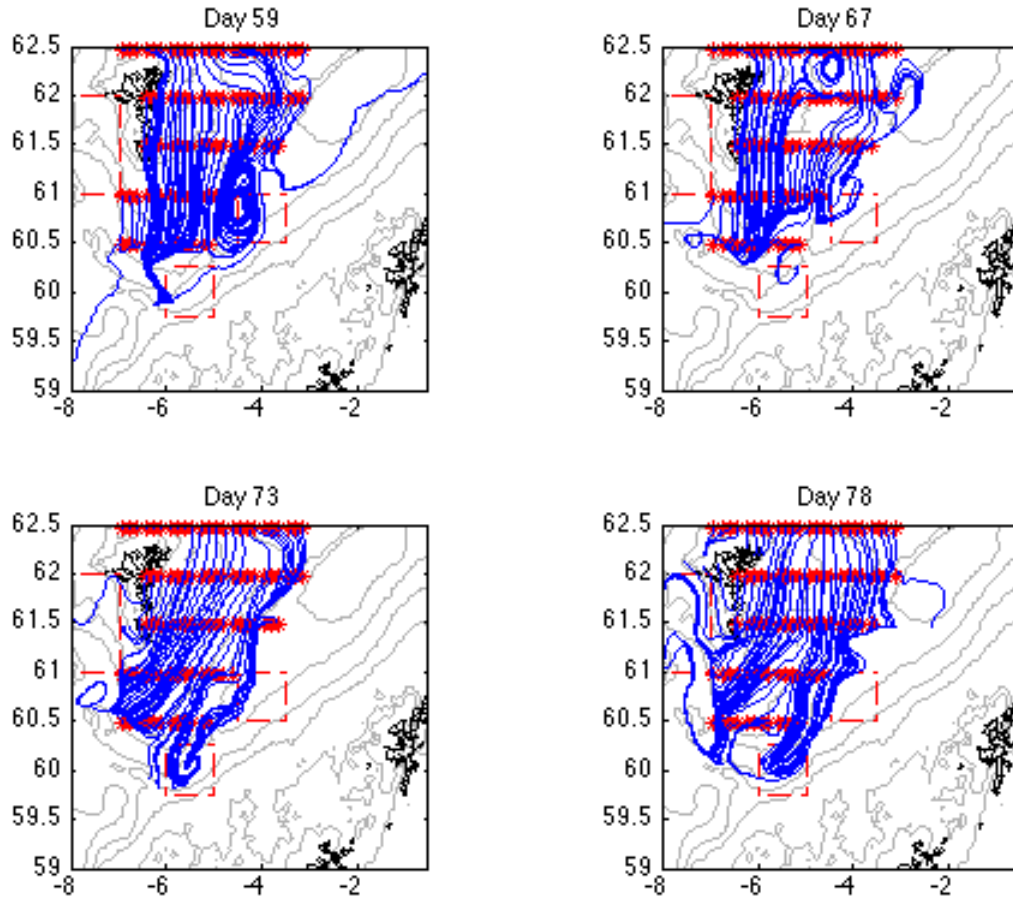
Figure 5.7: Daily streamlines originating from each node on the σ_t=27.6 isopycnal surface for a selection of dates. Bathymetry contoured at 50 m, 100 m, 200 m, and every 500 m from 500-3000 m.

5.4 Discussion

The likelihood of streamlines reaching the specified locations around the Faroes varies with depth and time. The relative proportion of streamlines crossing Boxes 1 - 3 around the Faroe shelf is generally preserved with increasing depth, however excluding the shallow Faroe shelf nodes reduces the total number of streamlines (Figure 5.8). The largest circulation features

on the western side of the Faroes are the inflow over the IFR and the FC along the IFF. To determine the relative importance of each, the temporal variability of the streamline positions are compared to the average current speed over the eastern half of the IFR between 62-63ºN (IFR inflow in Figure 5.8) and in the region of strongly eastward flows north and just west of the Faroes (FC in Figure 5.8). Highest time series correlations exist between the IFR inflow and Box 1 and the FC magnitude and Box 2, since the currents directly flow through each of these boxes. Weak, but statistically significant (p<0.05) correlations also exist between Boxes 1 and 3 (r=-0.37) and the IFR inflow and Box 3 (r=-0.31). This indicates that an increased inflow speed over the ridge often coincides with a decrease in southward circulation into the FSC. Since the strength of the FC and the number of streamlines entering Box 3 is not correlated, this further implies that the strength of the inflow across the eastern IFR has a greater effect on the southward flux into the FSC, than the magnitude of velocities north of the Faroes.

The lack of a significant correlation between the IFR inflow and streamlines in Box 2 suggests that the daily quantity of streamlines moving eastward, directly north of the Faroes depends more on changes in the FC strength than the magnitude of the IFR inflow. Further conclusions cannot be made without a longer time series, but this may introduce a temporal discrepancy when comparing transports collected along the Norröna section, which directly measures IFR inflows, to Line N, which includes contributions from both IFR inflows and the FC.

Upon reaching the FSC, the southward flowing MNAW is actively influenced by variations in the SSC strength and the active mesoscale eddy field of the central FSC. Similar to west of the Faroes, the mostly depth independent velocities over the Faroe Shelf and Slope result in a similar relative proportion of streamlines that reach each box with increasing depth/density (Figure 5.9). The decrease in the absolute number of streamlines reaching each box with increasing density is largely due to the exclusion of shallow streamlines and a smaller area of coverage by the streamlines. The quantity of streamlines entering the FAR box is generally less than for the SSC boxes, since these primarily originate from the shallower nodes. Temporal variability in the FAR box is moderately correlated (r=0.40, p<0.01) with the magnitude of the Faroe Shelf flow, suggesting that a stronger retroflection from north of the Faroes may be related to an increase in anticyclonic circulation around the Faroes. Streamlines entering SSC 2 on both isopycnal surfaces in Figure 5.9 (σ_t=27.5, 27.6) generally do so after crossing through
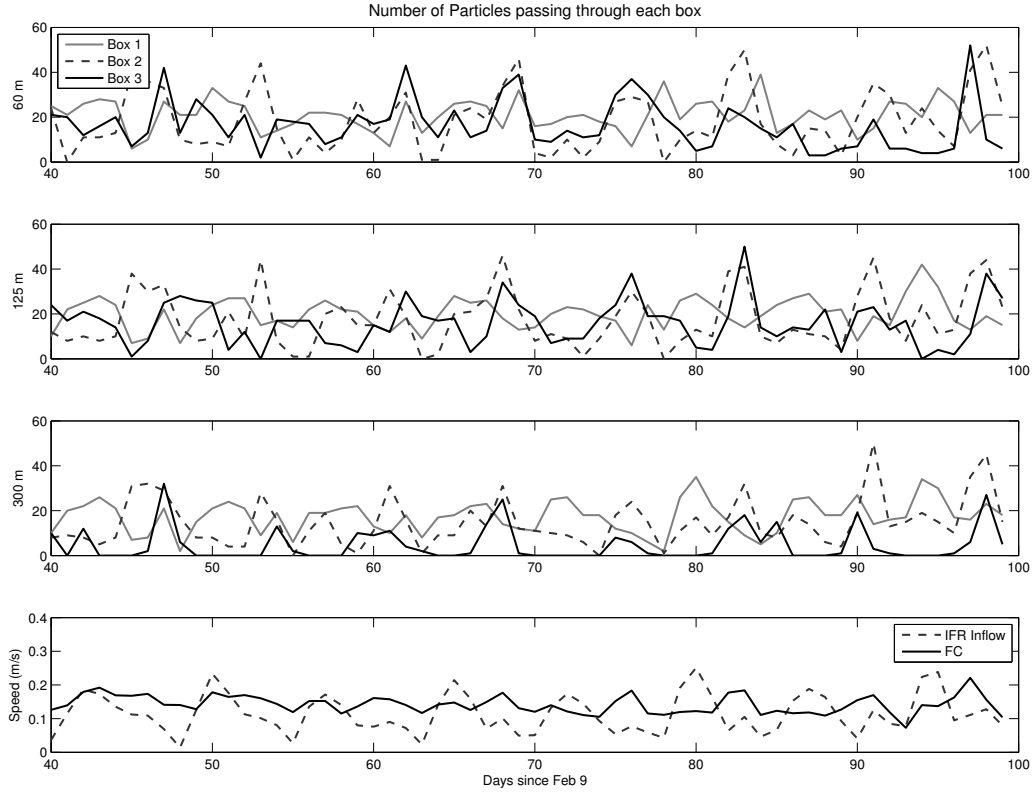
Figure 5.8: Temporal variability in the number of streamlines reaching boxes 1 - 3 for 60 m (top), 125 m (second), and 300 m (third) depth. The bottom panel shows the daily average speed for the IFR inflow and FC within the domain.

SSC 1 and continuing northeast with the SSC, however early in the simulation period and especially on the shallower isopycnal surface, some SSC 2 streamlines bypass the SSC 1 box and enter as part of southerly flows originating over the far eastern Faroes shelf and slope. This may be related to the strength of the inflow SSC since a moderate (r=-0.50) and statically significant (p<0.01) negative correlation exists between the number of SSC 2 streamlines and the magnitude of the SSC on σ_t=27.6 (also significant but slightly weaker on σ_t=27.5). This suggests that a weaker SSC corresponds to

99

less streamlines in SSC 2, perhaps due to greater central FSC eddy activity. The number of streamlines in the SSC 1 box is not significantly correlated with the strength of either the Faroe Slope flow or the SSC.

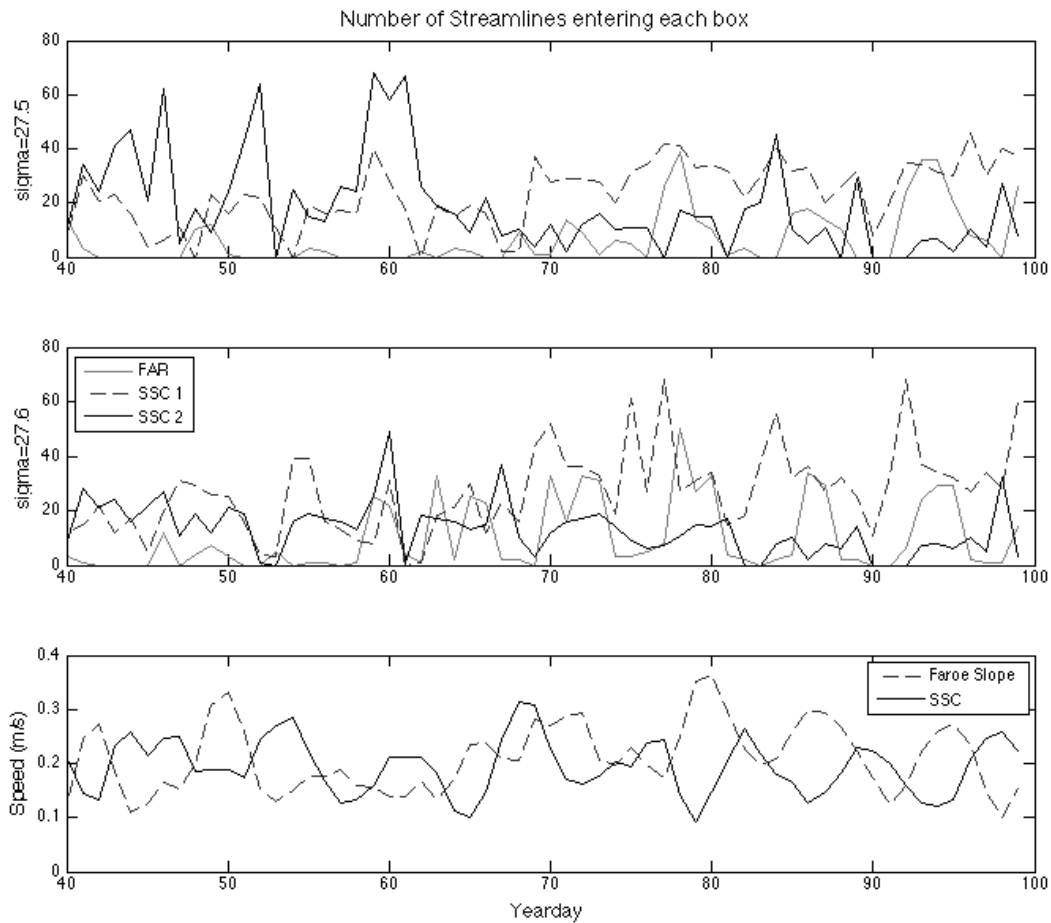Figure 5.9: Time Series of the number of streamlines in each box per day for σ_t=27.5 (top), σ_t=27.6 (second), and current speed (third). Note the varying y-axis scales. The bottom panel is a time series of the speed of the Faroe Slope flow and Shetland Slope Current averaged over the region of highest magnitude for each.

Topography strongly influences the velocity field throughout the region

and plays a significant role in the circulation around the Faroes. This is evident in the variable percentage of streamlines entering Box 1 from the Nuka Arctica track near the seamount at 60.8ºN 8.3ºW (Figure 5.3) and especially in the divergence of Faroe Shelf flows (Figure 5.6). A strong demarcation occurs around the 200-300 m isobaths east of the Faroes that separates the eastward and westward tending flows. Flows over the shelf regions shallower than 300 m are much more likely to circulate anticyclonically around the Faroes, and no water in regions deeper than 500 m follow the bathymetry of the Faroe Plateau westward. The eastern shelf regions and the steepest portions of the Faroe Slope are more likely to be entrained in the SSC, with half of the daily streamlines encountering the SSC at the southern end of the Faroe Plateau. Further entrainment may occur through the absorption of eddies comprised of MNAW farther north in the FSC (as described in the previous chapter), and occasionally (10-15% of model output period) flows shoreward of the 100 m isobath become entrained in the SSC.

Mean velocity profiles across the Norröna sections from observations and numerical simulations show a mean southward flux from the Faroes to just east of the 400 m isobath. The strongest southward velocity magnitudes (and greatest transport) occur between the 200-400 m isobaths. Results shown here imply that within that region the majority of the observed southward transport (∼1 Sv) is entrained in the SSC, with only a small fraction likely to circulate west around the Faroes. In contrast, the 0.2 - 0.5 Sv of observed southward transport over the shallower Faroe Shelf is more likely to circulate westward around the Faroes Plateau, with that likelihood increasing with decreasing shelf depth. Near contemporaneous sections of the IFR and FSC in the Norröna observations are currently limited, but if these results are any indication, it is expected that observations of heightened inflow speeds over the IFR will coincide with a decrease in surface outflow through the FSC.

5.5   Summary

Streamlines, representative of the path taken by a particle in a given velocity field over a one day snapshot, indicate the behavior of flow entering the FSC from the north and its subsequent divergence near the southern end of the Faroe Plateau. As anticipated, streamlines enter over the eastern IFR and then continue eastward along the IFF, before a variable portion of the flow diverges into the FSC. En route, an active mesoscale eddy field often disrupts

the mean flow. The number of streamlines reaching the Faroe Shelf and Slope from the IFR has a greater statistical relationship with the magnitude of IFR inflows over the eastern half of the ridge than with FC strength to the north of the Faroes. A decreased IFR inflow speed is correlated with an increase in streamlines east of the Faroes, implying a stronger anticyclonic circulation. Alternatively, temporal fluctuations in the FC are significantly correlated with the number of streamlines extending north of the Faroes, but do not have a significant influence over the quantity of streamlines entering the FSC.

Upon entering the FSC from the north, streamlines originating between the 200-500 m isobaths usually ($>$50% of model output days) turn eastward at the southern end of the Faroe Plateau, and are likely to be entrained in the SSC. A statistically significant correlation between the SSC 2 streamlines and the speed of the SSC implies that this is especially true when the SSC velocities are anomalously weak. Further entrainment into the SSC may occur through absorption of MNAW eddies that break off from the mean southward flow, or through an eastward turning of streamlines that exit the domain to the south. Faroe Shelf flows shallower than the 100 m isobath are more likely to circulate anticyclonically around the Faroes than be entrained into the SSC.

Temporal variability of the streamlines originating from the observational routes around the Faroes indicates a correspondence between inflows measured over the eastern portion of the Norrna's IFR section and southward flows along the Faroese slope in the FSC sections. Despite the necessity of the IFR inflows to cross Line N prior to entering the FSC, the temporal fluctuations north of the Faroes more closely resemble the strength of the FC, which masks the variations in IFR inflow speed. The streamlines further suggest that the majority of southward transport measured by the Norröna's FSC routes turns eastward at the southern end of the Faroe Plateau and is entrained in the SSC, with only the 0.2-0.5 Sv of shelf flow likely to follow an anticyclonic route. Furthermore, the divergence between the eastward and westward portions of the SFC occurs north of the FIM line, explaining the lack of southward flux observed crossing that section.

Chapter 6

Conclusions

Long term, repeated observations of the cross ridge exchanges provide essential insight into the spatially and temporally variable dynamics of the Iceland Faroes Scotland region. This dissertation emphasizes the contributions of ADCP measurements made by ships in regular traffic, by presenting direct observations of velocity over the full FSC and IFR sections (Chapter 2) and establishing internal consistency with similar observations over the basin and banks regions to the south (Chapter 3). The observations are complemented with high resolution numerical simulations, which clarify the spatial and temporal variability of the rates and pathways of surface flows through the FSC (Chapter 4) and illustrate the connectivity of the IFR and FSC (Chapter 5).

AW approaches the Iceland Faroes Shetland Ridge in bands of largely depth independent flow split almost equally between the Iceland Basin and the shallow regions east of Hatton and Rockall Banks (Chapter 3, Figure

To the east of the Iceland Basin, inflows are separated into a wider band along Bligh Bank and a narrower, but stronger contribution along the Scottish Slope. By 60ºN the Scottish Slope flow has developed into the >3 Sv Shetland Slope Current and continues as such over the eastern side of the FSC (Chapters 2, 3). Meanders of up to 60 km grow over weekly timescales along the western edge of the FSC, often shedding cyclonic eddies during their dissipation (Chapter 4). Along with eddies sourced at the northern edge of the Faroe Plateau, these rings disrupt the mean circulation of the channel and temporally alter the local volume flux (Chapter 4).

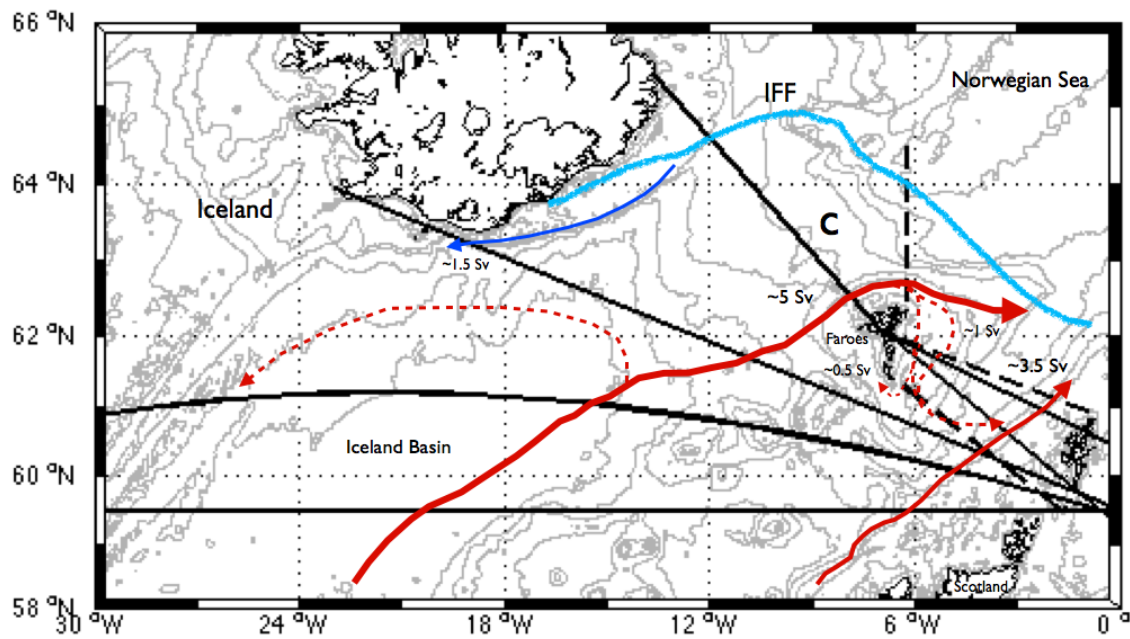Figure 6.1: Cartoon of the major surface currents crossing the Iceland Faroes Scotland Ridge. Ship of opportunity routes shown in black (Nuka Arctica and Norrona) and moored ADCP and repeat hydrographic routes shown in dotted black (Faire Isle Munken, Nulsa Flugga, Line N). Waters of Atlantic origin are colored red and Nordic Sea origin are blue. The light blue line is the mean position of the Iceland Faroes Front.

Bibliography

JT Allen, DA Smeed, and AL Chadwick. Eddies and mixing at the iceland-Færæ front. *Deep Sea Research Part I: Oceanographic Research Papers*, 41(1):51–79, 1994.

Nicholas Littlejohn Beaird. *Meridional Exchanges and Mixing at the Iceland-Faroe Ridge*. PhD thesis, 2013.

B. Berx, B. Hansen, S. Osterhus, K.M. Larsen, T. Sherwin, and K. Jochumsen. Combing in-situ measurements and altimetry to estimate volume, heat and salt transport variability through the Faroe Shetland Channel. *Ocean Science Discussions*, 10:153–195, 2013.

Karin M Borenäs, Irène L Lake, and Peter A Lundberg. On the intermediate water masses of the faroe-bank channel overflow. *Journal of Physical Oceanography*, 31(7):1904–1914, 2001.

AS Bower, B Le Cann, T Rossby, Walter Zenk, J Gould, K Speer, PL Richardson, MD Prater, and H-M Zhang. Directly measured mid-depth circulation in the northeastern North Atlantic Ocean. *Nature*, 419 (6907):603–607, 2002.

C Carollo, I Astin, J Graff, et al. Vertical structure of currents in the vicinity of the Iceland-Scotland Ridge. In *Annales Geophysicae*, volume 23, pages 1963–1975, 2005.

L Chafik, T Rossby, and C Schrum. On the spatial structure and temporal variability of poleward transport between Scotland and Greenland. *Journal of Geophysical Research: Oceans*, 2014.

Leon Chafik. The response of the circulation in the Faroe-Shetland Channel to the North Atlantic Oscillation. *Tellus*, 64(18423), 2012.

Lawrence K Coachman and Knut Aagaard. *Physical Oceanography of Arctic and Subarctic seas.* Springer, 1974.

Bob Dickson, Stephen Dye, Steingrimur Jonsson, Armin Kohl, Andreas Macrander, Marika Marnela, Jens Meincke, Steffen Olsen, Bert Rudels, Hedinn Valdimarsson, and Gunnar Voet. The overflow flux west of Iceland: Variability, origins and forcing. In *Arctic-subarctic Ocean Fluxes*, pages 443–474. Springer, 2008.

Harry D Dooley and Jens Meincke. Circulation and water masses in the Faroese Channels during Overflow '73. *Deutsche Hydrografische Zeitschrift*, 34(2):41–55, 1981.

Maureen Dunn. *A description of the barotropic tide on Georges Bank based upon five years of shipboard ADCP observations.* PhD thesis, State University of New York at Stony Brook, 2002.

Gary D Egbert and Svetlana Y Erofeeva. Efficient inverse modeling of barotropic ocean tides. *Journal of Atmospheric and Oceanic Technology*, 19(2):183–204, 2002.

E Gaard and B Hansen. Variations in the advection of calanus finmarchicus onto the faroe shelf. *ICES Journal of Marine Science: Journal du Conseil*, 57(6):1612–1618, 2000.

Adrian E Gill. *Atmosphere-ocean dynamics*, volume 30. Academic press, 1982.

R Lee Gordon and John M Huthnance. Storm-driven continental shelf waves over the Scottish continental shelf. *Continental Shelf Research*, 7(9):1015–1048, 1987.

RW Griffiths and PF Linden. The stability of buoyancy-driven coastal currents. *Dynamics of Atmospheres and Oceans*, 5(4):281–306, 1981.

Sirpa Häkkinen, Peter B Rhines, and Denise L Worthen. Northern North Atlantic sea-surface height and ocean heat content variability. *Journal of Geophysical Research: Oceans*, 2013.

B. Hansen, S. Osterhus, W.R. Terrell, S. Jonsson, H. Valdimarsson, H. Hatun, and S.M. Olsen. The inflow of Atlantic Water, heat, and salt to the

Nordic Seas across the Greenland-Scotland Ridge. In *Arctic-subarctic Ocean Fluxes*, pages 15–43. Springer, 2008.

B Hansen, H Hátún, R Kristiansen, SM Olsen, and S Østerhus. Stability and forcing of the Iceland-Faroe inflow of water, heat, and salt to the Arctic. *Ocean Sci*, 6:1013–1026, 2010.

Bogi Hansen and Svein Østerhus. North Atlantic–Nordic Seas exchanges. *Progress in Oceanography*, 45(2):109–208, 2000.

Bogi Hansen, Svein Østerhus, Hjalmar Hátún, Regin Kristiansen, and Karin Margretha Húsgar Larsen. The Iceland–Faroe inflow of Atlantic water to the Nordic seas. *Progress in Oceanography*, 59(4):443–474, 2003.

Hjálmar Hátún. *The Faroe Current*. University of Bergen, 2004.

Bjørn Helland-Hansen and Fridtjof Nansen. The norwegian sea. *Report on Norwegian Fishery and Marine Investigations 2, Kristiania*, page 390, 1909.

SL Hughes, WR Turrell, B Hansen, and S Østerhus. Fluxes of Atlantic Water (volume, heat and salt) in the färoe–shetland channel calculated from a decade of acoustic doppler current profiler data (1994–2005). frs collaborative report 01/06. *Fisheries Research Services Collaborative Report*, (01/06), 2006.

Philip K Jakobsen, Mads H Ribergaard, Detlef Quadfasel, Torben Schmith, and Christopher W Hughes. Near-surface circulation in the northern North Atlantic as inferred from Lagrangian drifters: Variability from the mesoscale to interannual. *Journal of Geophysical Research: Oceans (1978–2012)*, 108(C8), 2003.

Peter D Killworth, Nathan Paldor, and Melvin E Stern. Wave propagation and growth on a surface front in a two-layer geostrophic current. *Journal of Marine Research*, 42(4):761–785, 1984.

O. Knutsen, H. Svendse, S. Osterhus, T. Rossby, and B. Hansen. Direct measurements of the mean flow and eddy kinetic energy structure of the upper ocean circulation in the NE Atlantic. *Geophysical Research Letters*, 32(L14604), 2005.

G. Lagerloef. Topographically controlled flow around a deep trough transecting the shelf off Kodiak Island, Alaska. *Journal of Physical Oceanography*, 13:139–146, 1983.

Karin Margretha H Larsen, Bogi Hansen, Regin Kristiansen, and Svein Østerhus. Internal tides in the waters surrounding the Faroe Plateau. In *Proceedings of ICES 2000 Annual Conference*, 2000.

Karin Margretha H Larsen, Bogi Hansen, and Harald Svendsen. Faroe shelf water. *Continental Shelf Research*, 28(14):1754–1768, 2008.

Karin Margretha H Larsen, Bogi Hansen, and Harald Svendsen. The faroe shelf front: properties and exchange. *Journal of Marine Systems*, 78(1): 9–17, 2009.

Karin Margretha Húsgar Larsen. *Circulation and exchange of water masses on the Faroe Shelf and the impact on the Shelf ecosystem*. PhD thesis, The University of Bergen, 2009.

Svend-Aage Malmberg and SS Kristmannsson. Hydrographic conditions in icelandic waters, 1980–1989. In *ICES Marine Science Symposia*, volume 195, pages 76–92, 1992.

Dimitris Menemenlis, Ichiro Fukumori, and Tong Lee. Using green's functions to calibrate an ocean general circulation model. *Monthly weather review*, 133(5), 2005.

Dimitris Menemenlis, J-M Campin, Patrick Heimbach, Chris Hill, Tong Lee, An Nguyen, Michael Schodlok, and Hong Zhang. Ecco2: High resolution global ocean and sea ice data synthesis. *Mercator Ocean Q. Newsl*, 31: 13–21, 2008.

Håkon Mosby. *Atlantic water in the Norwegian Sea*. Universitetsforlaget, 1970.

L-Y Oey. Eddy energetics in the Faroe-Shetland channel: a model resolution study. *Continental Shelf Research*, 17(15):1929–1944, 1997.

Kjell Arild Orvik and Peter Niiler. Major pathways of Atlantic water in the northern North Atlantic and Nordic Seas toward Arctic. *Geophysical Research Letters*, 29(19):2–1, 2002.

Kjell Arild Orvik, Øystein Skagseth, and Martin Mork. Atlantic inflow to the Nordic Seas: Current structure and volume fluxes from moored current meters, VM-ADCP and SeaSoar-CTD observations, 1995–1999. *Deep Sea Research Part I: Oceanographic Research Papers*, 48(4):937–957, 2001.

Svein Østerhus, Toby Sherwin, Detlef Quadfasel, and Bogi Hansen. The overflow transport east of iceland. In *Arctic–Subarctic Ocean Fluxes*, pages 427–441. Springer, 2008.

L Otto and HM Van Aken. Surface circulation in the northeast Atlantic as observed with drifters. *Deep Sea Research Part I: Oceanographic Research Papers*, 43(4):467–499, 1996.

RT Pollard, JF Read, NP Holliday, and H Leach. Water masses and circulation pathways through the Iceland Basin during Vivaldi 1996. *Journal of Geophysical Research: Oceans*, 109(C4), 2004.

IS Robinson. Tidal vorticity and residual circulation. *Deep Sea Research Part A. Oceanographic Research Papers*, 28(3):195–212, 1981.

T. Rossby and C.N. Flagg. Direct measurement of volume flux in the Faroe-Shetland Channel and over the Iceland-Faroe Ridge. *Geophysical Research Letters*, 39(L07602), 2012.

T Rossby, MD Prater, and H Søiland. Pathways of inflow and dispersion of warm waters in the nordic seas. *Journal of Geophysical Research: Oceans (1978–2012)*, 114(C4), 2009.

Artem Sarafanov, Alexey Sokov, Alexander Demidov, and Anastasia Falina. Warming and salinification of intermediate and deep waters in the Irminger Sea and Iceland Basin in 1997–2006. *Geophysical Research Letters*, 34(23), 2007.

Artem Sarafanov, Anastasia Falina, Herlé Mercier, Alexey Sokov, Pascale Lherminier, Claire Gourcuff, Sergey Gladyshev, Fabienne Gaillard, and Nathalie Daniault. Mean full-depth summer circulation and transports at the northern periphery of the Atlantic Ocean in the 2000s. *Journal of Geophysical Research: Oceans (1978–2012)*, 117(C1), 2012.

TJ Sherwin, WR Turrell, DRG Jeans, and S Dye. Eddies and a mesoscale deflection of the slope current in the Faroe–Shetland Channel. *Deep Sea Research Part I: Oceanographic Research Papers*, 46(3):415–438, 1999.

Toby Sherwin, Sarah Hughes, and Bill Turrell. Analysis of the significance of short term (mesoscale) variability on the influx of material into the Arctic through the Faroe-Shetland Channel. Technical report, 2006a.

Toby J Sherwin, Martin O Williams, William R Turrell, Sarah L Hughes, and Peter I Miller. A description and analysis of mesoscale variability in the Färoe-Shetland Channel. *Journal of Geophysical Research: Oceans (1978–2012)*, 111(C3), 2006b.

Toby J Sherwin, Sarah L Hughes, William R Turrell, Bogi Hansen, and Svein Østerhus. Wind-driven monthly variations in transport and the flow field in the Faroe–Shetland Channel. *Polar Research*, 27(1):7–22, 2008.

K Simonsen. Tides and tidal simulation in the area around the faroe islands. nansen environmental and remote sensing center. Technical report, Technical Report, 1999.

Michael A Spall and James F Price. Mesoscale variability in Denmark strait: The PV outflow hypothesis. *Journal of physical oceanography*, 28(8):1598–1623, 1998.

James H Swift and Knut Aagaard. Seasonal transitions and water mass formation in the Iceland and Greenland seas. *Deep Sea Research Part A. Oceanographic Research Papers*, 28(10):1107–1129, 1981.

John Barclay Tait. *Hydrography of the Faroe-Shetland Channel, 1927-1952.* HM Stationery Office, 1957.

W.R. Turrell, G. Slesser, R.D. Adams, R. Payne, and P.A. Gillibrand. Decadal variability in the composition of Faroe Shetland Channel bottom water. *Deep-Sea Research Part I*, 46:1–25, 1999.

National Oceanic U.S. Department of Commerce and National Geophysical Data Center Atmospheric Administration. 2-minute Gridded Global Relief Data (ETOPO2v2), 2006. Available at http://www.ngdc.noaa.gov/mgg/fliers/06mgg01.html.

Kjetil Våge, Robert S Pickart, Michael A Spall, GWK Moore, Héinn Valdimarsson, Daniel J Torres, Svetlana Y Erofeeva, and Jan Even Ø Nilsen. Revised circulation scheme north of the Denmark Strait. *Deep Sea Research Part I: Oceanographic Research Papers*, 79:20–39, 2013.

Héinn Valdimarsson and Svend-Aage Malmberg. Near-surface circulation in icelandic waters derived from satellite tracked drifters. *Rit Fiskideild*, 16: 23–40, 1999.

Wilken-Jon von Appen, Robert S Pickart, Kenneth H Brink, and Thomas WN Haine. Water column structure and statistics of Denmark Strait Overflow Water cyclones. *Deep Sea Research Part I: Oceanographic Research Papers*, 84:110–126, 2014.

Yu-Huai Wang, Ling-Yun Chiao, Kamazima MM Lwiza, and Dong-Ping Wang. Analysis of flow at the gate of Taiwan Strait. *Journal of Geophysical Research: Oceans (1978–2012)*, 109(C2), 2004.

MO Williams and TJ Sherwin. Mesoscale dynamics in the Faroes Channels. Technical report, 2002.

Igor Yashayaev, N Penny Holliday, Manfred Bersch, and Hendrik M van Aken. The history of the Labrador Sea Water: Production, spreading, transformation and loss. In *Arctic–Subarctic Ocean Fluxes*, pages 569–612. Springer, 2008.

JTF Zimmerman. Topographic generation of residual circulation by oscillatory (tidal) currents. *Geophysical & Astrophysical Fluid Dynamics*, 11(1): 35–47, 1978.

JTF Zimmerman. Dynamics, diffusion and geomorphological significance of tidal residual eddies. 1981.